Elucidating the reaction mechanism of cobalt-based Fischer-Tropsch Synthesis

A microkinetic model on Co FCC(110)

van der Meijs, Joost

Award date:
2020

Technische Universiteit
Eindhoven
University of Technology

Department of Chemical Engineering & Chemistry
Inorganic Materials & Catalysis
Postbus 513, 5600 MB Eindhoven
The Netherlands
www.tue.nl

Author
J. van der Meijs (S111746)

Committee
Prof.dr.ir. E.J.M. Hensen
Dr.ir. I.A.W. Filot
Ir. M.P.C. van Etten
Dr.ir. I. Roghair

Date
11 february 2020

Version
1.0

Elucidating the reaction mechanism of cobalt-based Fischer-Tropsch Synthesis

A microkinetic model on Co FCC(110)

J. van der Meijs (S111746)
j.v.d.meijs@student.tue.nl

Abstract

The Fischer-Tropsch Synthesis is a Feedstock-to-Liquid process which has the potential to produce hydrocarbon based fuels on a renewable basis. These conventional fuels will still have a use in the future due to their high energy density. Experiments have shown that cobalt is a viable catalyst for this process and has the ability to generate olefins and parafins. In this work, the Fischer-Tropsch mechanism is explored on the cobalt FCC(110) facet. Previous work by Zijlstra focussed on a dual site model using the HCP($11\bar{2}1$), or B_5-site, and the HCP(0001). Molecular Dynamics simulated annealing calculations have shown that this specific site is not present on the catalytic surface of cobalt nanoparticles in the range of 2-9nm. Molecular Dynamics annealing simulations also have shown that the surface site distribution of the FCC(110) site has a similar trend to the exprimentally observed structure sensitivity trend. In addition CO scission is relatively easy on this facet with a barrier of approximately 130kJ/mol. Therefore, the FCC(110) surface facet could be a good candidate active site for describing the Fischer-Tropsch Synthesis on cobalt. The exploration in this study is done using Density Functional Theory calculations using VASP and microkinetic modelling using MKMCXX. This work will focus on building a microkinetic model for a large system of elementary reaction steps. We found that the cobalt FCC(110) facet shows activity in the temperature range 200 to 250°C with a selectivity of around 50% towards CO_2. We also studied the behaviour of the FCC(110) facets by varying the reaction conditions such as: (1) reactant ratios, (2) the pressure and (3) the temperature. We showed that by changing the H_2:CO-ratio from 1:1 to 10:1 there is no significant change in the formation of long hydrocarbons. Varying the pressure between 1 to 20 bars by incresing the partial pressures of H_2 and CO shows no increase in CO consumption. Varying the temperature to from the regime 200-250°C to the regime of 320-350°C shows an increase in the selectivity towards CO_2 to approximately 60%. During this study we found it is highly unlikely that the cobalt FCC(110) facet is responsible for the majority of the activity observed during Fischer-Tropsch reaction conditions.

Contents

List of Figures

List of Tables

1 Introduction

1.1 Relevance

1.1.1 Catalysis

In many chemical processes catalysts are utilized to make a process more economicly viable due to a lower pressure or temperature needed, or make it applicable at large scale due to an increase in reaction speed. A catalyst is a substance that changes the reaction path without altering the thermodynamic equilibrium of the starting reactants and the products, see Figure 1.1. Intelligent catalyst design is regarded as difficult due to the many different effects at play within the reactor the catalyst is applied. At the macroscopic scale there are pressure, temperature, flow rate and stream compositions to consider. At a mesoscopic scale there is the form of the catalyst particles, micro or meso pores and possible diffusion limitations at play. At the microscopic scale there are quantum effects, the potential energy landscapes on the catalyst surface and lateral interactions to take into account. This study will mainy focus on the microscopic scale.

1.1.2 Fischer-Tropsch synthesis

The Fisher-Tropsch synthesis (FTS) is a process in which syngas (a mixture of carbon monoxide and hydrogen) react on a catalytic surface to form long chain hydrocarbons. The FT-process is a so called Gas-to-Liquid (GtL) process. These kind of processes gain importance due to the use of natural gas being the feedstock for fuels [1]. FT can also be used for Biomass-to-Liquid (BtL) or Coal-to-Liquid (CtL) [2, 3], the former being the more interesting of the two due to the implication that it is able to convert waste, or biomass, into useful products. Converting biomass to conventional fuels or other oil derivatives could lead to a circular economy[4].

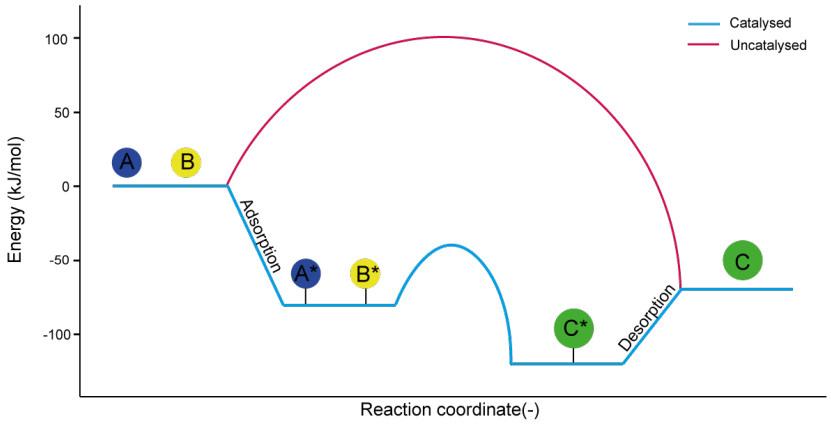

Figure 1.1: A potential energy diagram for a reaction of A and B in the gas phase to product C. A^*, B^* and C^* are adsorbates on the catalytic surface. The one step reaction is the reaction without the catalyst present (red line). The blue line represents the reaction with the catalyst present. The barriers and steps in this example are arbitrarily chosen and only to illustrate the change in reaction pathway. The potential energy diagram does not represent a specific reaction. The diagram is with regards to the initial state of $A + B$ and a positive energy in this case only means that the energy of the state is higher than the initial state.

1.2 State of the art

The Fischer-Tropsch (FT) synthesis is a synthesis of hydrocarbons with many proposed reaction pathways. Within the FT-process the following transition metals can be used[5]: iron, cobalt, nickel and ruthenium. Although ruthenium shows the most activity it is also by far the most expensive of the four. Thus rendering ruthenium not economically viable for industrial use. Nickel shows the most activity in the FT-synthesis after ruthenium, however nickel is a very good hydrogenation catalyst leading to the less valuable and less desired methane instead of longer hydrocarbons. This leaves iron and cobalt as viable candidates as FT catalyst. Iron is most seen in industrial applications due to its low cost and high yield in olefins. Iron is also known for high activity in the water gas shift (WGS) reaction. Cobalt, although more expensive than iron, shows less sintering, agglomeration and a possible higher product selectivity than iron. This could make cobalt a more desired catalyst over iron. A deeper understanding of the FT synthesis would allow us to design better catalysts for the chemical reactions and better select the outcome of the process [6]. There is an ongoing debate on the rate limiting step in the FT synthesis, there is evidence that would support the hypothesis that the CO-dissociation is the most critical [7], evidence can also be found that the carbon hydrogenation is the rate determining factor of the FT-synthesis [8, 9]. Research has shown that cobalt shows a growing activity with increasing particle size up to around 6 nm [10, 11, 12], it is also proposed that there is a dependence on the type of facets available for the reaction to take place upon [6, 12]. Beyond approximately 6 nm, the activity shows no increase with increasing particle size[10]. It is thought that below this threshold there are not enough step-edge sites (B_5-site) available to facilitate CO-dissociation[13].

A change of diameter of the catalytic cobalt nanoparticles can also bring a change in different surfaces that are available for reaction and even different bulk phases[6, 14]. The bulk structure dictates which facets are available on the outside of the particles, as shown by Liu et al.[6] from the Wulff construction of the cobalt nanoparticles[15]. The drawback from the Wulff construction is that only one bulk phase is present, either HCP or FCC, while experimental evidence suggest the presence of both. Different surfaces show different activities for different reactions, such as CO-dissociation or hydrogenation of a carbon-species[16, 17]. Often different types of reactive or adsorption sites are present on one type of surface such as the four-fold, three-fold, top-bridged or top [17], an example can be seen in Figure 1.2. Due to different facets having different coordination they stabilize species differently.

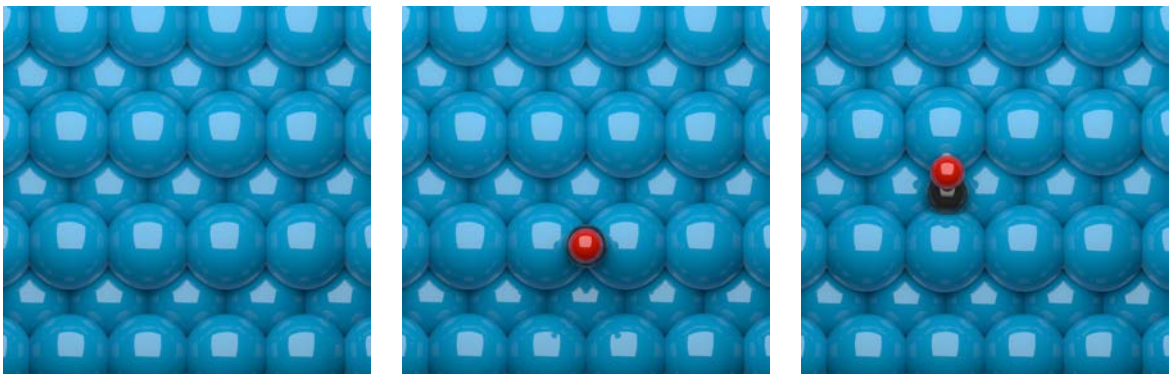

a b c

Figure 1.2: On the left (a): an empty cobalt FCC (110) surface; clearly visible are the ridges and valleys. The combination of which provide different reactive sites on the surface. It allows for top (on top of the ridges), two fold bridged (also on top of the ridge), Three-fold and three-fold in the valley. In the middle (b): a CO-molecule adsorbed on the bridged position on the cobalt surface. On the right (c): a CO-molecule in a four-fold position in the valley.

Research by Zijlstra et al.[13], Filot[20] and others [8, 21, 22] show that the cobalt HCP $(11\bar{2}1)$, also called the B_5-site, would be a highle reactive surface for the Fischer-Tropsch synthesis due to its ability to dissociate CO[23]. Recent molecular dynamics annealing simulations in combination with pattern recognition show that the HCP $(11\bar{2}1)$ does not appear on cobalt nanoparticles with a particle size in the range of 2 to 9 nm, see Figure 1.3. Therefor another surface should be responsible for the activity

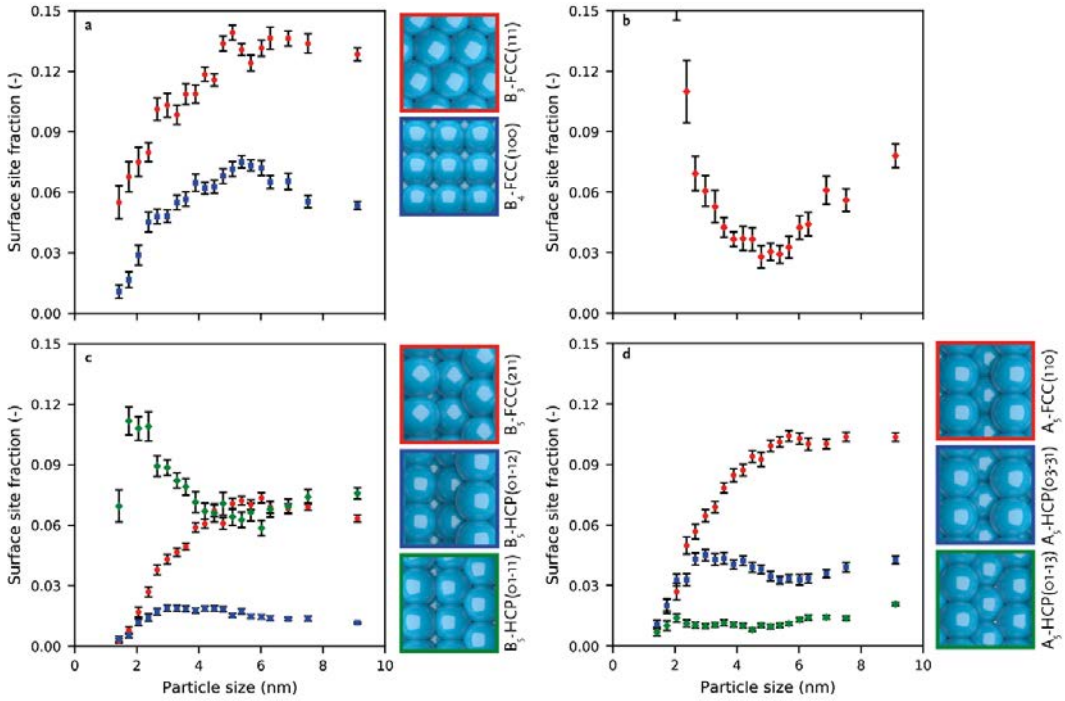

Figure 1.3: The distributions of different facets for different cobalt particle sizes. The image is taken from the work of ir. M.P.C. van Etten. It can be seen that the fraction of the FCC(110), or A_5-site, increases to 6 nm and has a plateau for larger particle sizes.

and selectivity trends observed in experiments for the FT-synthesis. When looking at the interaction that carbon and oxygen have with the cobalt surface, see Figure 1.4, it can be clearly seen that the HCP(01$\bar{1}$1) and the FCC(100) facets have stronger interactions with carbon and oxygen. The HCP(01$\bar{1}$2) and FCC(211) both show weaker interaction with the oxygen and stronger interaction with the carbon. These stronger interactions are unfavourable for the Fischer Tropsch. Thus the main focus is the weaker interaction with carbon and the metal. The candidate that is the closest to the HCP(11$\bar{2}$1) in terms of M-O and M-C interaction is the FCC(110). The FCC(110) shows a slightly weaker interaction with carbon and a much weaker interaction with oxygen when compared to the HCP(11$\bar{2}$1). The cobalt FCC(110), also called the A_5-site, surface provides a varied surface with many different reactive sites. Thus allowing it potentially to have the different sites needed for the CO-dissociation, the hydrogenation of the carbon species and the coupling of carbon species to form hydrocarbon chains. This potential makes it possible that it could be the most active site during FT operation conditions.

Current FT reaction conditions are in the range of 473-523K for low temperature FT-synthesis (LTFT) and 593-623K for high temperature FT synthesis (HTFT)[24, 25, 26, 27]. For LTFT the choice of reactor is the fixed-bed reactor and the slurry bubble column. The choice of reactor for HTFT is the fluidized bed reactor. This study will focus on the LTFT reaction conditions with a pressure of 1bar[24, 28, 22].

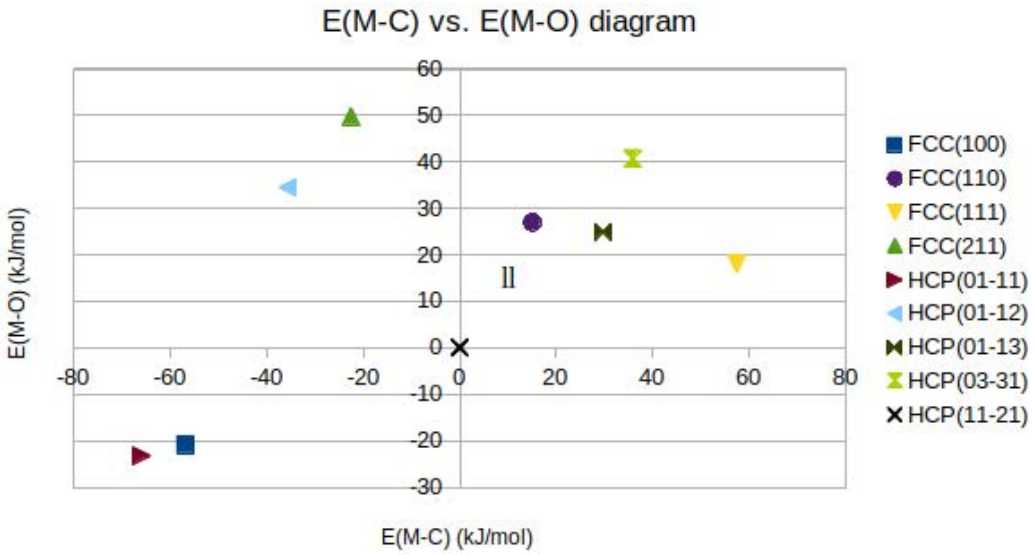

Figure 1.4: The distribution of diffent facets. On the vertical axis is the interaction energy of oxygen with cobalt and on the horizontal axis the interaction energy of carbon with cobalt. All points are in relation to the cobalt HCP(11$\bar{2}$1). The location of the cobalt FCC(110)-facet is the circle in the first quadrant of the diagram.

1.3 Goals and research questions

The aim of this project is to gain insight in the behaviour of the cobalt FCC(110) facet under Fischer Tropsch reaction conditions. To achieve this, DFT-calculations will be done on the cobalt FCC(110) surface and a microkinetic model will be build to study the FTS on this cobalt facet. In order to get to the research goal these of research questions will be investigated:

1. What are the barriers & pre-exponential factors for each of the elementary reactions in the Fischer-Tropsch Synthesis?
2. What are the activities and selectivities for cobalt based Fischer-Tropsch on the FCC(110) surface?
3. What is the influence of reaction conditions on the Fischer-Tropsch Synthesis on the cobalt FCC(110) facet?

To answer the first question DFT-calculations on the Co FCC(110)-surface for the formation of methane, ethylene and ethane will be done. To answer the second question three steps will be taken: (1) a microkinetic model will be build for the microkinetic description based on the DFT data, (2) lateral interactions on the surface will be added and (3) the extrapolation of the network to describe FT-synthesis up to C_{25} parafins and olefins. In order to answer the last question the following influences will be investigated on the overall consumption of CO and the formation of hydrocarbonchains: (1) the influence of varying the H_2:CO-ratio, (2) the influence of the pressure, both with and without an inert carrier gas, and (3) the influence of temperature.

2 Method

2.1 Density Functional Theory

Density Functional Theory[29, 30, 20], or DFT for short, will be used to explore the different states, calculate the corresponding electronic energies and zero-point-energy corrections. The DFT data is in turn used to calculate the activation barriers for the set of elementary reactionsteps for the cobalt based FTS on FCC(110). For finding the transition state, TS, between the initial state, IS, of a reaction and the final state, FS, the climbing Nudged Elastic Band, NEB or cNEB, method was used. For all chemical surface reactions, Arrhenius behaviour is assumed. The total contribution of the vibrational partition functions (eq 2.1) is calculated at a temperature of 500K. The rate constant k is then calculated according to the Eyring equation (Equation 2.2).

$$Q_{vib} = \prod_{\omega} \frac{1}{1 - e^{-h\omega/k_b T}} \tag{2.1}$$

$$k = \frac{k_b T}{h} \cdot \frac{Q^{\dagger}_{TS}}{Q_{IS}} \cdot e^{-\Delta E_{act}/RT} \tag{2.2}$$

2.1.1 Software and settings

VASP

The software used for the DFT calculations is the Vienna ab initio Simulation Package[31], or VASP for short. The version used is VASP/5.3.5. Unless otherwise mentioned all calculations have been performed with the Perdew-Burke-Ernzerhof (PBE) exchange-correlation GGA-functional[32]. Within VASP the method used is Potential Projector Augmented-Wave method (PAW)[33]. In short the PAW method solves the radial schrödinger equations under the assumption of a frozen core system in which each shell around an atom is projected onto a plane to produce planar waves. The full derivation of the equations used during DFT-calculations is outside of the scope of this study. For the different types of calculations different settings are used, a full overview of all settings can be found in appendix B. For more detailed information on the settings view the VASP wiki[31].

VeeVee

The Software used for building an visualizing the different states is VeeVee. VeeVee can read VASP output and generate the geometry input for VASP. The version used is 1.5.1. VeeVee is a custom software package developed by dr.ir. I.A.W. Filot. It is available for free from https://www.ivofilot.nl/software

Material Studios

To construct the Co FCC(110) slab, Material Studios is used. First the FCC structure is generated and the FCC (110) face is cut. After generation of the unitcell, a 3 by 3 unitcell surface is constructed with 7 atomic layers. In order to create a surface slab a 7.5 Å vacuum slab was added to both the top and the bottom

Blender

To create the images found in appendix C, the software Blender is used. The software is free and can be found at https://www.blender.org/. The version of the software used is 2.79. In combination

with the software blender a set of scripts was used, developed by dr.ir. B. Zijlstra for loading and rendering the images. The settings for the script can be found in appendix G. The script can be found at https://gitlab.tue.nl.

Jmol

In order to check the vibrations of the transition states the program Jmol was used. Jmol is a Java based open source molecular viewer. The version used is Jmol 14.6.4. The software is free for download at https://sourceforge.net/projects/jmol.

2.1.2 Calculations on Reactions

For an explanation of the names of the VASP in and output files see Table A.2 in appendix A. For all calculations on the cobalt FCC(110) slab a unit cell of 7.46Å by 10.55Å by 22.46Å used, this gives a cell with an volume of $1.8 \cdot 10^3 \text{Å}^3$. The number of K-points used is 5 by 5 by 1 giving 25 K-points. All calculations are done in reciprocal space unless mentioned otherwise. For the IS and FS of a elementary reaction step the ionic relaxation, or geometry optimization, is done first. For fast and accurate geometry optimization, four runs are done. The INCAR settings for the first run are displayed in Table B.1. The first run done has 10 ionic steps, with an energy cutoff of 300eV. The changes made to the INCAR for the second, third and final run can be found in Tables B.2, B.3 and B.4. As can be seen in those tables, the precision mode of VASP is set to normal for the first, second and third run. The final run is done with accurate precision. The energy cutoff for the fourth run is also 400eV as is more conventional instead of 300eV than the runs that have come before it. The amount of ionic steps are 120, 100 and 40 for the second, third and fourth run, respectively. The setting IBRION = 2 allows VASP to make rigorous adjustments to the geometry to achieve a minimum in energy. From the fourth run of the geometry optimization it is first checked using VeeVee (see section 2.1.1 for more information on the program) seeing if the result yields a desired state for further calculation. Secondly a calculation is done to retrieve the Zero-Point-Energy Correction (or ZPE for short) and the contribution of the vibrational partition function, see equation 2.1 at 500K. This calculation is also called the frequency analysis. The same POTCAR and K-POINTS are used as in the previous calculation step. The setting for the INCAR can be found in Table B.5. The energy cutoff is set to 400eV with 100 ionic steps to reach conversion. After the frequency analysis a calculation is performed, in the first NEB calculation there are 8 images (NEB8). The same POTCAR and number of K-POINTS are used as for the IS and FS. The settings for the INCAR can be found in Tables B.6, B.7 and B.8. There are three runs in total with the settings as mentioned above. The Setting IBRION = 1 allows VASP to make very minor adjustments to the geometry to find a local minimum in energy. This setting is also used in the upcoming few calculations with exceptions to the frequency analysis of the TS. The results of the NEB8 are retrieved and the images with the highest energy as well as the image bellow and above it are retrieved for further calculation. These will be used to do the NEB calculation again but this time with three images (NEB3). The NEB3 just like the NEB8 has three runs to allow for quick and accurate results. The settings of the first, second and final run can be found in Tables B.9, B.10 and B.11, respectively. From the NEB3, the middle image is supposed to have the highest energy level. This is presumed now to be te TS, to confirm this another soft geometry optimization (IBRION = 1) is required as well as a frequency analysis. For the geometry optimization there are two runs for which the same POTCAR and number of K-POINTS are used as the IS/FS. The settings for the first and second run can be found in Table B.12 and B.13. Finally to confirm there is a transition state a frequency analysis is performed. The same POTCAR and K-POINTS are used as in the geometry optimization for the TS. The settings for the analysis can be found in Table B.14. The results of this calculation should, in case of a double sided reaction on the slab, yield two imaginary frequencies. If there is only one side of the slab that has an adsorbate there should only be one imaginary frequency. VASP generates different types of output this study will focus mainly on:

(1) the geometry for the continuation of further calculations, (2) the energy of the system to generate the barriers needed for the microkinetic model and (3) in case of a frequency analysis the vibrational levels of the adsorbates to determine the contributions of the vibrational partition function. In order to verify there is a TS, the vibrations are checked in Jmol and one has to lie in the direction of the reaction coordinate.

The final step is to determine the activation barrier (ΔE_{act}) for the elementary reaction step according to the equations 2.3 and 2.4. The factor $\frac{1}{2}$ is there to correct for a slab with a reaction on both the top and bottom. In case there is only a one sided reaction, this factor is not needed. The ϵ_{state} is the energy of the state as calculated by VASP in eV, the $\epsilon_{state,zpe}$ is the ZPE as determined by the frequency analysis.

$$\Delta E_{act}^{forward} = \frac{1}{2}\left((\epsilon_{TS} + \epsilon_{TS,zpe}) - (\epsilon_{IS} + \epsilon_{IS,zpe})\right) \times 96.485[kJ \cdot mol^{-1} \cdot eV^{-1}] \tag{2.3}$$

$$\Delta E_{act}^{backward} = \frac{1}{2}\left((\epsilon_{TS} + \epsilon_{TS,zpe}) - (\epsilon_{FS} + \epsilon_{FS,zpe})\right) \times 96.485[kJ \cdot mol^{-1} \cdot eV^{-1}] \tag{2.4}$$

In case of an ad- or desorption step, the following equation is used:

$$\Delta E_{ads} = \left((\epsilon_{gas} + \epsilon_{zpe}) - \frac{1}{2}(\epsilon_{adsorbate} + \epsilon_{ZPE} - \epsilon_{surface})\right) \times 96.485\left[kJ \cdot mol^{-1} \cdot eV^{-1}\right] \tag{2.5}$$

With $\epsilon_{surface}$ the energy of the relaxed surface in eV. In case of a one sided reaction, more information in the next sub-section, the term $\frac{1}{2}$ of course is not needed. For desorption: ΔE_{des} the gas-phase and surface energy terms are the other way around: $\Delta E_{des} = -\Delta E_{ads}$

2.1.3 One sided reactions vs. two sided reactions

To negate dipole-effects, calculation are done on two sides of the surface slab. It was however soon apparent that doing the calculations on only one side would use less computational time. The VASP package offers the possibility to correct for these dipole-effects. The calculations with an adsorbate on only one side are done with freezing the bottom half of the surface where there is no adsorbate. Thus many calculations are done using the one-sides reaction to save on computational time. Due to the geometry optimizing algorithm single sided calculations proved easier to converge than double sides reactions. The saved time and ease of use come with the cost of the loss of accuracy. To correct for the dipole-dipole interactions of the slabs, the settings mentioned in Table B.15 were used.

2.2 MicroKinetics

2.2.1 Software & settings

MKMCXX

For the microkinetic modeling the program MKMCXX was used. Which can be found at https://mkmcxx.nl/. More detailed information on the program can be found at the MKMCXX wiki at https://wiki.mkmcxx.nl/. MKMCXX is a TU/e inhouse developed microkinetic modeling software package by prof.dr.ir. E.J.M. Hensen, dr.ir. I.A.W. Filot and dr.ir. B. Zijlsta. The version used is 2.14.6. For the mathmatical description and derivations see "introduction to microkinetic modelling" by dr. I.A.W. Filot [34]

The input files for MKMCXX can be found in Appendix H. The regex section contains the rules for the regular expressions used to drive the variable section. In the compounds-section all the different gasphase and surface components of the reaction were defined. The H_2:CO-ratio is set to 2:1. The concentration of all products was set to 0 [-]. The initial concentration of empty sites was set to 1 [-] and

the initial concentration to all other components was set to 0 [-]. The reaction-section contains the ad- & desorption reactions using HK-kinetics and surface reactions using LH-kinetics. For the HK-kinetics a adsorption site size of $5.38 \times 10^{-20} m^2$ is assumed and the sticking coëfficient was set to unity. The settings used were a pressure of 1000 mbar and the type of run was set to "*SEQUENCERUN*". The "*REAGENTS*" are set to CO and H_2. In the run sections the runs are defined via the temperature, time, absolute tolerance and relative tolerance. For the gasphase substances the thermochemistry data is used from ref [35], these are in term used for the Shomate equations (equations 2.6, 2.7 and 2.8) [35]. The latter two are used in MKMCXX.

$$C_{p,i} = A_i + B_i T' + C_i (T')^2 + D_i (T')^3 + \frac{E_i}{(T')^2} \tag{2.6}$$

$$H_{T,i} - H_{298.15,i} = A_i T' + \frac{B_i (T')^2}{2} + \frac{C_i (T')^3}{3} + \frac{D_i (T')^4}{4} - \frac{E_i}{T'} + F_i - H_i \tag{2.7}$$

$$S_{i,T} = A_i \ln (T') + B_i T' + \frac{C_i (T')^2}{2} + \frac{D_i (T')^3}{3} - \frac{E_i}{2(T')^2} + G_i \tag{2.8}$$

In equations 2.6, 2.7 and 2.8 T' is defined as in equation 2.9 with T the temperature in Kelvin.

$$T' = \frac{T(K)}{1000} \tag{2.9}$$

The parameters for the Shomate equations can be found in appendix F. For ethane there is no Shomate parameter data available from ref [35], here the Herz-Knudsen parameters are used.

2.2.2 Lateral interactions

To improve the microkinetic model of the network, lateral interactions were added. Here the data for the quantization for the lateral interactions is taken from the dataset on Co-FTS from dr. B. Zijlstra [23]. For the hydrocarbons, the lateral interactions are based upon the sum of their elements. The values for the lateral interactions can be found in Table 2.1. The values for the lateral interactions are at 1 monolayer (ML). The lower limit for the effect of the lateral interactions is set to 0ML. The lateral interactions will be taken into account for the following reactions:

- Carbon-carbon coupling when the growing chain is lifted from the surface, see Figure 2.1.
- Hydrogenation of the growing carbon chain leading to a fully hydrogenated second carbon atom, see Figure 2.2

Table 2.1: The values for the lateral interactions per adsorbate. For hydrocarbons the values for the lateral interactions is the sum of the elements. The values are taken from the model of dr.ir. B. Zijlstra [23].

adsorbate	$E_{lateral}$ [kJ/mol]
CO	450
C	300
O	300
H	100

2.2.3 Modeling Fischer-Tropsch in a microkinetic model

In order to model the Fischer-Tropsch synthesis better, longer hydrocarbons need to be produced. The production of longer hydrocarbons will be extrapolated using the data from the production of C_2. Here the chain extending from the carbon species on the surface will be treated as if it is one hydrogen atom, see Figure 2.3. The FTS is modelled up to C_{25}-species for both the alkanes and the alkenes. Only the α-alkenes are taken into consideration.

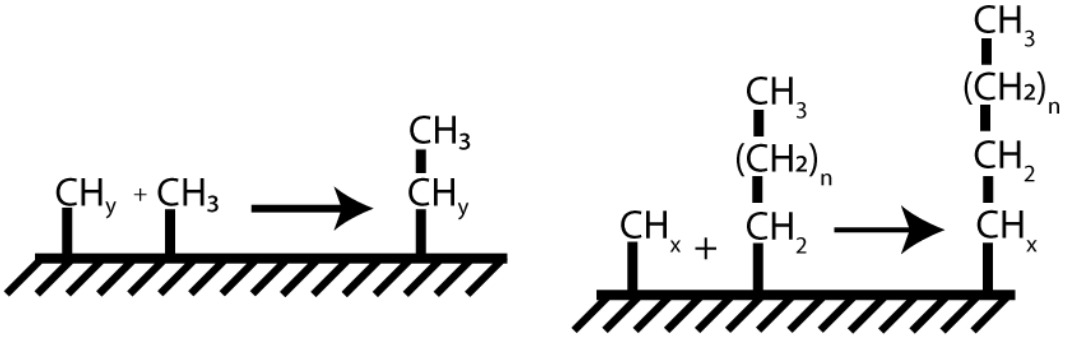

Figure 2.1: Schematic views for the reactions that will be taken into account for the lateral interactions. The left image shows the first carbon-carbon coupling when the chain starts. The right image shows the carbon-carbon coupling with a longer hydrocarbon.

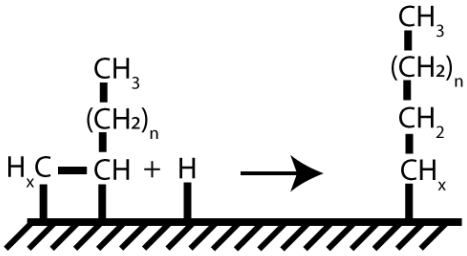

Figure 2.2: Schematic view of the hydrogenation reaction on the secon carbon in the growing hydrocarbon chain.

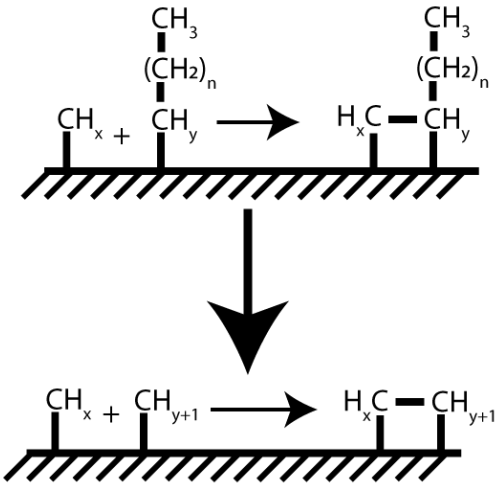

Figure 2.3: Schematic view of the approximation for reactions with longer hydrocarbonchains.

3 Results & discussion

3.1 Density Functional Theory

3.1.1 Network

In order to obtain a full reaction mechanism for the FT Synthesis, an inventory was made for which elementary reaction steps were possible. In Figure 3.1 the reaction network can be seen, here the adsorption of hydrogen, with an adsorption energy of 74.83 kJ/mol, is not displayed. In Figure 3.1 the energy barriers for the FTS can be found. These values can also be found in the tables in Appendix D. Note that the formation of methanol and other alcohols are not taken into consideration as experimental research does not suggest the formation of these alcohols, but rather the parafins and 1-olefins are obtained[36]. For all reactions, Arrhenius behaviour is assumed. In this network plot it can clearly be seen that the last hydrogenation step in the formation of methane is in the same order in terms of energy barrier (50-80 kJ/mol) in comparison with the other steps in the formation of methane. The formation of ethane is very easy by combining two methyl-adsorbates with a barrier of 20.3 kJ/mol. Since the coupling of two methyl groups is a termination step, this might have a significant negative impact on the ability for long hydrocarbon chains to form. In the coming sections, the different facets of this network plot will be discussed and explained in more detail.

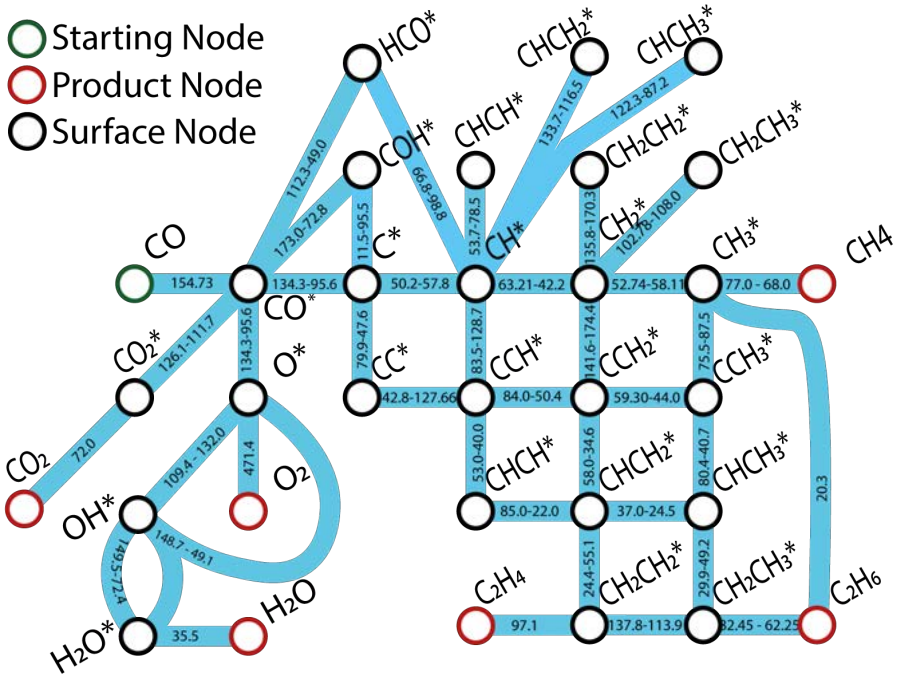

Figure 3.1: An overview of the reaction network up to C_2H_6. The values displayed are the activation energies in kJ/mol. Line segments containing only one value are considered stepped reactions and segments with two values are reactions containing a transition state. In this figure the dissociative adsorption of hydrogen is not displayed and has an adsorption energy of 74.83kJ/mol. The network starts at CO and ends at H_2O, CO_2, CH_4, C_2H_4 and C_2H_6.

3.1.2 CO-dissociation

First the CO-dissociation was studied, with the method described in section 2.1. In Figure 3.1 this is the first reaction from the starting node to the formation of C* and O*. As can be seen in Figure 3.2, the IS of CO on the surface is in the 4-fold position in the valley. The CO dissociates over the ridge and the carbon and oxygen atoms each end up at a different side of the ridge. Figure 3.3 shows the potential energy diagram (PED) with respect to CO in the gas phase and the corresponding values for the barriers can be found in Table D.1. The IS and FS assist in generating the TS. The calculated barriers are with respect to the most stable adsorption site of an adsorbate. From Figure 3.1 it can be seen that the forward barrier for direct CO-dissociation equals 134.25kJ/mol and the barriers for CO scission for the route that is hydrogen assisted are 66.81 kJ/mol for the route via the HCO-intermediate and 11.51 kJ/mol via the COH-intermediate. The hydrogenation of the CO-species to the HCO species is easier than direct dissociation, the overall reaction barrier is roughly equal to the direct dissociation. The formation of the COH intermediate is significantly more difficult than the direct dissociation. Therefore, these two pathways, direct CO-dissociation and the H-assisted CO-dissociation via the HCO-intermediate, are more likely to occur than the H-assisted pathway via the COH-intermediate. Detailed microkinetic modelling is needed in order to give more insight in which pathway will happen.

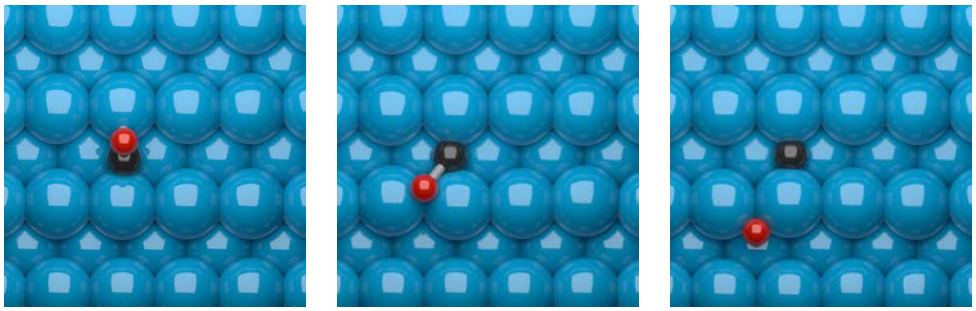

Figure 3.2: The dissociation of CO on the cobalt FCC(110) surface. Left is the IS, in the middle the TS and the right shows the FS.

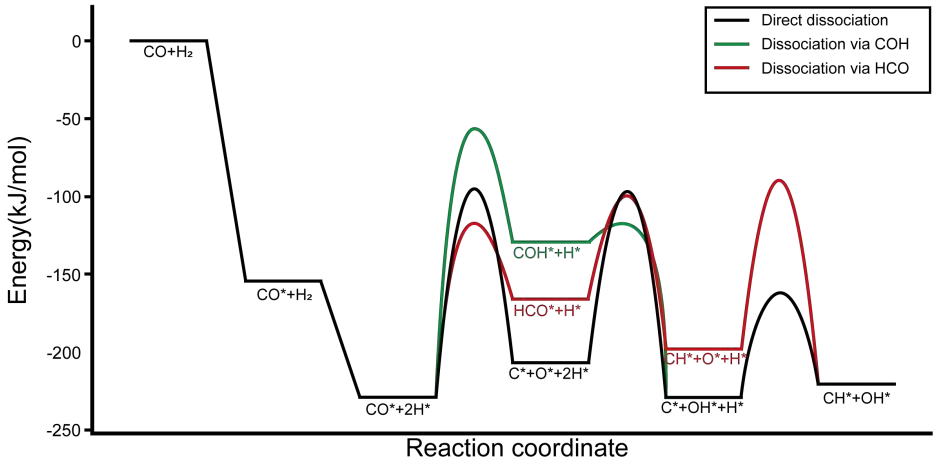

Figure 3.3: The potential energy diagram for the adsorption and dissociation of CO on the Co FCC(110) surface. The diagram is with respect to CO(g) and H_2(g). The first step is adsorption of the CO with ΔE=-154.73 kJ/mol. The adsorption of hydrogen is a step of ΔE=-74.83 kJ/mol. The barrier for direct dissociation (black line) after the adsorption steps are $\Delta E_{act}^{forward}$=134.25 kJ/mol and a backwards energy barrier of $\Delta E_{act}^{backward}$= 101.05 kJ/mol. The red line shows the hydrogen assisted dissociation via the HCO-intermediate, the green line shows the hydrogen assisted dissociation via the COH-intermediate.

.

3.1.3 Methanation

The methane formation has been studied using DFT and the obtained PED can be seen in Figure 3.4. In Figure 3.1 this is the horizontal pathway starting at C* and going to the product node CH_4. The configurations on the surface for the corresponding reactions can be found in appendix C, figures C.7, C.8, C.9 and C.10. The excact values for the energy barriers can be found in Table D.2. From Table D.2 it can be seen that the barrier for the formation of methane, CH_3+H $\rightarrow$ CH_4 + 2*, is only slightly higher than the other hydrogenation steps of the single carbon-species. Due to this relative low barrier for the formation of methane it is expected that in the microkinetic model methane is a large part of what will be produced. The calculated reaction enthalpy for the formation of methane is -228.9 kJ/mol, more information on the reaction enthalpy can be found in section 3.1.6.

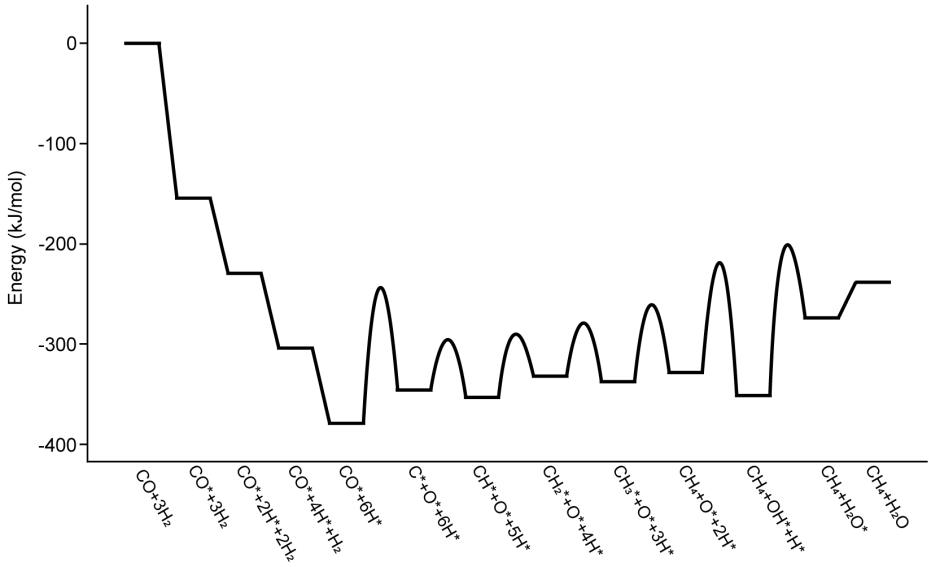

Figure 3.4: The energy diagram for the methanation reactions with respect to carbonmonoxide and hydrogen in the gas phase. The values for the steps and barriers needed for the dissociation of CO can be found in Table D.1. The barriers for the other reactions can be found in Table D.2. The calculated ΔH_r^0=-228.9 kJ/mol.

3.1.4 Oxygen Removal

As a result of the CO-dissociation there will be oxygen species on the surface. Staring from the oxygen node in the lower left corner of Figure 3.1 going to the H_2O, CO_2 and O_2 product nodes. Three possible pathways for oxygen removal are: (1) the formation of H_2O, (2) the formation of CO_2 and (3) the desorption of molecular oxygen which is very unlikely to occur with a barrier of 471.4kJ/mol. The PED of the formation of water and carbondioxide can be seen in Figure 3.5, due to the high barrier for the formation of molecular oxygen this is not taken into account. The activation energies can be found in Table D.4. Figure 3.5 shows the two pathways explored for the formation of water. It shows the direct hydrogenation of the oxygen species and the protonshuffle. The protonshuffle is the transfer of a hydrogen from one OH-species to another, creating H_2O and oxygen on the surface. From Figure 3.5 it looks like the overall barrier in the formation of water is the lowest for the protonshuffle pathway. Therefore it is expected that the dominant pathway in the formation of water will be via the protonshuffling. Looking at the PED in Figure 3.5 the more likely removal of oxygen is the formation of CO_2. Microkinetic modelling has to be done in order to confirm this.

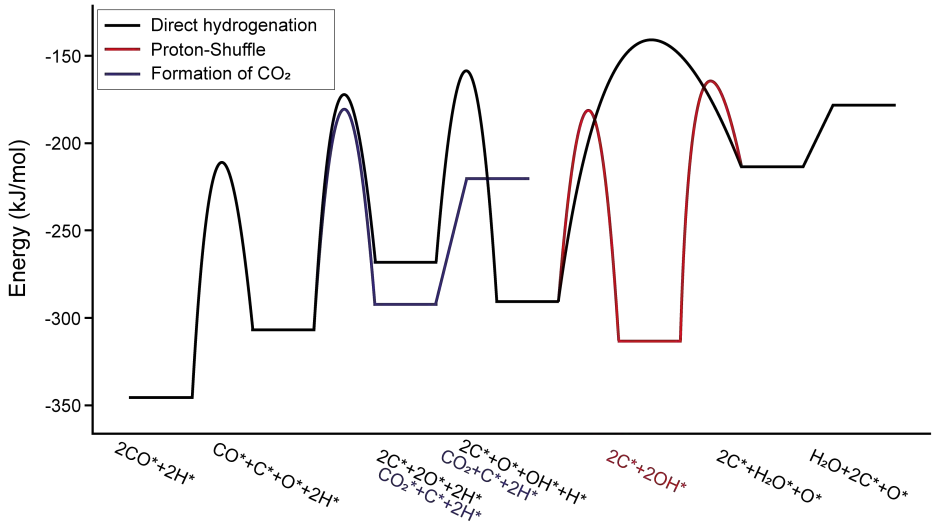

Figure 3.5: The PED for the removal of oxygen via the formation of water (black and red) and the formation of CO_2 (blue). The red line displays the protonshuffle, the combination of two hydroxygroups to form water and an oxygen-adsorbate. The refrence is two CO and two hydrogen on the surface. The PED is with respect to two CO and two H on the surface.

3.1.5 Carbon-carbon coupling and hydrogenation

The carbon-carbon coupling and hydrogenation steps for C_2H_n-species ($0 \leq n \leq 6$) was also investigated. These are all the pathways in Figure 3.1 not yet covered in the previous sections. The activation energies can be found in Table D.3, the corresponding images for the reaction can be found in appendix C. The PED for the formation of C_2H_6 can be found in Figure 3.6. In Figure 3.6 it can be seen that the formation of ethane via the combination of CH_3 intermediate (red line) is a stepped reaction. A stepped reaction means that there was no TS found. This reaction has a forward barrier of 20.34kJ/mol. Due to this low barrier for coupling after the formation of the CH_3 it is very easy to combine these and form ethane. The black line represents the formation of ethane via the CH intermediate and the blue line represents the synthesis with the CH_2-intermediate. Due to the low barrier for the formation of ethane it is very likely that this will be a dominant pathway. Which may inhibit the formation of longer hydrocarbons.

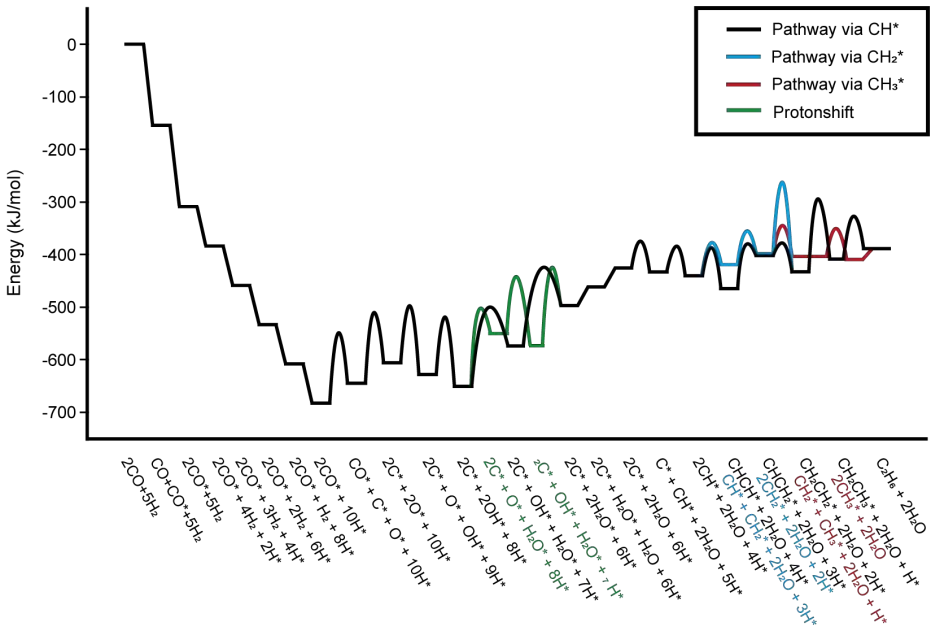

Figure 3.6: The PED for the formation of C_2H_6. Shown are the different pathways with regards to oxygen removal and three possible pathways with regards to coupling reactions.

3.1.6 Enthalpic contribution

Using the DFT values found, the reaction enthalpy was calculated for the following reactions: (1) the formation of methane, (2) the water gas shift reaction, (3) the formation of ethane, (4) the formation of ethylene, (5) the formation of propane and (6) the formation propylene and compared to the reaction enthalpy that was calculated from the formation enthalpies as reported by NIST[35]. The values for the different species can be found in Table E.1. To overcome the difference in DFT-values to the reported values from NIST, energy penalties on CO and CO_2 are introduced. The values can be found in Table E.1. The square error was calculated using Equation 3.1 and minimized using the non-linear Generalized Reduced Gradient method in MS Excel. The calculated reaction enthalpies can be found in Table E.2 along with the calculated reaction enthalpy using the formation. For the evaluation for the model, the sum of squares will be evaluated and minimized. The result can be found in Figure 3.7.

$$\sigma^2 = \left(E_{DFT+penalty}\,[kJ/mol] - \Delta H_{r,NIST}\,[kJ/mol]\right)^2 \tag{3.1}$$

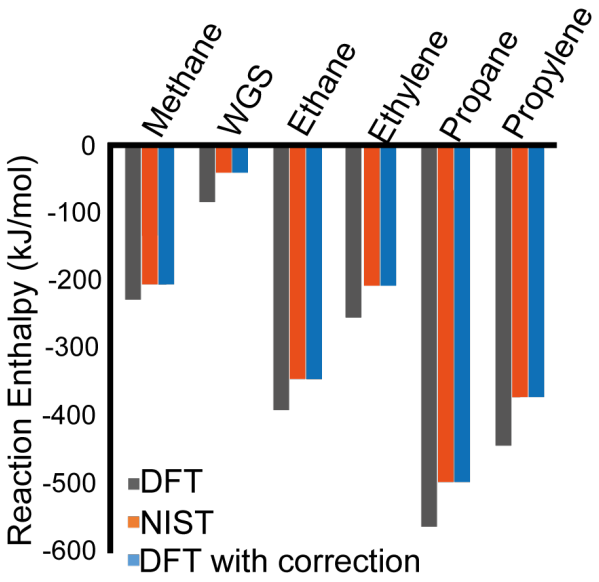

Figure 3.7: The Calculated reaction enthalpies for the DFT-values reported in gray, the reaction enthalpy using the values found in the NIST-database (orange) and the DFT-values with a energy penalty on CO and CO_2. The calculated DTF values have been calculated using the PBE-functional.

So far, all calculations have been done using the PBE-functional. However there is a debate on the CO-overbinding effect. The solution could be the use of the revised-PBE (rPBE) functional, it is speculated that that would lead to less overbinding effects and thus the need for smaller or no energetic penalties. For this purpose the chemical compounds from Table E.1 were reversed using the rPBE-functional. The results are in Table E.3. The reaction enthalpies can be found in Table E.4 along with the corresponding error an each reaction. The fit with the parameters was done the same way as for the PBE-functional.

However, instead of using just a correction factor for some components, it is also possible to use the thermodynamic approach, this does not per se yield better results due to the accuracy of the DFT. The corrections that can be done is the correction for the expansion of a gas, Equation 3.2.

$$\Delta H_r = \sum_i \nu_i \left(E_i + RT\right) \tag{3.2}$$

Note that in equation 3.2 R is the gas constant in kJ/(mol·K) and T = 298.15K as the formtion enthapies are given at that temperature. The next iteration would be to consider the influence of the rotation and translation. For a detailed mathmatical derivation please see "Introduction to microkinetics" by I.A.W.

Filot version 1.6.

$$\Delta H_r = \sum_i \nu_i \left(E_i + \left(\frac{3}{2} + \frac{2+\delta}{2} \right) \cdot RT \right) \tag{3.3}$$

In Equation 3.3 the term $\left(\frac{3}{2}\right)$ is the thermodynamic correction for translation and the $\left(\frac{2+\delta}{2}\right)$ is the thermodynamic correction for the rotation of the gasphase molecules, here $\delta = 0$ for linear molecules and $\delta = 1$ for non-linear molecules. The calculated values for the reaction enthalpy can be found in Table E.5 for both the PBE and de rPBE functionals along with the difference to the $\Delta H_{r,NIST}$. From Table E.5 it may be aparrent that the rBPE gives a better overall fit as the error is smaller. However by using a correction factor for CO and CO_2, a better fit for the overall model is obtained. The error on the reaction enthalpy for the formation of methane is $2.5 \cdot 10^{-8}$kJ/mol and the formation of propylene has an error of 3.4kJ/mol.

3.2 MicroKinetics

The microkinetic model was build in three stages: (1) the reaction network that was investigated using DFT, (2) the addition of lateral interactions to this model and (3) the extrapolation towards longer hydrocarbons. For the microkinetic model, the energetic correction from Table E.1 will be used and the barriers in Tables D.1, D.2, D.3 and D.4 will be used. Next to building the microkinetic model, there will also be a look into different operating regimes: (1) different H_2:CO-ratios ranging from 1:1 to 10:1, (2) a range of total operating pressures ranging from 1 to 20 bar both with and without the use of a carrier gas and (3) how the catalyst operates in the HTFT regime. Lastly the apparent activation energy, selectivity and chaingrowth will be discussed. The overall reaction rate will be evaluated based on the consumption of CO.

3.2.1 The reaction network

Firstly the full reaction network that was investigated using DFT was build in MKMCXX. For the adsorption/desorption reactions Hertz-Knudsen kinetics are used and for elementary reactions on the surface the Langmuir-Hinselwood kinetics were used. The thermochemistry data were taken from https://webbook.nist.gov/ an overview can be found in appendix F. The HK-parameters are calculated within MKMCXX based on the Shomate equations. The sticking coëfficient was set to unity and the site area is set to $5.38 \cdot 10^{-20} m^2$. The CO/H_2 ratio is set to 1:2. At this point no lateral interactions are taken into account. The inputfile can be found in Appendix H.1. Figure 3.8a shows the coverage of the surface under LTFT conditions with a pressure of 1 bar. Here it can be seen that the surface is completely covered with CO. Experimentally CO coverage of around 40% are observed[22]. This can be explained due to lateral interactions, which are not taken into account yet. Hence, lateral interactions need to be taken into account to make a more realistic model. From the DRC-plot in Figure 3.8b it can also be seen that CO-dissociation is the rate determining step.

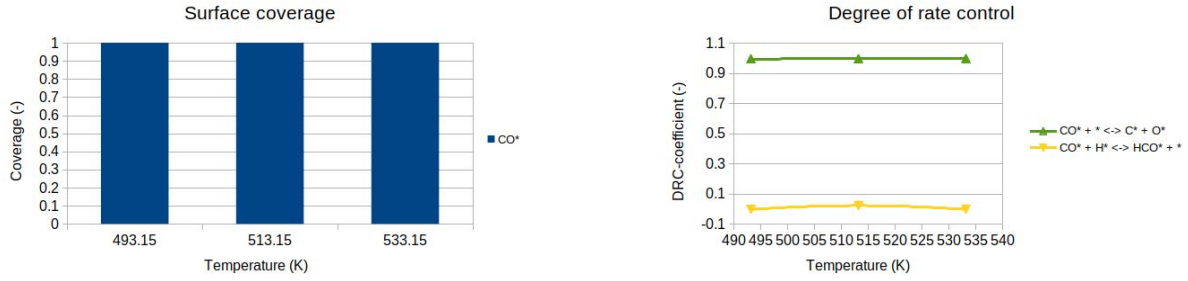

(a) (b)

Figure 3.8: The reaction network up to C_2H_6 for the temperatures: 493.15, 513.15 and 533.15K at P=1000mbar and H_2:CO = 2:1. No lateral interactions are taken into account. (a) The coverage of the surface for the network up to C_2H_6. It can be seen from the bar-plot that for all temperatures the surface is completely covered in CO*. (b) The degree of rate control for the reaction network, here it can be seen that the reaction rate is fully determined by the dissociation of CO (upward triangles)

3.2.2 Addition of lateral interactions

Secondly the lateral interaction were implemented, as mentioned in section 2.2.2, Table 2.1. The results can be found in Figure 3.9. The first thing to notice is that the coverage of CO drops and the surface is now covered with multiple species, like O, OH, C, CH, CCH and CCH_3, and has free sites available. For the limiting factors in the reaction rate it can be seen in Figure 3.9b that there are a lot more reactions contributing to the overall reaction rate when compared to the model without lateral interactions. The formation of water is rate limiting step while the dissociation of CO is inhibiting the reaction. The inputfile for MKMCXX can be found in Appendix H.2.

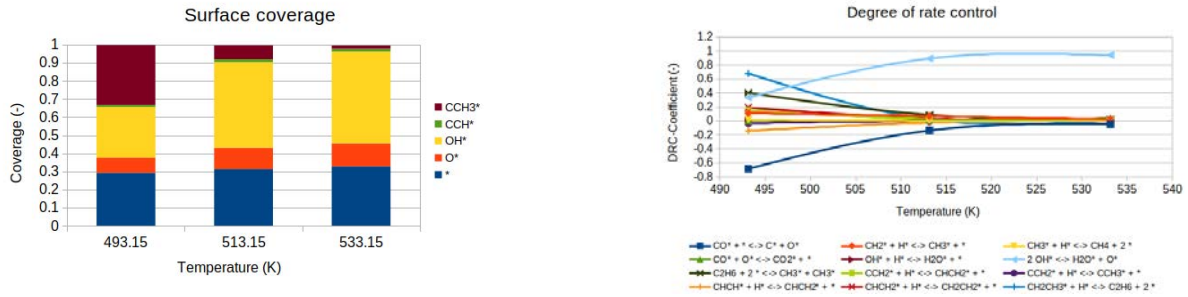

(a) (b)

Figure 3.9: The coverage and degree of rate control for the reaction network up to C_2H_6 for the temperatures: 493.15, 513.15 and 533.15K at P=1000mbar and H_2:CO = 2:1. For the simulations lateral interactions are taken into account as can be found in Table 2.1. (a) The coverage of the surface for the reaction network including the lateral interactions, the surface is covered in multiple surface species such as O*, OH*, CCH* and CCH_3 there are also free sites available (*). (b) The DRC-plot for the reaction network, here it can be seen that multiple have an influence on the overall reactionrate.

3.2.3 Extrapolated network

For a better description of the FT-synthesis, the barriers found for the formation of ethane and ethylene were used to extrapolate to C_{25} olefins and parafins as described in Section 2.2.3. Only α-unsaturated hydrocarbons are considered as far as olefins go. The inputfile can be found in Appendix H.3. In Figure 3.10a it can be seen that the surface is for about 40% consistent of free sites under operating conditions, adsorbed CO make up an approximate 50% of the surface and the remaining surface sites are distributed among H*, O* and OH*. Figure 3.10b shows that the formation of CO_2 has the most influence on the overall reaction, followed by the dissociation of carbon monoxide into C* and O*. It is clear from Figure 3.10c that hydrocarbons longer than C_{12} are not produced and for hydrocarbons C_{3+} the production is very limited and could even be considered almost zero as well. From Figure 3.10c it can also be seen that the production for C_2 or C_1 species does not differ much (a TOF of $4.4\times10^{-5}s^{-1}$ and $3.4\times10^{-5}s^{-1}$ respectively). Figure 3.10d shows the reaction orders of CO and H_2 for the FTS, here it can be seen that H_2 has a positive reaction order thus adding more hydrogen will improve the consumption of CO. However increasing the amount of hydrogen changes the H_2:CO-ratio, the effects of this change are discussed in 3.2.4.

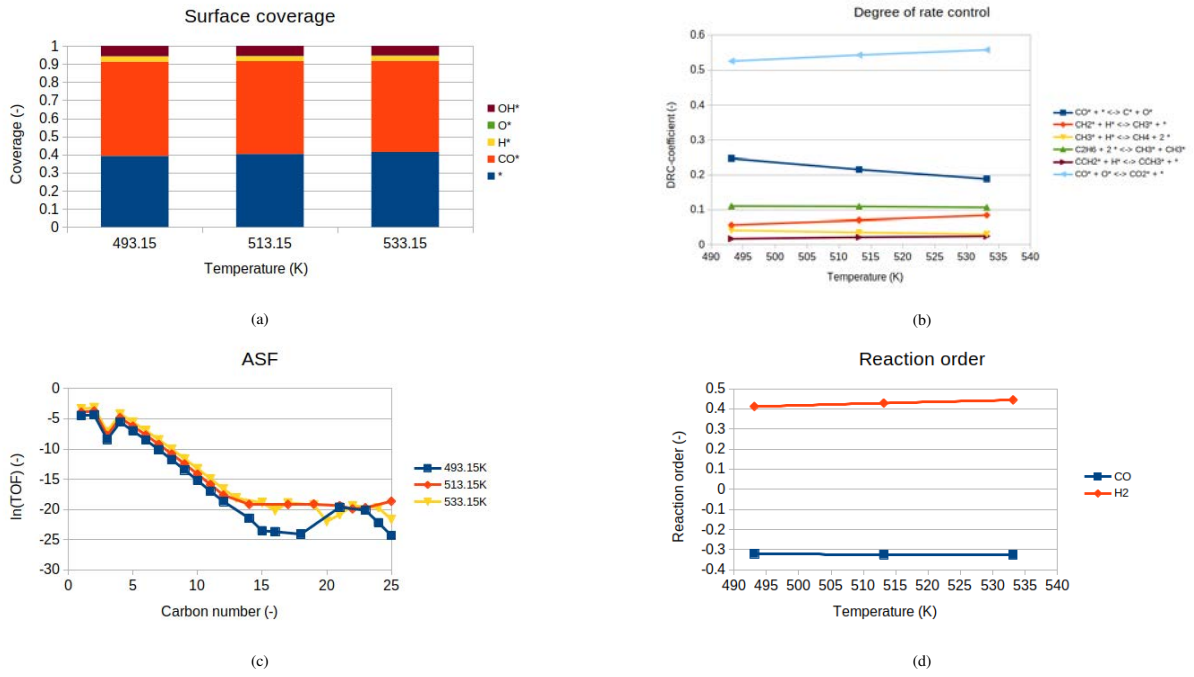

Figure 3.10: Full FT-synthesis (up to C_{25}-species), H_2:CO=2:1, P=1000mbar, temperatures: 493.15, 513.15 and 533.15K. Lateral interactions are taken into account according to section 2.2.2. (a) The surface coverage of CO FCC(110) under FTS conditions, on the surface OH*, O*, H* and CO* species are present. (b) The degree of rate control for FT-synthesis. As can be seen there is not just one reaction controlling the entire reactionrate. The biggest influence is still the dissociation of CO* into C* and O*. For hydogenation the step CH_2 to CH_3 is limiting and the combination of two single carbon species is most limited by the combination of two CH_3-species. (c) The production of the different lengths hydrocarbons. After C_{10} the production goes below the computational threshold and can be considered to not happen. (d) The reaction orders for FT-syntesis on the cobalt FCC(110). The reaction order of CO goes from -0.32 at 493.15K to -0.33 to 533.15K and the reaction order in hydrogen goes from 0.41 at 493.15K to 0.44 at 533.15K.

In the previous section PED's were constructed from the DFT-data. When combining the PED of the formation of methane, Figure 3.4, and the PED for the formation of ethane, Figure 3.6 into Figure 3.11 it can be seen that the formation of methane would be favourable with regards to the formation of C_{2+}. This would lead to the surface generating relativly large amounts of methane. This however gives rise to the question if the surface is able to generate long hydrocarbons. As can be seen in Figure 3.12d, the production of hydrocarbons of C_3 and longer is low or non-existent. When the PED shown in Figure 3.11 is compared to the work of Dr.ir. I.A.W. Filot [20] where the position of methane higher compared to ethane it can be seen that it is opposite from the situation here. In the case as shown in Figure 3.11 it would be thermodynamical favourable to produce methane.

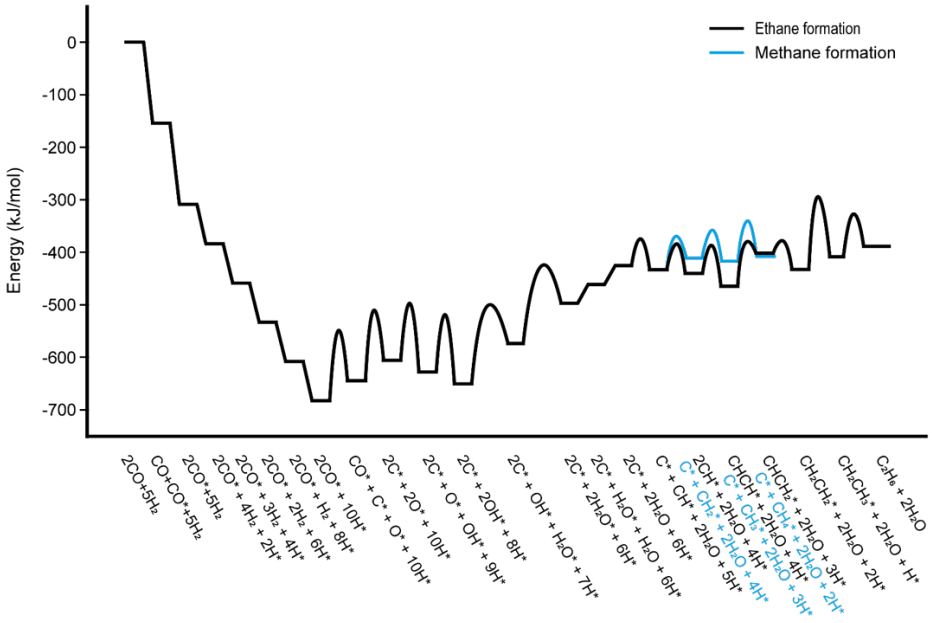

Figure 3.11: The PED for the production of methane (blue) and ethane (black). The production of methane leaves one carbon and two hydrogen atoms on the surface. The Energy level for the production of methane is lower then the energy level of Ethane, this could indicate a surface that would be good for the producion of methane.

3.2.4 Scanning the network

Varying the H_2:CO-ratio

Different H_2/CO-ratios are explored at T=220/240/260°C with P_{total}=1bar. The explored ratios are 1:1, 1.5:1, 2:1, 3:1, 4:1, 5:1 and 10:1. The coverages are given in Figure 3.12. Here is can be seen that the coverage of hydrogen changes slightly with an increasing H_2/CO-ratio. The number of free sites increases slightly with an increase in temperature and with higher ratios. It can be seen in the production plot, Figure 3.12d, that the production does not change significantly in the lower carbon regime (C_1 and C_2). Due to the lower regime staying constant the products with carbon count of three or more are not produced.

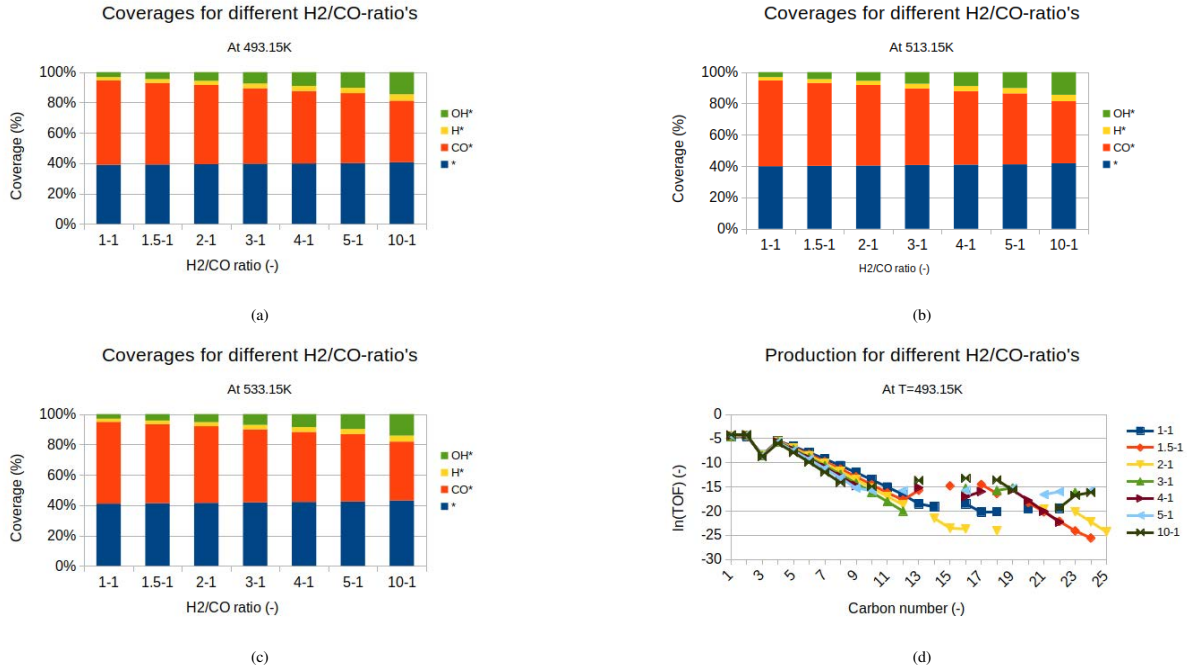

Figure 3.12: The surface coverage of different species on the surface using three different temperatures (a) 220, (b) 240 and (c) 260^{o}C. The tested H_2:CO-ratios for each temperature are 1:1, 3:2, 2:1, 3:1, 4:1, 5:1 and 10:1. It can be seen that the coverage of OH* increased with increasing H_2:CO-ratio. The amount of free sites stays rougly the same. And the CO* coverage decreases with increasing H_2:CO-ratio. (d) The production of different products, after a carbonlength of 12 the production is inconsistent. This is a simulation done at 220^{o}C. The production is slightly higher with increasing H_2:CO-ratio.

Restricting the chaingrowth

Although the FTS is modelled up to C_{25}-species a scan was done restricting the carbon growth from C_4 to C_{24} with increments of 2. This was done at 220, 240 and 260°C. Figures 3.13a, 3.13b and 3.13c show the production of hydrocarbons on the cobalt FCC(110) at 1000mbar, H2:CO-ratio 2:1. All three figures show that there is no significance to letting the model run for longer hydrocarbons as there is no difference in production when comparing the run with a cap at C_4 with a run that is allowed to go up to C_{25}-species. This would suggest that the growth of hydro carbons is very minimal on the cobalt FCC(110) facet.

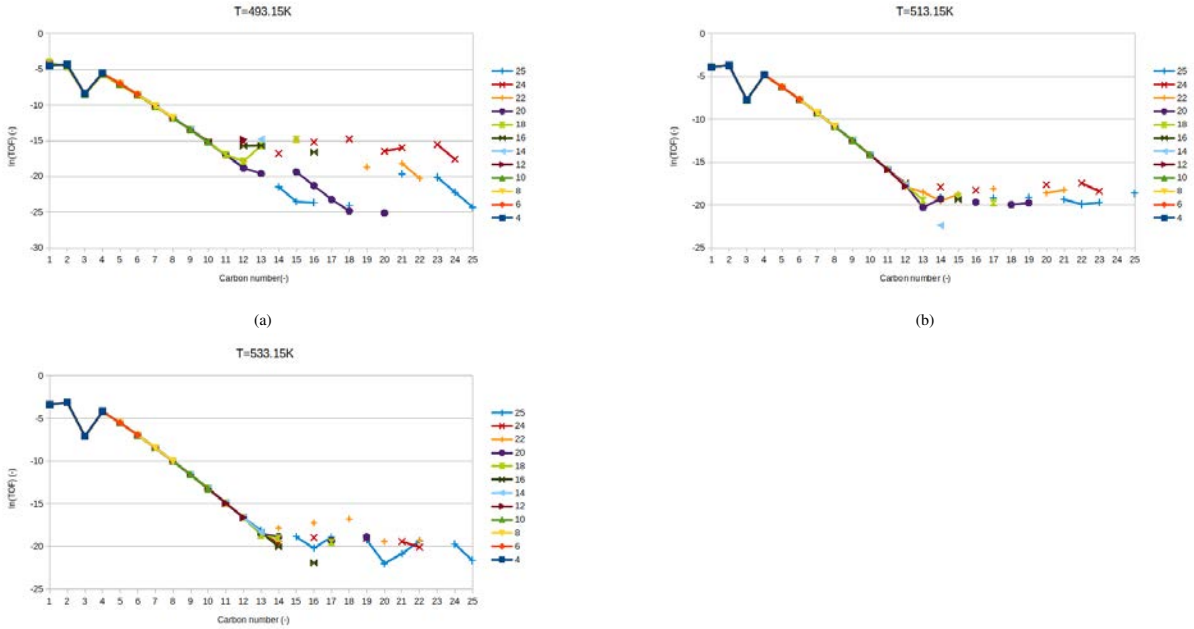

Figure 3.13: Production plots for FTS at T= (a) 220, (b) 240 and (c) 260°C, P=1000mbar and H_2/CO=2. In each of the plots after C_{12} the production is not consistent and can be consirered zero. By increasing the temperature the production goed up slightly, however the cuttoff has no significant effect on the production. This indicates that the production of C_{3+} is difficult on the surface.

Varying the pressure

The simulations are conducted for LTFT temperatures and at a pressure of 1000mbar, industrial FT-processes however operate at a higher pressure of around 20bars. Thus a scan was done checking the influence of the pressure on the microkinetic simulations. This scan was done with and without an inert carrier gas. The runs that were done can be found in Table 3.1. Figure 3.14b shows that the run with a pressure of 10 bar shows a very steep slope, this run showed convergence problems. It can clearly be seen in Figure 3.15c and 3.15d that increasing the pressure by using a carrier gas has no influence on the reaction orders of CO and H_2. However increasing the pressure without the use of a inert gas component present shows a dependency. In Figure 3.15a and 3.15b it can be seen that the reaction order in CO increases with an increase in pressure and the reaction order decreases with an increase in pressure for hydrogen. In Figure 3.16 the consumption of hydrogen and carbon monoxide can be found, here it can be seen that the consumption is non-dependend on the overall pressure of the system and increases with an increasing temperature. From Figure 3.14 it can be seen that the pressure has no influence on the production of longer hydrocarbons. It can also be seen in Figure 3.14b that the run with a pressure of 10 bar shows a very steep slope, this run showed convergence problems.

Table 3.1: The different simulations done with changing pressure. P_{H_2} is the partial pressure in hydrogen, P_{CO} the parial pressure in carbon monoxide and P_{inert} the partial pressure of the carrier gas, all pressures are in mbar. P_{total} is the total pressure in mbar. For every run the H_2/CO-ratio is kept constant at 2:1. The temperatures of the simulation runs per pressure are 220, 240 and 260°C.

P_{total} (bar)	P_{H_2} (mbar)	P_{CO} (mbar)	P_{inert} (mbar)
1	667	333	0
2	667	333	1000
2	1333	667	0
5	667	333	4000
5	3333	1667	0
10	667	333	9000
10	6667	3333	0
20	667	333	19000
20	13333	6667	0

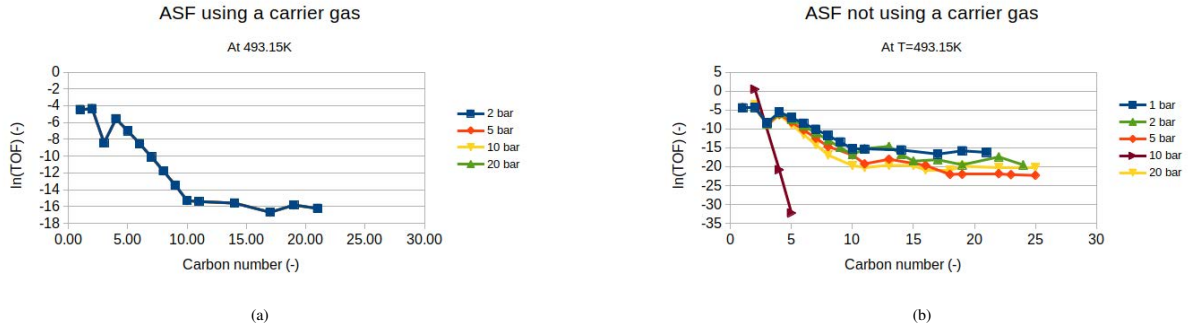

(a) (b)

Figure 3.14: The production of hydrocarbons for different pressures at a temperature of 493.15K. (a) Shows the ASF plot for the runs that have a carrier gas. (b) Shows the ASF plot for the runs without the use of carrier gas.

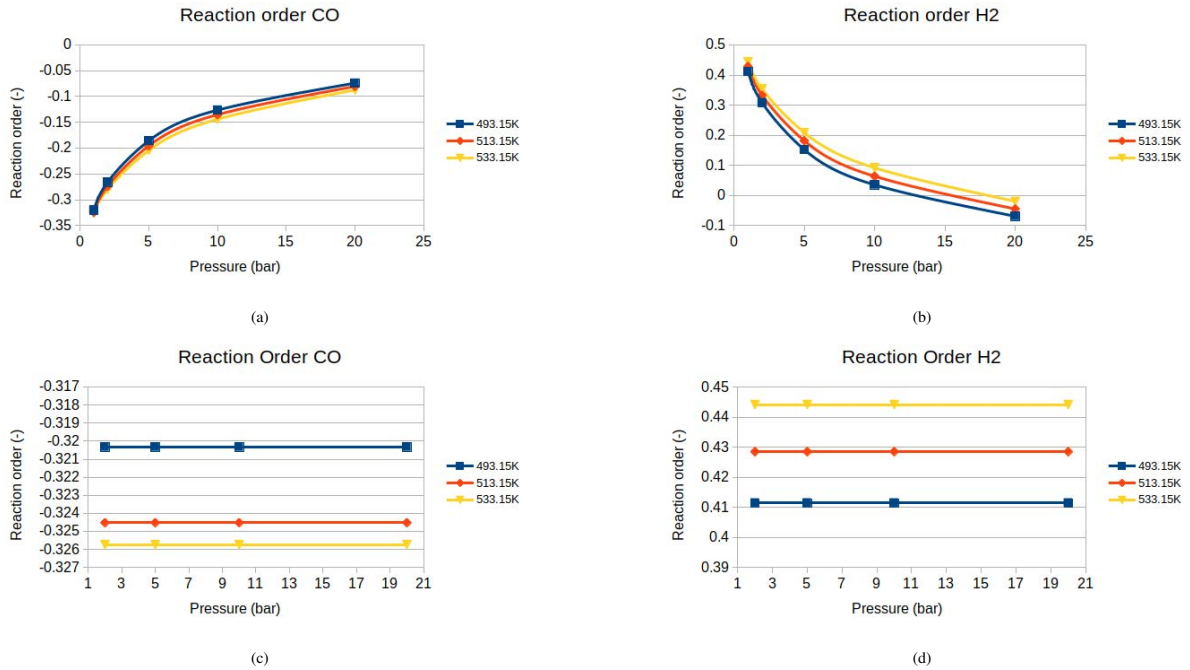

Figure 3.15: The reaction orders in CO and H_2 for the pressures of 1, 2, 5, 10 and 20 bar with simulation temperatures of 220, 240 and 260°C. The H_2/CO-ratio is 2:1. The exact settings for the runs can be found in Table 3.1. Increasing the pressure by adding a carrier gas has no noticable effect on the reaction order. Increasing the pressure by increasing the pressure of CO and H_2 has a noticable effect on the reactionorder as both CO and H_2 go to zero with increasing temperature, in the case for hydrogen it goes slightly below zero and into the negative region. (a) and (b) are without carrier gas. (c) and (d) are with the use of an inert gas component and keeping P_{H_2}=667mbar and P_{CO}=333mbar

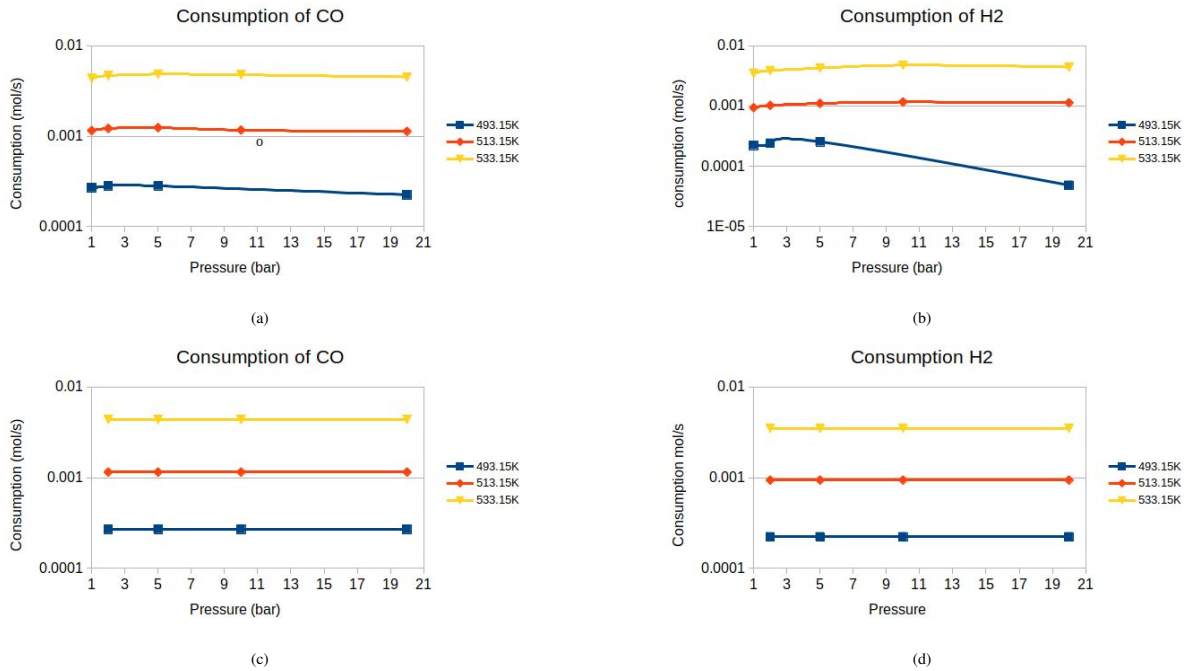

Figure 3.16: The consumption of hydrogen and carbon monoxide under LTFT conditions. P_{total}=1/2/5/10/20bar, T=220/240/260°C. For every run the H_2:CO-ratio is kept to 2:1. For the runs using an inert carrier gas the P_{CO}=333mbar and the P_{H_2}=667mbar, the P_{inert} is set to 1/4/9/19bar. Overall it can be said that the consumption is not dependend on the pressure of the system. The runs of T=493.15K without carrier gas at high pressures (10 and 20 bar) were troublesome. The run of 10bar did not finish on steady state before reaching $t_{max} = 1 \cdot 10^4$s. (a) The consumption of carbon monoxide is not dependend on the pressure and goes up by increasing temperature, no carrier gas used. (b) The consumption of Hydrogen is not dependend on the pressure and goes up by increasing temperature, no carrier gas used. (c) The consumption of carbon monoxide is not dependend on the pressure and goes up by increasing temperature, using a carrier gas. (d) The consumption of H_2 is not dependend on the pressure and goes up by increasing temperature, using a carrier gas.

Increasing the resolution

The initial runs for the microkinetic model were done for 220, 240 and 260°C, LTFT however spans the temperature range 200 to 250°C (473.15 to 523.15K). Therefor runs with smaller temperature increases were done to increase the resolution within the operating temperature range. The runs were done from 200°C up to and including 250°C using 5°C increments. The pressure is set to 1bar and the H_2:CO-ratio is set to 2:1. The results can be found in figure 3.17. Increasing the resolution has no effect on the results, these are in agreement with the three temperature runs shown before.

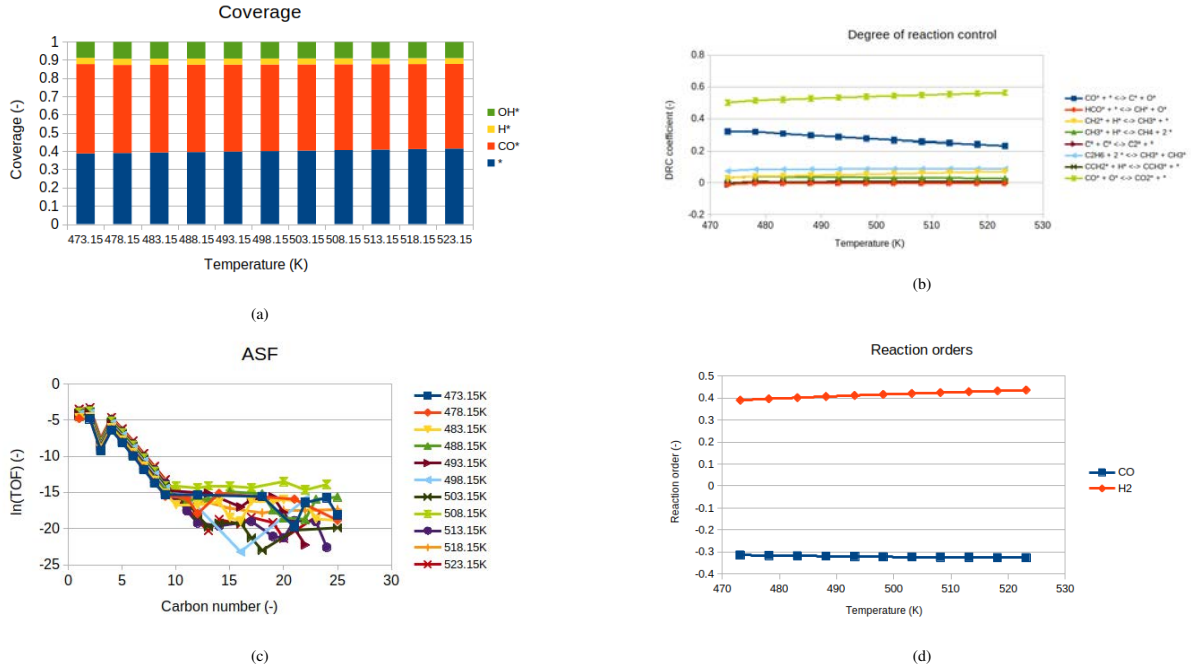

Figure 3.17: A detailed scan of the network in a higher resolution. P=1000mbar, H_2:CO=2:1. Temperature ranges from 473.15 to 523.15K with 5K increments. (a) The coverage of the surface under LTFT-conditions. The higher resolution is congruent with the lower resulution seen in 3.10a. (b) The DRC-coefficient for FTS under LTFT-conditions. The higher resolution shows the trend as in 3.10b. (c) The production of carbon chains under LTFT-conditions. Chains with more than 12 carbons are not being produced. (d) The reaction orders of H_2 and CO under FTS LTFT conditions. The positive reaction order in hydrogen shows that an increase in hydrogen leads to a faster reaction rate. The negative reaction order in CO shows that an decrease in the amount of CO leads to an increase in the overall reaction speed.

Varying the temperature regime

The LTFT is not the only operating regime for FTS however, thus the HTFT is also explored. Figure 3.18 shows the surface coverage, DRC-coefficient, production and reaction orders. From the production (Figure 3.18c) it can be seen that although the production of methane and ethane is higher, production of longer hydrocarbons is still lacking. The surface coverage (Figure 3.18a) in the HTFT regime shows the same trend as in the LTFT-regime. Figure 3.18b shows that less reactions have an influence on the overall reaction rate, with the formation of CO_2 capping at around 60%. The reaction order (Figure 3.18d) in H_2 is higher then for the LTFT and also seems to flatten out, the order in CO is also flattening out at these higher temperatures.

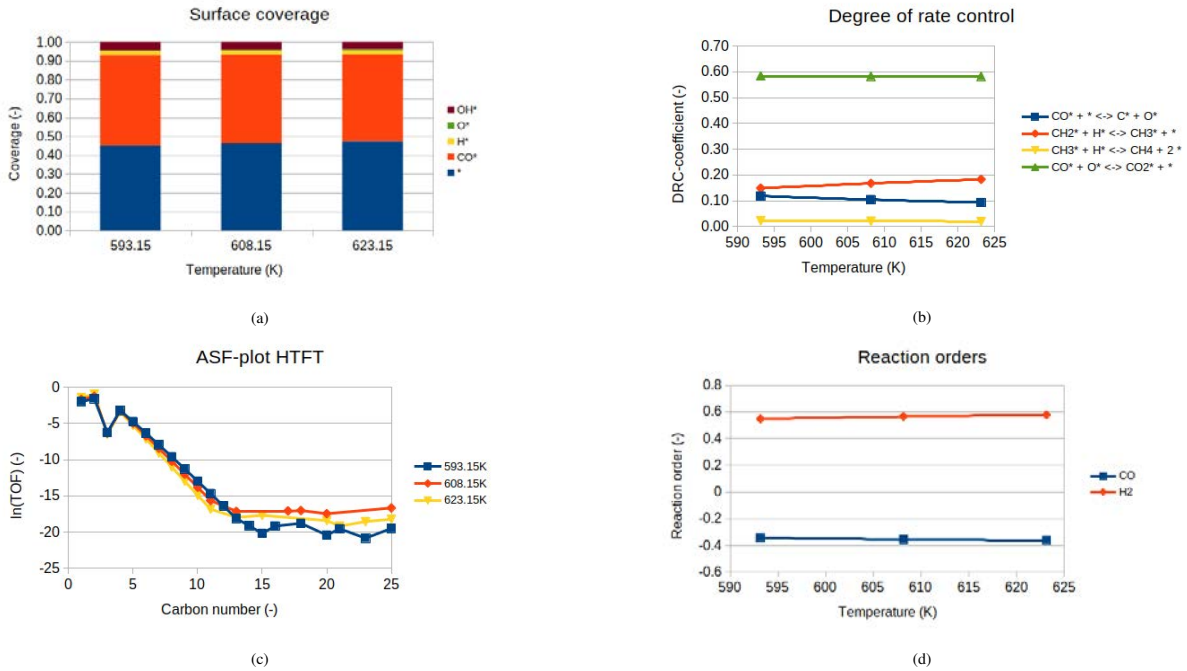

Figure 3.18: Fischer-Tropsch synthesis under HTFT conditions. P_{total}=1000mbar, P_{CO}=333mbar and P_{H_2}=667mbar, T=320/335/350$^{\circ}C$. (a) The surfacce coverage of the surface, on the surface CO*, O* OH* and H* adsorbates are present. (b) The degree of rate control, the formation of carbondioxide via the oxygenation of CO is the rate limiting step (upward triangles). The DRC coefficient fot the dissociations of CO (squares) is around 0.1 for the entire temperature range. The hydrogenation of the single carbon species to CH_3 and CH_4 are of influence on the overall reaction rate. (c) The production of hydrocarbons C_{12+} is inconsistent and can be considered zero. for $C_{2<n<12}$ hydrocarbons the production is very low. (d) The reaction orders in hydrogen and carbon monoxide. The positive order in hydrogen means that the reaction rate will increase with an increase in the partial pressure of hydrogen. The negative reaction order in carbonmonoxide indicates that the reaction rate will increase by decreasing the partial pressure in CO.

3.2.5 The apparent activation energy, selectivity and chaingrowth

The apparent activation energy

The overall apparent activation energy for both the LTFT and HTFT were evaluated. It can be seen in Figure 3.19 that with increasing temperature the apparent activation energy for FTS decreased thus the overall reaction rate will go up with increasing temperature. The range of the apparent activation energy for the LTFT regime is from 153.8 kJ/mol at 220°C to 151.5 kJ/mol at °C. For the HTFT-regime the apparent activation energy starts at 144.9kJ/mol at 32°C and goes down to 143.9kJ/mol at 350°C. This is higher then reported in literature [37] were it is reported that for cobalt Fischer-Tropsch the apparent activation enegy is 93 kJ/mol at 220°C. This could mean that the cobalt FCC(110) is not the dominant surface during FTS under reaction conditions.

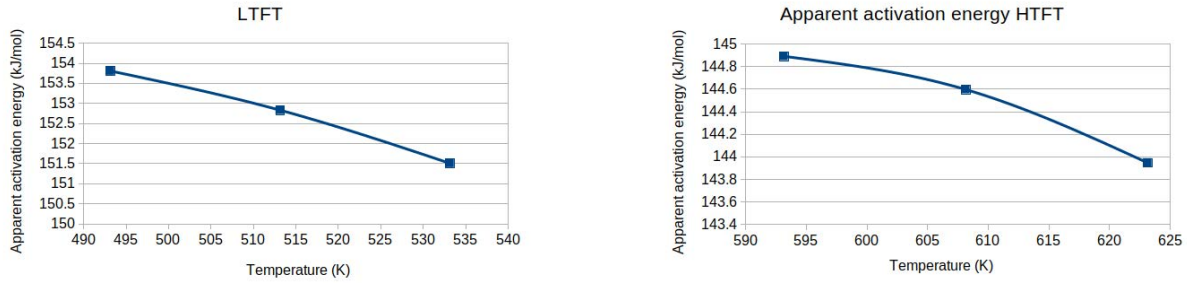

(a) (b)

Figure 3.19: The apparent activation enegry for FTS under LTFT conditions and HTFT conditions. (a) T=220/240/260°C, P=1000mbar and H_2:CO=2:1, (b) T=320/335/350°C, P=1000mbar and H_2:CO=2:1. With increasing the temperature the apparent activation energy goes down. However even in the HTFT-range the ΔE_{act}^{app} is still larger then the CO-dissociation barrier.

The selectivity

The selectivity was calculated using MKMCXX. The results for both LTFT and HTFT can be found in Figure 3.20. Here it can be seen that in the LTFT regime (Figure 3.20a) the selectivity towards CO_2 is about 50% and in the HTFT regime (Figure 3.20b) the selectivity towards carbondioxide is even around 60%. The selectivity towards methane in the HTFT regime is about 8% and in the LTFT regime 10-12%. While the cobalt FCC(110) facet shows a large selectivity for CO_2, it is not the main product observed during FTS where a selectivity of 7.8% are observed at 220°C[22].

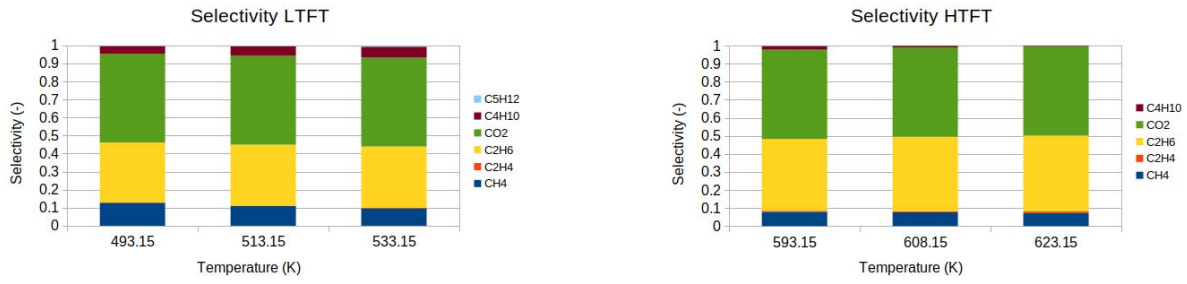

(a) (b)

Figure 3.20: The selectivity for FTS under LTFT and HTFT conditions. (a) T=220/240/260°C, P=1000mbar and H_2:CO=2:1, (b) T=320/335/350°C, P=1000mbar and H_2:CO=2:1. The selectivity is determined on the bases of the carbon balance.

The chaingrowth parameter

From the ASF plots (Figure 3.10c and Figure 3.18c) the chain growth parameter (α) can be determined. Figure 3.21 shows the chaingrowth parameter and the asf-plot for both the LTFT and HTFT range. The chaingrowth parameter was determined from C_5 to C_{10}. For the LTFT-regime the chaingrowth parameter is increasing and for the HTFT the chaingrowth parameter is decreasing. This could suggest an optimum inbetween the two regimes. Compared to the PhD-thesis of dr.ir. B. Zijlstra, α around 0.6 at 220°C, the found growth parameters for the cobalt FCC(110) are very low compared to an α of 0.023 for the FCC(110) facet at 220°C.

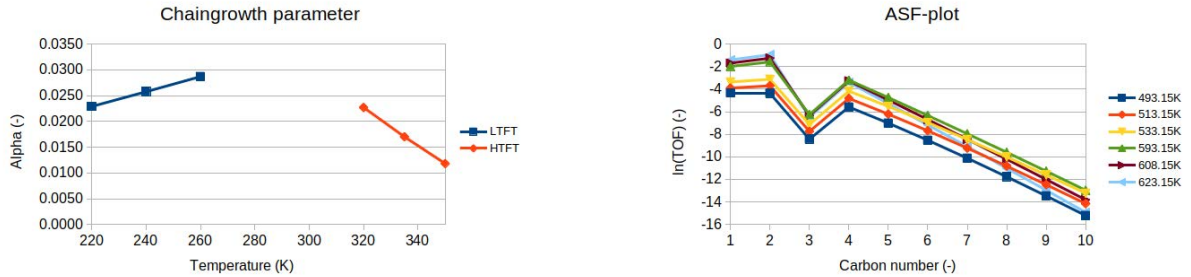

(a) (b)

Figure 3.21: (a) The chaingrowth parameter for both the LTFT regime (squares) and the HTFT regime (diamonds). The chaingrowth parameter was determined from C_5 tot C_{10}. (b) The ASF-plot for both LTFT and HTFT. Although the production of hydrocarbons is lower in the LTFT regime the maximum α was found at the upper limit of the LTFT.

4 Conclusions

The aim of this study was to bring insight into the elementary reaction steps involved in the FT-process on the cobalt FCC(110)-facet using a microkinetic model. Two main questions were asked at the beginning of this thesis: (1) what are the barriers & pre-exponential factors for each of the elementary reactions in the Fischer-Tropsch Synthesis, (2) what are the activities and selectivities for cobalt based Fischer-Tropsch on the FCC(110) surface and (3) what is the influence of reaction conditions on the Fischer-Tropsch Synthesis on the cobalt FCC(110) facet. To answer the first question DFT-calculations were done on the Co FCC(110)-surface for the formation of methane, ethylene and ethane. For the second question: (1) a microkinetic model was build for the microkinetic description of the formation of methane and ethane, (2) the lateral interactions on the surface will be added and (3) the extrapolation of the network to describe FT-synthesis up to C_{25} olefins and parafins. To answer the last question the operation conditions such as the reactant ratio, the pressure and the temperature were varied.

From the DTF data it can be seen that the last hydrogenation step of the single carbon atom has a similar energy barrier to the rest of the hydrogenation steps. It was also shown that the formation of ethane via the CH_3-intermediate would be fairly simple using a step reaction to form C_2H_6 due to the low barrier of that elementary reaction step.

In the microkintic model the lack of lateral interactions made it such that the surface was filled with CO. This result is in contradiction with experimental data thus underlining the need for lateral interactions. Adding the lateral interactions showed coverages that are more in agreement with experimental data. The extrapolation of the microkinetic model to include the production of long hydrocarbons shows that on the cobalt FCC(110) no long hydrocarbons, C_{12+}, are being produced under reaction conditions. The cobalt FCC(110) surface shows relatively high activity for the dissociation of carbon monoxide. However, it is highly unlikely that this A_5-site is the predominant active site during Fischer-Tropsch synthesis. The cobalt surface also shows activity for the production of methane and ethane. In comparison to the work of Zijlstra[23] on the cobalt HCP($11\bar{2}1$), the activity of the FCC(110) facet is very low.

In order to answer the last question the following influences were investigated on the overall consumption of CO and the formation of hydrocarbon chains: (1) The influence of the H_2:CO-ratio by changing it from 1:1 to 10:1, (2) The influence of the pressure by increasing it from 1 bar to 20 bar both with and without the use of an inert carrier gas and (3) The influence of temperature by investigating the HTFT-regime. Changing the H_2:CO-ratio did not change the chain growth by much and the effect on the surface coverage is minimal. Increasing the pressure by using an inert carrier gas did nothing to the overall reaction. However, when increasing the pressure without the use of an inert carrier gas the dependence of the reaction order is significant. The consumption of the reactants H_2 and CO do not seem to change with the increase in pressure.

Lastly the apparent activation energy, selevtivity and chaingrowth-parameter were investigated in both the LTFT and HTFT regime with P_{total}=1000mbar and H_2:CO=2:1.The apparent activation energy shows a declining trend with an increasing temperature. The selectivity in the LTFT regime is about 50% CO_2, in the HTFT regime the is even higher at around 60%. This CO_2 selectivity is not observed in expriments where the selectivity is reported to be around 7.8% at 220°C with H_2:CO = 2:1 [22].

5 Outlook

Although the HCP($11\bar{2}1$), HCP(0001) described by Zijlstra[23] and FCC(110) are good starting points for different site types to describe the activity of a nano particle with, a cobalt nano particle has more than these two facets, if at all present, at a certain particle size. Thus the description of more different facets is needed. The microkinetic description of a nanoparticle would than imply that the full Fischer-Tropsch Synthesis should be modelled on all facets using DFT, like done in this work for the FCC(110).

However it would be computational and economically expensive and thus the unfavorable option. Work done by Abild-Pedersen et al.[38] shows that different adsorbates can be modelled on the same facet on different metals by using a Brönsted-Evans-Polanyi relation. Perhaps, such a feature can also be achieved on different facets using the same transition metal. Although in the work by Abild-Pedersen et al. there is a linear correlation, in this case there might be a quadratic relation, because changing the facet changes the potiental energy surface. The method of using a Brönsted-Evans-Polanyi relation could lead to fast scanning of facets for activity of desired reactions.

Another approach is to make use of neural networks and deep learing techniques in order to simulate the behaviour of the different facets of the cobalt nanoparticles. Neural networks, when used correctly, can give fast and accurate results. However the big drawback of neural networks is the necessity to train them, possibly taking a lot of time and effort itself. The modelling of all facets using DFT would take more time than the training and using of neural networks and the use of neural networks would provide an improvement in the time investment.

It can be speculated that the cobalt FCC(110) can supply other facets with the monomers needed to obtain adequate long chain growth, although this was not the focus of this study. This mechanism would imply that the single carbon species diffuse to other facets, where carbon-carbon coupling reactions are relatively easy compared to the FCC (110) facet. This would lead to two or more different facets brought together in a model and is shown in the work by Zijlstra[23]. However the diffusion and migration on the surface cannot be moddeled to a precise degree due to one of the underlying assumptions of microkinetic models, namely the mean field approximation. The approximation states that one species on the surface can interact with any other species on the surface independend of their repective locations. Consequently, moddeling of migration of species on surfaces should take a different route, for instance kinetic Monte Carlo simulations.

6 Acknowledgements

At this point only one thing remains: to thank everybody for their incredible support and I would like to show my gratitude. I would like to start with Emiel Hensen for the opportunity to do my master project here at IMC. I would like to thank Ivo Filot for the guidence and wisdom troughout the project. I would also like to thank Ivo Roghair for your time and effort in participating in my graduation committee. Of course I would like to thank Michel van Etten for the supervision, it has been a great experience to have you as my daily supervisor. I cannot imagine a someone better suited for the job, I can only say "*douze points pour Michel!*'".

I also would like to thank my office buddies: Anouk, Tim, Michelle, Koen, Jasper & Roos. It was awesome to share an office with you guys (and girls ofcourse!). The spontaneous discussions that would sometimes erupt in the most diverse of subjects were great fun. I liked the hike during my lunchbreak very much with you Roos and always looked forward to it. Jasper you have amazing stories of what you and your friends are always up to. Koen when you were building the Raspberry Pi cluster I was most facinated by it and our discussions on computer related stuff were always interesting. Michelle you are a source of pure positive energy in the office and were always down to go to the F.O.R.T. on thursdays at 4pm. Tim your general knowledge amazed me and your ability to connect to seemingly untied subjects using wikipedia is in my eyes of legendary proportions. Anouk you are always ready to help everybody and you're always ready to make another case.

A large thank you goes to Bart Zijlstra, you have helped me immensely during my graduation project. The testament to that is the amount of times your name comes up in this thesis. You have explained the possibilities of MKMCXX to me and showed me how everything works. It was a pleasure to see you receive the title of doctor and you have most definitly earned it in my eyes. I can ofcourse not forget to mention Robin and Bart jr. you guys have helped me from time to time and I am grateful that you guys have taken the time to do so.

I also would like to thank my parents for the support you have shown during my time as a student here at the TU/e. You have given me the motivation I needed to get through my bachelor and master. You have tried to make me the best version of myself, and I will do everything I can to make you proud.

Lastly I would like to thank Mayra, you are my best buddy and I know that you'll have my back at all times. I can honestly say that I could absolutely not have done it without you by my side. Rakastan sinua koko sydämestäni ja haluan jakaa elämäni kanssasi.

Bibliography

[1] Akram Tavakoli, Morteza Sohrabi, and Ali Kargari. "Application of Anderson-Schulz-Flory (ASF) equation in the product distribution of slurry phase FT synthesis with nanosized iron catalysts". In: *Chemical Engineering Journal* 136.2-3 (2008), pp. 358–363. ISSN: 13858947. DOI: 10.1016/j.cej.2007.04.017.

[2] B. Kamm. "Production of platform chemicals and synthesis gas from biomass". In: *Angewandte Chemie - International Edition* 46.27 (2007), pp. 5056–5058. ISSN: 14337851. DOI: 10.1002/anie.200604514.

[3] Alireza Asiaee and Kenneth M. Benjamin. "A density functional theory based elementary reaction mechanism for early steps of Fischer-Tropsch synthesis over cobalt catalyst. 2. Microkinetic modeling of liquid-phase vs. gaseous-phase process". In: *Molecular Catalysis* 436 (2017), pp. 210–217. ISSN: 24688231. DOI: 10.1016/j.mcat.2017.04.006. URL: http://dx.doi.org/10.1016/j.mcat.2017.04.006.

[4] Vasileios Rizos, Katja Tuokko, and Arno Behrens. *The Circular Economy - A review of definitions. processes, and impacts*. 2017/08. 2017, pp. 1 –36. ISBN: 9789461385970.

[5] Andrei Y. Khodakov, Wei Chu, and Pascal Fongarland. "Advances in the development of novel cobalt Fischer-Tropsch catalysts for synthesis of long-chain hydrocarbons and clean fuels". In: *Chemical Reviews* 107.5 (2007), pp. 1692–1744. ISSN: 00092665. DOI: 10.1021/cr050972v.

[6] Jin Xun Liu et al. "Crystallographic dependence of CO activation on cobalt catalysts: HCP versus FCC". In: *Journal of the American Chemical Society* 135.44 (2013), pp. 16284–16287. ISSN: 00027863. DOI: 10.1021/ja408521w.

[7] R. A. Van Santen et al. "Mechanism and microkinetics of the Fischer-Tropsch reaction". In: *Physical Chemistry Chemical Physics* 15.40 (2013), pp. 17038–17063. ISSN: 14639076. DOI: 10.1039/c3cp52506f.

[8] Wei Chen et al. "Mechanism of Cobalt-Catalyzed CO Hydrogenation: 2. Fischer-Tropsch Synthesis". In: *ACS Catalysis* 7.12 (2017), pp. 8061–8071. ISSN: 21555435. DOI: 10.1021/acscatal.7b02758.

[9] Wei Chen et al. "Mechanism of Carbon Monoxide Dissociation on a Cobalt Fischer–Tropsch Catalyst". In: *ChemCatChem* 10.1 (2018), pp. 136–140. ISSN: 18673899. DOI: 10.1002/cctc.201701203.

[10] G. Leendert Bezemer et al. "Cobalt particle size effects in the Fischer-Tropsch reaction studied with carbon nanofiber supported catalysts". In: *Journal of the American Chemical Society* 128.12 (2006), pp. 3956–3964. ISSN: 00027863. DOI: 10.1021/ja058282w.

[11] Rutger A van Santen. "Insensitive Catalytic Relationships". In: *Accounts of Chemical Research* 42.1 (2009).

[12] Jin Xun Liu et al. "Particle Size and Crystal Phase Effects in Fischer-Tropsch Catalysts". In: *Engineering* 3.4 (2017), pp. 467–476. ISSN: 20958099. DOI: 10.1016/J.ENG.2017.04.012. URL: http://dx.doi.org/10.1016/J.ENG.2017.04.012.

[13] Bart Zijlstra et al. "Coverage effects in CO dissociation on Metallic Cobalt Nanoparticles". In: *ACS Catalysis* 9 (2019), acscatal.9b01967. ISSN: 2155-5435. DOI: 10.1021/acscatal.9b01967. URL: http://pubs.acs.org/doi/10.1021/acscatal.9b01967.

[14] Ravi Agrawal, Prasad Phatak, and Leonardo Spanu. "Effect of phase and size on surface sites in cobalt nanoparticles". In: *Catalysis Today* 312.March (2018), pp. 174–180. ISSN: 09205861. DOI: 10.1016/j.cattod.2018.03.064. URL: https://doi.org/10.1016/j.cattod.2018.03.064.

[15] Georgios D. Barmparis et al. “Nanoparticle shapes by using Wulff constructions and first-principles calculations”. In: *Beilstein Journal of Nanotechnology* 6.1 (2015), pp. 361–368. ISSN: 21904286. DOI: 10.3762/bjnano.6.35.

[16] Lennart Joos et al. “Reactivity of CO on carbon-covered cobalt surfaces in fischer-tropsch synthesis”. In: *Journal of Physical Chemistry C* 118.10 (2014), pp. 5317–5321. ISSN: 19327455. DOI: 10.1021/jp4109706.

[17] Chuan Qin et al. “Crystal-Plane-Dependent Fischer-Tropsch Performance of Cobalt Catalysts”. In: *ACS Catalysis* 8.10 (2018), pp. 9447–9455. ISSN: 21555435. DOI: 10.1021/acscatal.8b01333.

[18] Jens K. Nørskov et al. “The nature of the active site in heterogeneous metal catalysis”. In: *Chemical Society Reviews* 37.10 (2008), pp. 2163–2171. ISSN: 03060012. DOI: 10.1039/b800260f.

[19] J. Matthiesen et al. “The Brønsted–Evans–Polanyi relation and the volcano curve in heterogeneous catalysis”. In: *Journal of Catalysis* 224.1 (2004), pp. 206–217. ISSN: 00219517. DOI: 10.1016/j.jcat.2004.02.034.

[20] Ivo A.W. Filot. “Quantum Chemical and Microkinetic Modeling of the Fischer-Tropsch Reaction”. PhD thesis. Technische Universiteit, 2015, pp. 28–36. ISBN: 978-90-386-3793-8. URL: https://www.ivofilot.nl/thesis.

[21] Wei Chen et al. “Mechanism of Cobalt-Catalyzed CO Hydrogenation: 1. Methanation”. In: *ACS Catalysis* 7.12 (2017), pp. 8050–8060. ISSN: 21555435. DOI: 10.1021/acscatal.7b02757.

[22] Wei Chen. *A Transient Kinetics Study of Fischer-Tropsch Synthesis Mechanism on Cobalt Catalysts*. 2017. 2017, p. 159. ISBN: 978-90-386-4394-6.

[23] Bart Zijlstra. “Microkinetic modeling of Fischer-Tropsch synthesis on cobalt”. English. Proefschrift. PhD thesis. Department of Chemical Engineering and Chemistry, Jan. 2020. ISBN: 978-90-386-4956-6.

[24] Mark E. Dry. “The fischer–tropsch process: 1950–2000”. In: *Catalysis Today* 71 (2002), pp. 227–241. DOI: https://doi.org/10.1016/S0920-5861(01)00453-9. URL: https://www.sciencedirect.com/science/article/pii/S0920586101004539.

[25] Joseph W Pratt. “A Fischer-Tropsch Synthesis Reactor Model Framework for Liquid Biofuels Production”. In: *Sandia Report* September (2012).

[26] B Jager and R Espinoza. “Advances in low temperature Fischer-Tropsch synthesis”. In: *Catalysis Today* 23 (1995), pp. 17–28.

[27] Mark E. Dry. “The fischer-tropsch process - commercial aspects”. In: *Catalysis Today* 6.3 (1990), pp. 183–206. ISSN: 09205861. DOI: 10.1016/0920-5861(90)85002-6.

[28] Sio-iong Ao Haeng and Kon Kim. *Transactions on Engineering Technologies*. 2015. ISBN: 978-981-10-7487-5. DOI: 10.1007/978-981-10-7488-2. URL: http://link.springer.com/10.1007/978-981-10-7488-2.

[29] Craig P. Plaisance, Rutger A. Van Santen, and Karsten Reuter. “Constrained-Orbital Density Functional Theory. Computational Method and Applications to Surface Chemical Processes”. In: *Journal of Chemical Theory and Computation* 13.8 (2017), pp. 3561–3574. ISSN: 15499626. DOI: 10.1021/acs.jctc.7b00362.

[30] Benjamin Kaduk, Tim Kowalczyk, and Troy Van Voorhis. “Constrained density functional theory”. In: *Chemical Reviews* 112.1 (2012), pp. 321–370. ISSN: 00092665. DOI: 10.1021/cr200148b.

[31] Universitat Wien. *VASP wiki*. 2019. URL: https://cms.mpi.univie.ac.at/wiki/index.php (visited on 07/22/2019).

[32] Joachim Paier et al. “The Perdew-Burke-Ernzerhof exchange-correlation functional applied to the G2-1 test set using a plane-wave basis set”. In: *Journal of Chemical Physics* 122.23 (2005), pp. 1–13. ISSN: 00219606. DOI: 10.1063/1.1926272.

[33] P.E. Blochl. “Projector augmented-wave method”. In: *Physical Review B* 50.24 (1994), pp. 17953–17979. DOI: 10.1142/9789814365031_0023.

[34] Ivo A.W. Filot. *Introduction to Microkinetic Modeling*. 1.5.0. Eindhoven: TU/e, 2018. ISBN: 978-90-386-3793-8.

[35] NIST. *NIST chemistry webbook*. 2018. URL: https://webbook.nist.gov/chemistry/ (visited on 08/28/2019).

[36] Wilson D. Shafer et al. “Fischer-tropsch: Product selectivity-the fingerprint of synthetic fuels”. In: *Catalysts* 9.3 (2019). ISSN: 20734344. DOI: 10.3390/catal9030259.

[37] Ian C. Yates and Charles N. Satterfield. “Intrinsic Kinetics of the Fischer-Tropsch Synthesis on a Cobalt Catalyst”. In: *Energy and Fuels* 5.1 (1991), pp. 168–173. ISSN: 15205029. DOI: 10.1021/ef00025a029.

[38] F. Abild-Pedersen et al. “Scaling properties of adsorption energies for hydrogen-containing molecules on transition-metal surfaces”. In: *Physical Review Letters* 99.1 (2007), pp. 4–7. ISSN: 00319007. DOI: 10.1103/PhysRevLett.99.016105.

A Nomenclature

Table A.1: Abbriviations

Abbriviation	Full text
FT(S)	Fischer-Tropsch (Synthesis)
GtL	Gas-to-Liquid
CtL	Coal-to-Liquid
BtL	Biomass-to-Liquid
WGS	Water Gas Shift
FCC	Face Centred Cubic
HCP	Hexagonal Closed Packing
ASF	Anderson-Schulz-Flory
LTFT	Low Temperature Fischer-Tropsch
HTFT	High Temperature Fischer-Tropsch
IS	Initial State
FS	Final State
TS	Transition State
VASP	Vienna ab initio Simulation Package[31]
GGA	Generalized Gradient Approximation
DFT	Density Functional Theory
PBE	Perdew-Burke-Ernzerhof
PAW	Potential Projector Augmented-Wave
NEB/cNEB	climbing Nudged Elastic Band
NEB8	NEB with 8 images
NEB3	NEB with 3 images
PED	Potential Energy Diagram
MFA	Mean-Field approximation
AAE	Apperent Activation Energy
DRC	Degree of Rate Control
DSC	Degree of Selectivity Control
HK	Hertz-Knudsen
LH	Langmuir-Hinselwood
BEP	Brønsted-Evans-Polanyi
NIST	National Institute of Standards and Technology

Table A.2: File names and their explanations.

Name	Description
INCAR	A VASP file that contains the settings for the calculation
POSCAR	A VASP input file that contains the positions of the atoms for a calculation
CONTCAR	A VASP output file that contain the positions of the atoms after the calculation is finished, can be used for further calculations.
OUTCAR	A VASP output file that contains all information on the system such as: atom locations, total energy of the system and depending on the type of calculation also the frequencies of the adsorbates.

Table A.3: Physical quantities, their units and a short description.

Symbol	Units	Description
Q	[-]	Vibrational partition function
h	$J \cdot s$	Plancks-constant
ω	$J \cdot s^{-1}$	Frequency
k_b	$m^2 \cdot kg \cdot s^{-2} \cdot K^{-1}$	Boltzmann constant
T	K	Temperature
ΔE_{act}	$J \cdot mol^{-1}$	Activation energy barrier
R	$J \cdot mol^{-1} \cdot K^{-1}$	Gas constant
k	Dependent on reaction order	reaction rate constant
K	[-]	Equilibrium constant
ν_i	[-]	Stochimetric factor for component i
[i]	$mol \cdot L^{-1}$	concentration in component i
r_i	$mol \cdot L^{-1} \cdot s^{-1}$	reaction rate in component i
Θ_i	[-]	fractional coverage of component i
ϵ_{state}	$kJ \cdot mol^{-1}$	The calculated energy of a state, without ZPE correction
$\epsilon_{state,zpe}$	$kJ \cdot mol^{-1}$	The ZPE correction for a state
E_{state}	$kJ \cdot mol^{-1}$	The calculated energy of a state, with ZPE correction
V	m^3	Volume
N	mol	Amount of reactive sites
P	$N \cdot m^2$	Pressure
p_i	$N \cdot m^2$	Partial pressure of comopnent i
$C_{p,i}$	$J \cdot mol^{-1} \cdot K^{-1}$	Specific heat of component i
$H_{T,i}$	$kJ \cdot mol^{-1}$	Specific Enthalpy for component i
$S_{T,i}$	$J \cdot mol^{-1} \cdot K^{-1}$	Specific entropy for component i
A to G	$J \cdot mol^{-1} \cdot K^{-1}$	experimental shomate parameters
T_x	K	$\frac{T}{1000}$
χi	[-]	DRC coëfficient for reaction i
$\epsilon_{i,c}$	[-]	DSC coëfficient for reaction i component c
η_c	[-]	Selectivity towards component c
$\Delta_f H^0$	$kJ \cdot mol^{-1})$	Formation enthalpy at 298.15K
ΔH_r	$kJ \cdot mol^{-1}$	Reaction enthalpy
$\Delta(\Delta H_r)$	$kJ \cdot mol^{-1}$	The change in reaction enthalpy

B INCAR settings per calculation

Table B.1: INCAR settings for the first calculations pass done on the initial state and final state.

Setting	Value
LREAL	Auto
LCHARG	.TRUE.
LWAVE	.TRUE.
PREC	Normal
ADDGRID	.FALSE.
ENCUT	300
ISMEAR	1
SIGMA	0.2
EDIFF	$1 \cdot 10^{-4}$
EDIFFG	$1 \cdot 10^{-3}$
NSW	10
ISIF	2
IBRION	2
ISPIN	2
POTIM	0.1
ALGO	FAST
NELMIN	2
NELM	100
ISTART	1
MAGMOM	$106 \cdot 3$
NCORE	8
KPAR	1

Table B.2: Changes to the INCAR for the second run for an initial or final state. The changes are with respect to the first run

Setting	Old value	New value
POTIM	0.1	1.0
NSW	10	120
ALGO	FAST	VeryFast
EDIFF	$1 \cdot 10^{-4}$	$1 \cdot 10^{-5}$
EDIFFG	$1 \cdot 10^{-3}$	$1 \cdot 10^{-4}$

Table B.3: Changes to the INCAR for the thrid run for an initial or final state. The changes are with respect to the second run

Setting	old value	new value
ENCUT	300	400
POTIM	1.0	0.5
NSW	120	100
ALGO	VeryFast	Normal
ISTART	1	0

Table B.4: Changes to the INCAR for the fourth and final run for an initial or final state. The changes are with respect to the third run

Setting	old value	new value
NSW	100	40
LREAL	Auto	.False.
PREC	Normal	Accurate
ISTART	0	1

Table B.5: Setting for a frequency analysis for the inital and final state to retrieve the Zero-Point-Energy Correction and the vibritional partition function at 500K

Setting	Value
LREAL	.FALSE.
LCHARG	.TRUE.
LWAVE	.TRUE.
PREC	Normal
ADDGRID	.FALSE.
ENCUT	400
ISMEAR	1
SIGMA	0.2
EDIFF	$1 \cdot 10^{-5}$
EDIFFG	$1 \cdot 10^{-4}$
NSW	100
ISIF	2
IBRION	5
ISPIN	2
POTIM	0.02
ALGO	NORMAL
NELMIN	4
NELM	300
ISYM	0
MAGMOM	$106 \cdot 3$
NCORE	8
KPAR	1
IDIPOL	1
DIPOL	0.5 0.5 0.5
LDIPOL	.FALSE.

Table B.6: The INCAR setting for the first run of a Nudged Elastic Band calculation with 8 images.

Setting	Value
LREAL	.FALSE.
LCHARG	.TRUE.
LWAVE	.TRUE.
PREC	Single
ADDGRID	.FALSE.
ENCUT	300
ISMEAR	1
SIGMA	0.2
EDIFF	$1 \cdot 10^{-4}$
EDIFFG	$1 \cdot 10^{-3}$
NSW	10
ISIF	2
IBRION	1
ISPIN	2
POTIM	0.05
ALGO	Fast
NELMIN	6
NELM	40
ISTART	1
MAGMOM	$120 \cdot 3$
NCORE	6
KPAR	1
IMAGES	8

Table B.7: The changes to the settings for the second run of the Nudged Elastic Band calculation with 8 images. The changes are with respect to the first run

Setting	Old value	New Value
POTIM	0.05	0.2
NSW	10	20
ALGO	Fast	VeryFast

Table B.8: The changes to the settings for the third and final run of the Nudged Elastic Band calculation with 8 images. The changes are with respect to the second run

Setting	Old value	New Value
ALGO	VeryFast	Normal
PREC	Single	Normal
ENCUT	300	350
EDIFF	$1 \cdot 10^{-4}$	$1 \cdot 10^{-5}$
EDIFFG	$1 \cdot 10^{-3}$	$1 \cdot 10^{-4}$
ISTART	1	0

Table B.9: The INCAR setting for a Nudged Elastic Band calculation with 3 images.

Setting	Value
LREAL	Auto
LCHARG	.TRUE.
LWAVE	.TRUE.
PREC	Single
ADDGRID	.FALSE.
ENCUT	300
ISMEAR	1
SIGMA	0.2
EDIFF	$1 \cdot 10^{-4}$
EDIFFG	$1 \cdot 10^{-3}$
NSW	10
ISIF	2
IBRION	1
ISPIN	2
POTIM	0.05
ALGO	Fast
NELMIN	6
NELM	40
ISTART	1
MAGMOM	$106 \cdot 3$
NCORE	8
KPAR	1
IMAGES	3

Table B.10: The changes to the settings for the second run of the Nudged Elastic Band calculation with 3 images. The changes are with respect to the first run.

Setting	Old value	New Value
POTIM	0.05	0.2
NSW	10	20
ALGO	Fast	VeryFast

Table B.11: The changes to the settings for the third and final run of the Nudged Elastic Band calculation with 3 images. The changes are with respect to the second run.

Setting	Old value	New Value
ALGO	VeryFast	Normal
LREAL	Auto	.FALSE.
PREC	Single	Normal
ENCUT	300	350
EDIFF	$1 \cdot 10^{-4}$	$1 \cdot 10^{-5}$
EDIFFG	$1 \cdot 10^{-3}$	$1 \cdot 10^{-4}$
ISTART 1	0	

Table B.12: The INCAR setting for the first run of a Transition State geometry optimization.

Setting	Value
LREAL	.FALSE.
LCHARG	.TRUE.
LWAVE	.TRUE.
PREC	Normal
ADDGRID	.FALSE.
ENCUT	400
ISMEAR	1
SIGMA	0.2
EDIFF	$1 \cdot 10^{-5}$
EDIFFG	$1 \cdot 10^{-4}$
NSW	100
ISIF	2
IBRION	1
ISPIN	2
POTIM	0.05
ALGO	Normal
NELMIN	4
NELM	100
NCORE	8
MAGMOM	$106 \cdot 3$

Table B.13: The INCAR setting for the second run of a Transition State geometry optimization. The changes are with respect to the first run

Setting	Old value	New Value
POTIM	0.05	0.1
NSW	100	80
PREC	Normal	Accurate
ADDGRID	.FALSE.	.TRUE.

Table B.14: The INCAR setting for a frequency analysis on the Transition State geomerty optimization.

Setting	Value
LREAL	.FALSE.
LCHARG	.TRUE.
LWAVE	.TRUE.
PREC	Normal
ADDGRID	.FALSE.
ENCUT	400
ISMEAR	1
SIGMA	0.2
EDIFF	$1 \cdot 10^{-5}$
EDIFFG	$1 \cdot 10^{-4}$
NSW	100
ISIF	2
IBRION	5
ISPIN	2
POTIM	0.02
ALGO	Normal
NELMIN	4
NELM	100
ISYM	0
MAGMOM	$106 \cdot 3$
NCORE	8
KPAR	1
IDIPOL	3
DIPOL	0.5 0.5 0.5
LDIPOL	.FALSE.

Table B.15: The settings that are added for a single sided calculation

	Setting	Value
[]	IDIPOL	3
	DIPOL	0.5 0.5 0.5

C Elementary Reaction steps on Co(110)

C.1 CO Dissociation

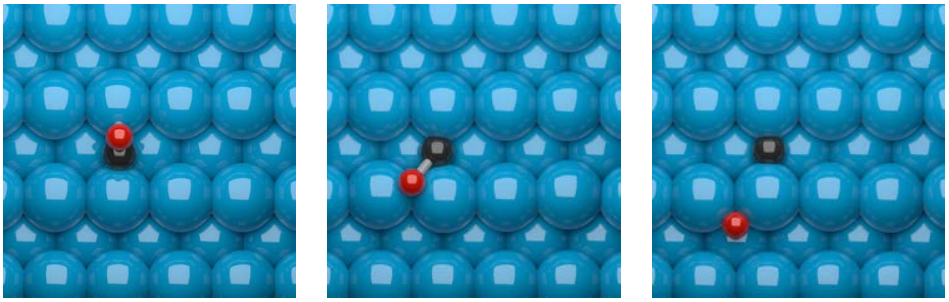

IS TS FS

Figure C.1: $CO^* + * \rightarrow C^* + O^*$

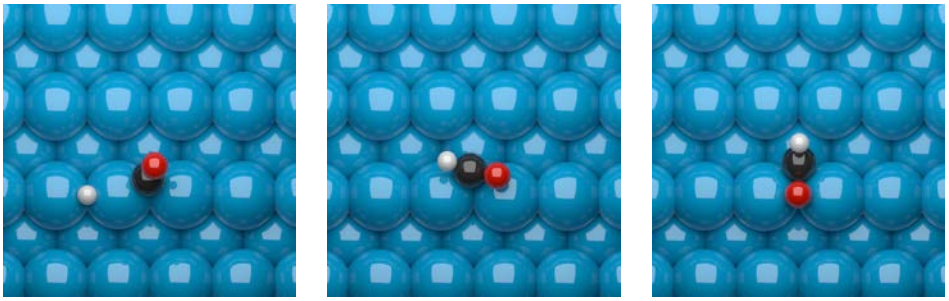

IS TS FS

Figure C.2: $CO^* + H^* \rightarrow HCO^* + *$

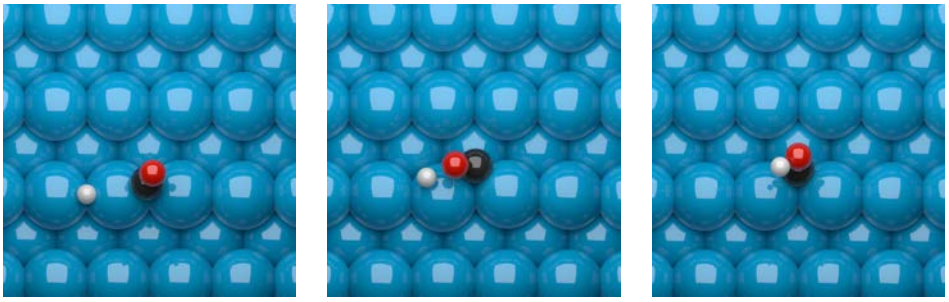

IS TS FS

Figure C.3: $CO^* + H^* \rightarrow COH^* + *$

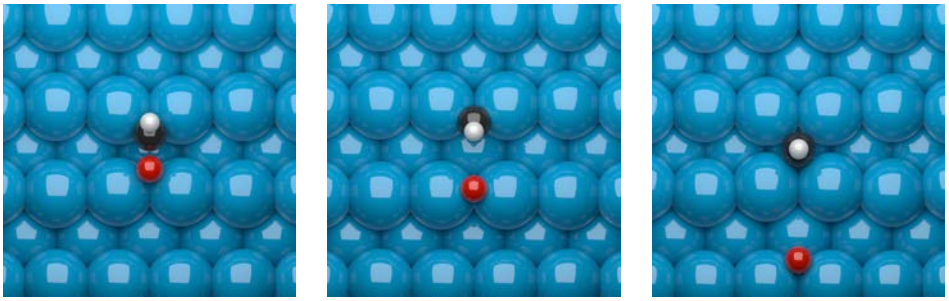

IS TS FS

Figure C.4: $HCO^* + * \rightarrow CH^* + O^*$

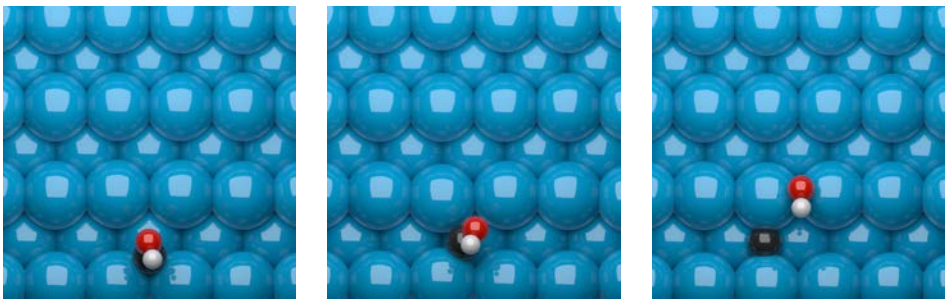

IS TS FS

Figure C.5: $COH^* + * \rightarrow C^* + OH^*$

C.2 Elements on the surface

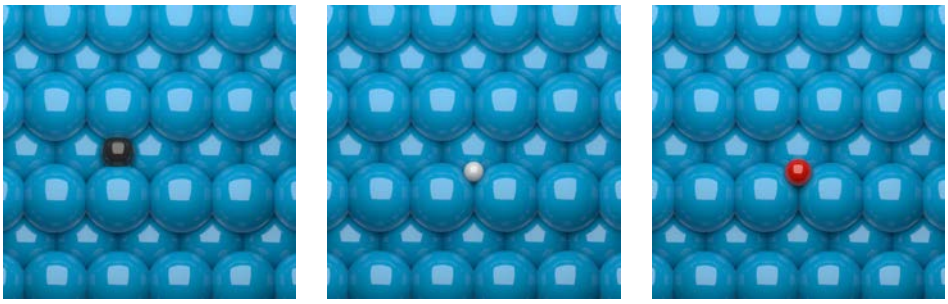

Figure C.6: On the leftside, a single Carbon atom on the cobalt surface. In the middle image a single hydrogen atom on the surface. In the right image a single oxygen on the surface.

C.3 Methanation

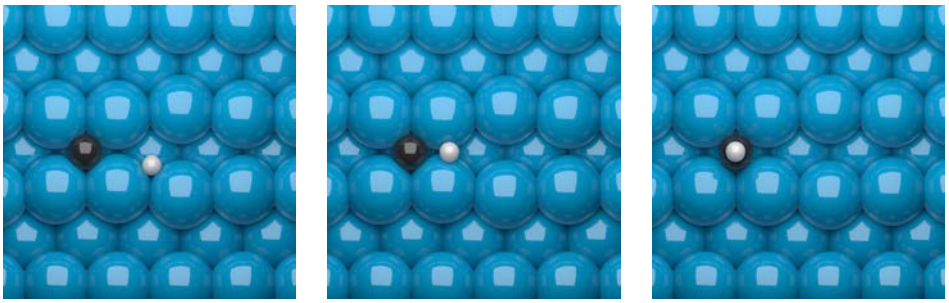

IS TS FS

Figure C.7: $C^* + H^* \rightarrow CH^* + *$

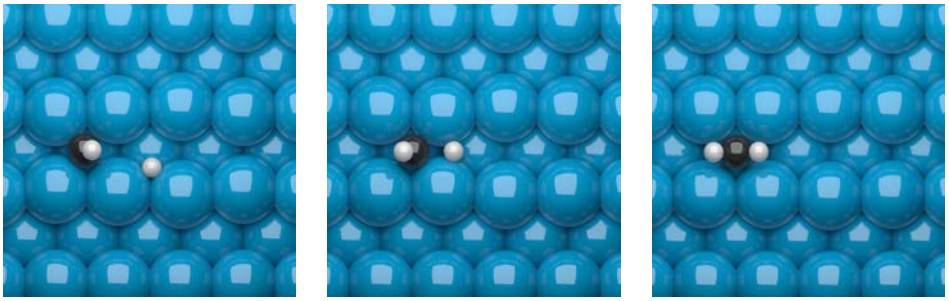

IS TS FS

Figure C.8: $CH^* + H^* \rightarrow CH_2^* + *$

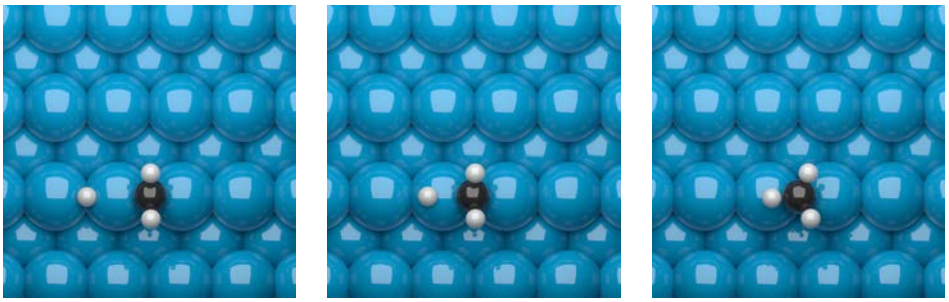

IS TS FS

Figure C.9: $CH_2^* + H^* \rightarrow CH_3^* + *$

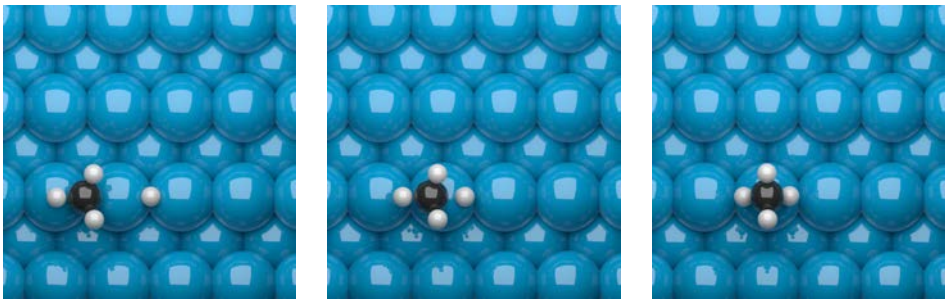

IS FS

Figure C.10: $CH_3^* + H^* \rightarrow CH_4 + 2*$

C.4 Carbon Carbon coupling and Hydrogenation of C_2-species

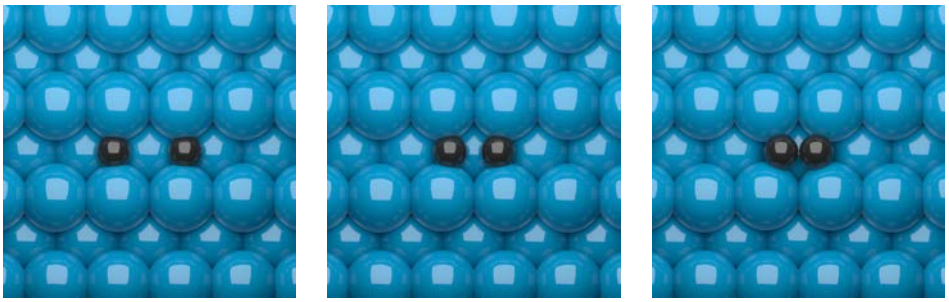

IS TS FS

Figure C.11: $2C^* \rightarrow C_2^* + *$

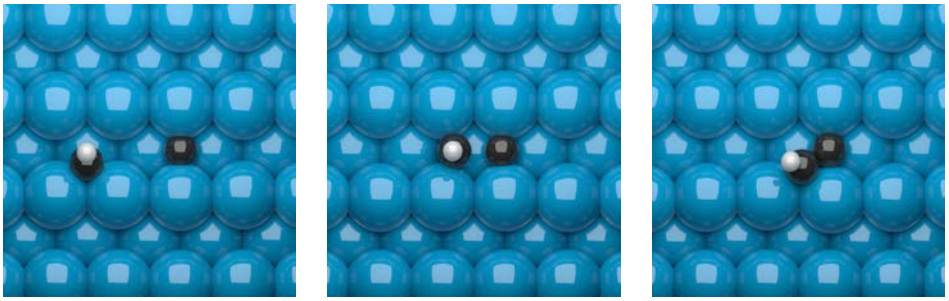

IS TS FS

Figure C.12: $CH^* + C^* \rightarrow CCH^* + *$

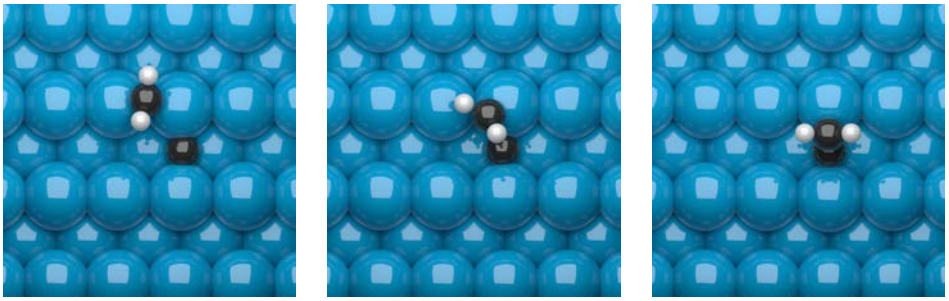

IS TS FS

Figure C.13: $CH_2^* + C^* \rightarrow CCH_2^* + *$

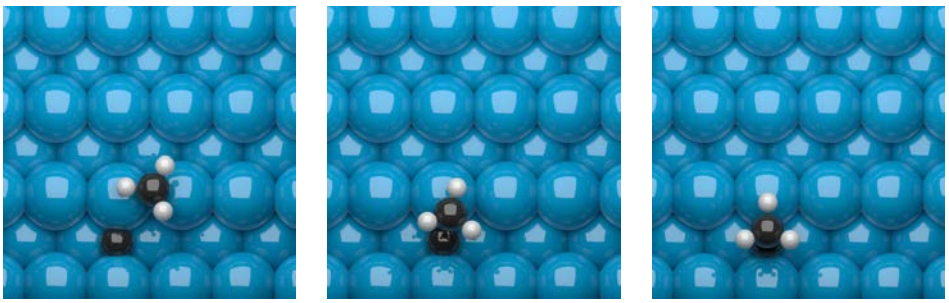

IS TS FS

Figure C.14: $CH_3^* + C^* \rightarrow CCH_3^* + *$

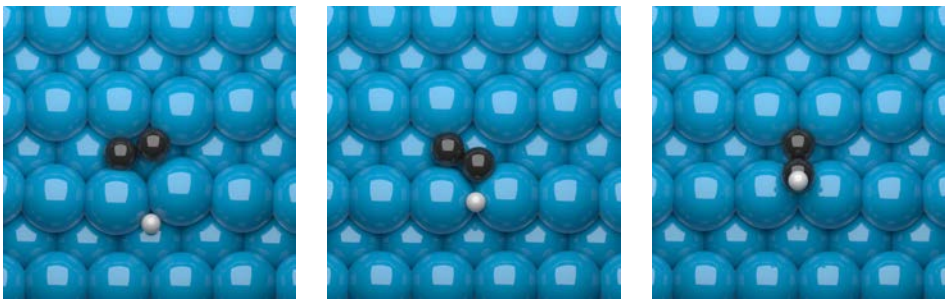

IS TS FS

Figure C.15: $C_2^* + H^* \rightarrow CCH^* + *$

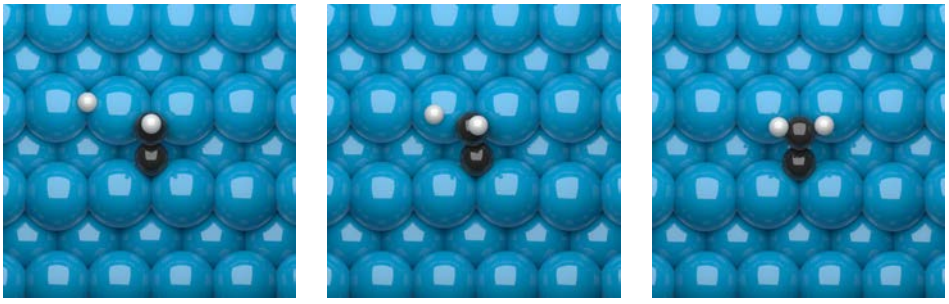

IS TS FS

Figure C.16: $CCH^* + H^* \rightarrow CCH_2^* + *$

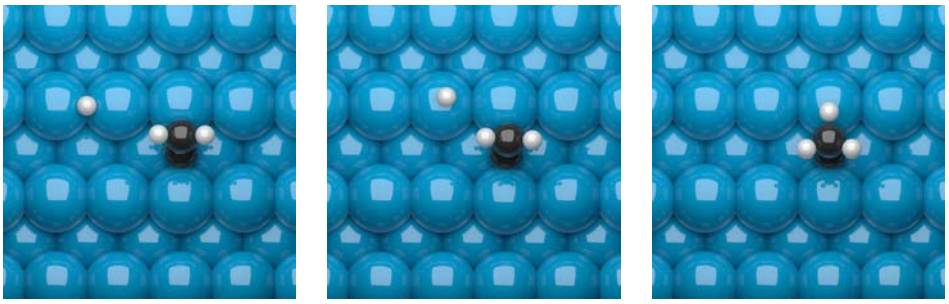

IS TS FS

Figure C.17: $CCH_2^* + H^* \rightarrow CCH_3^* + *$

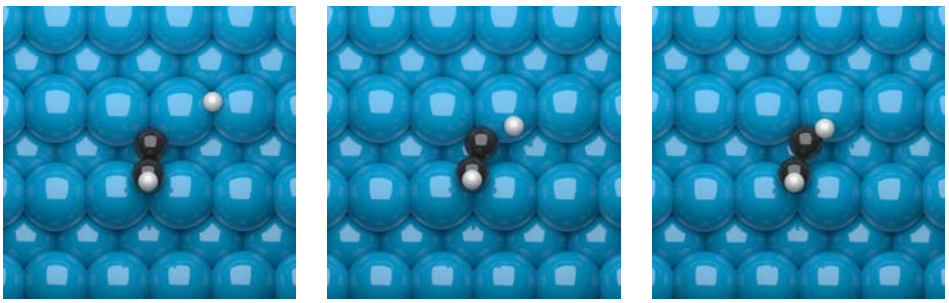

IS TS FS

Figure C.18: $CCH^* + H^* \rightarrow CHCH^* + *$

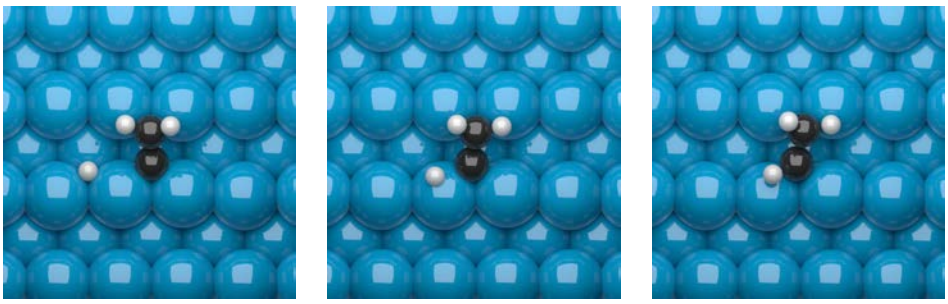

IS TS FS

Figure C.19: $CCH_2^* + H^* \rightarrow CHCH_2^* + *$

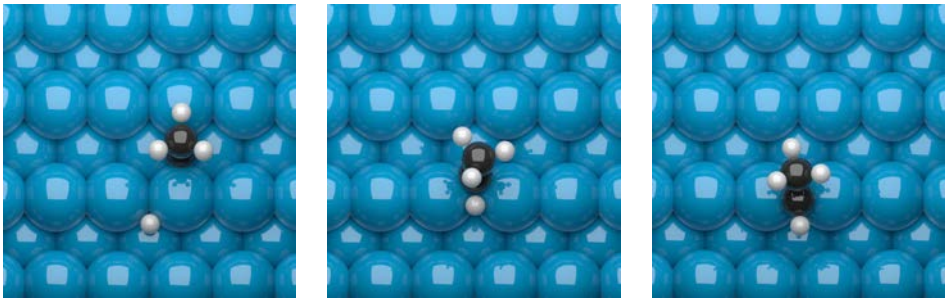

IS TS FS

Figure C.20: $CCH_3^* + H^* \rightarrow CHCH_3^* + *$

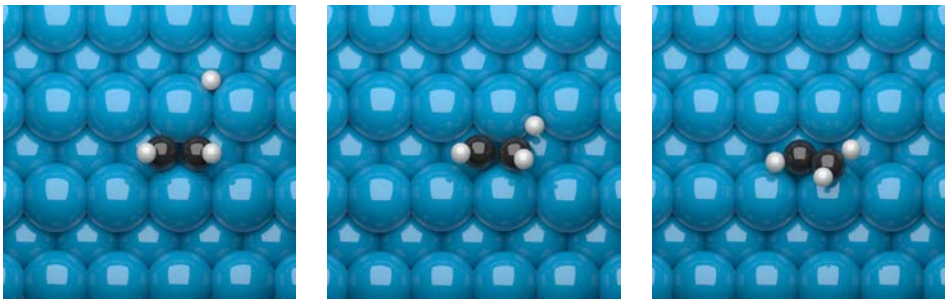

IS TS FS

Figure C.21: $CHCH^* + H^* \rightarrow CHCH_2^* + *$

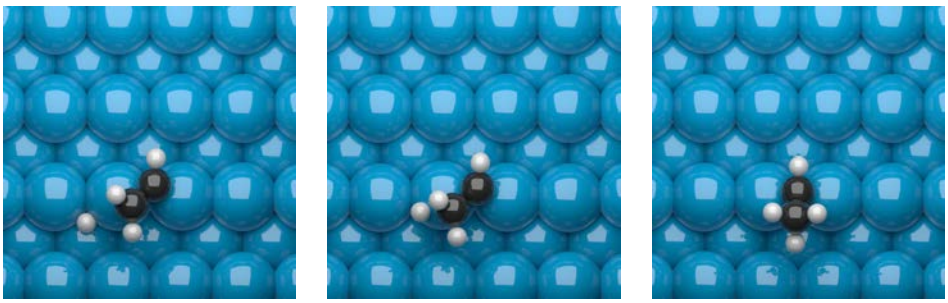

IS TS FS

Figure C.22: $CHCH_2^* + H^* \rightarrow CHCH_3^* + *$

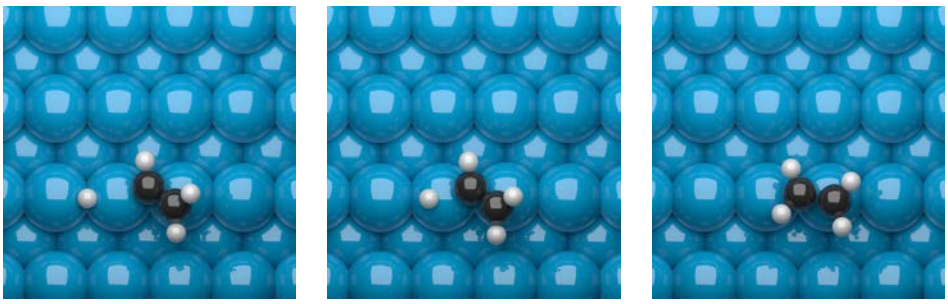

IS TS FS

Figure C.23: $CHCH_2^* + H^* \rightarrow CH_2CH_2^* + *$

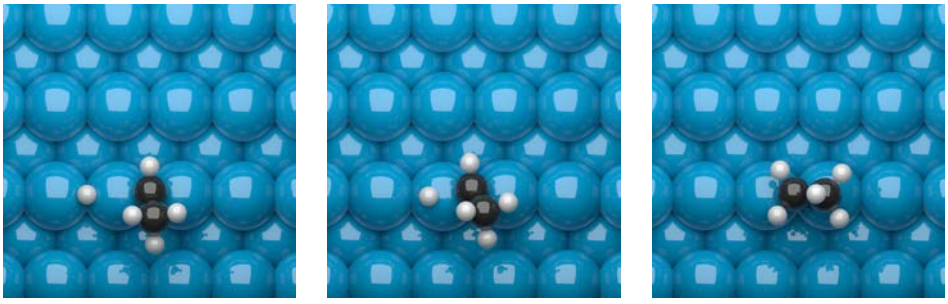

IS TS FS

Figure C.24: $CHCH_3^* + H^* \rightarrow CH_2CH_3^* + *$

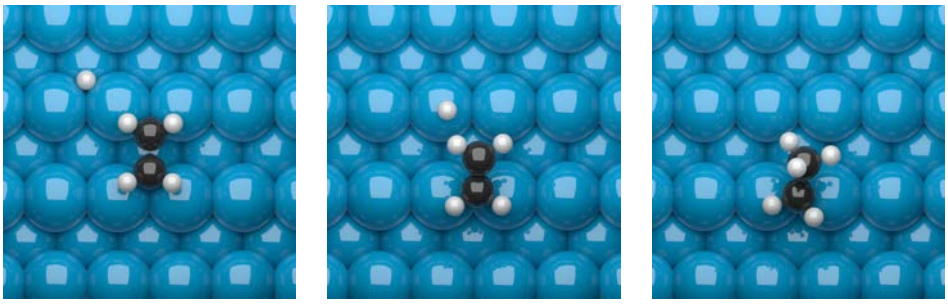

IS TS FS

Figure C.25: $CH_2CH_2^* + H^* \rightarrow CH_2CH_3^* + *$

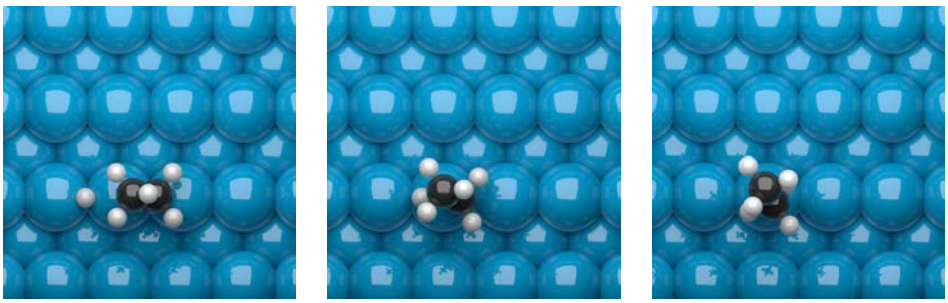

IS TS FS

Figure C.26: $CH_2CH_3^* + H^* \rightarrow C_2H_6 + 2*$

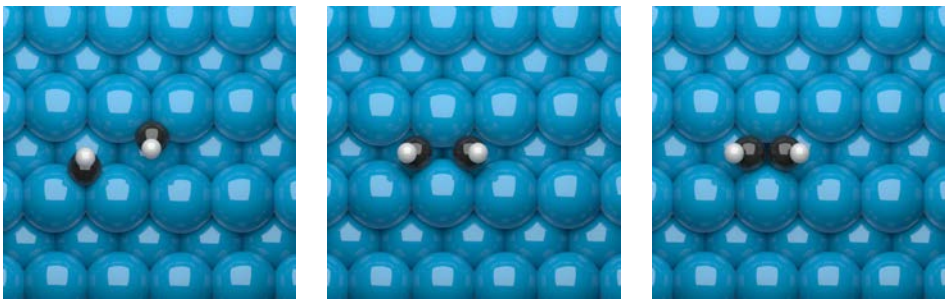

IS TS FS

Figure C.27: $2CH^* \rightarrow CHCH^* + *$

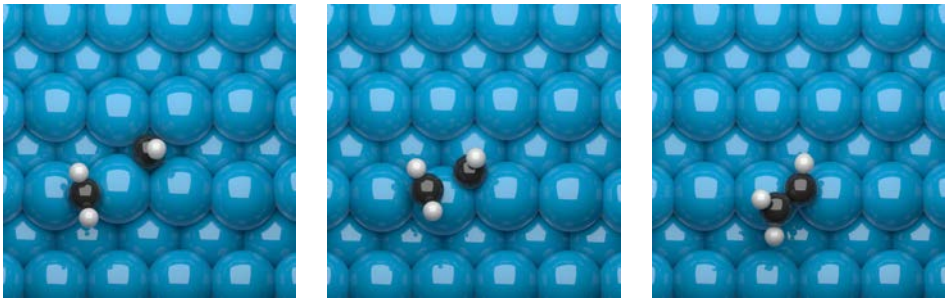

IS TS FS

Figure C.28: $CH^* + CH_2^* \rightarrow CHCH_2^* + *$

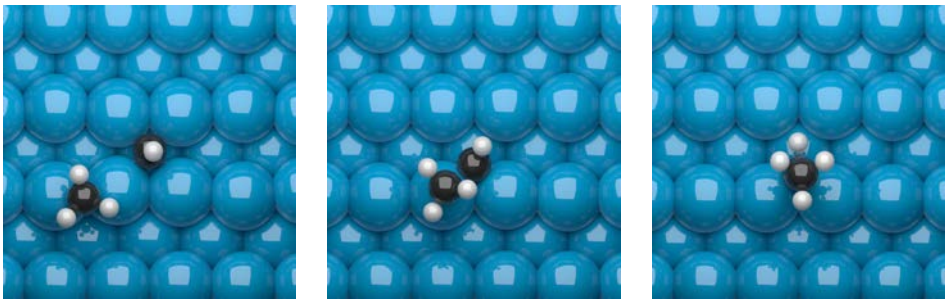

IS TS FS

Figure C.29: $CH^* + CH_3^* \rightarrow CHCH_3^* + *$

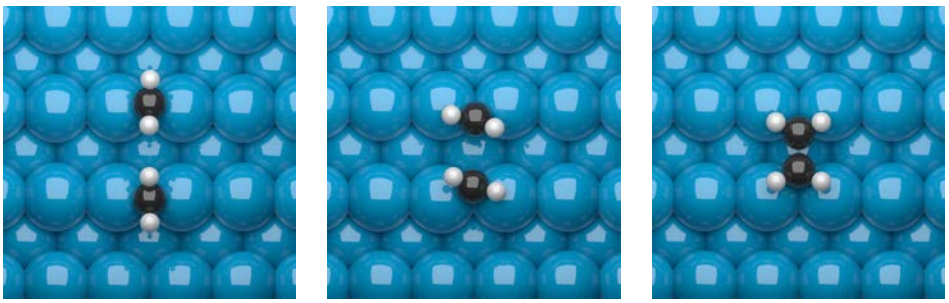

IS TS FS

Figure C.30: $2CH_2^* \rightarrow CH_2CH_2^* + *$

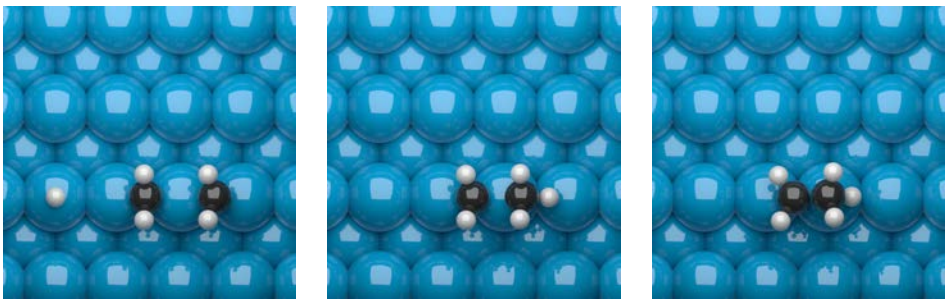

IS TS FS

Figure C.31: $CH_2^* + CH_3^* \rightarrow CH_2CH_3^* + *$

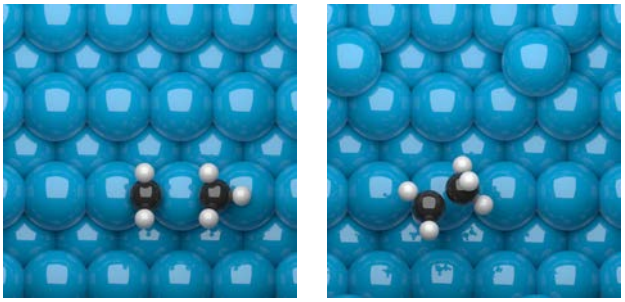

IS FS

Figure C.32: $2CH_3^* \rightarrow C_2H_6 + 2*$

C.5 Oxygen removal

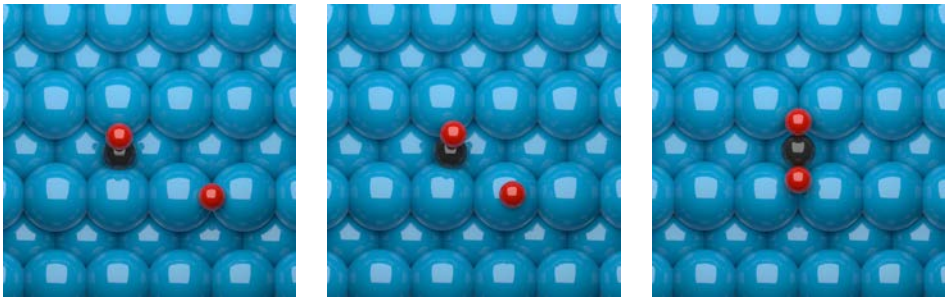

IS TS FS

Figure C.33: $CO^* + O^* \rightarrow CO_2^* + *$

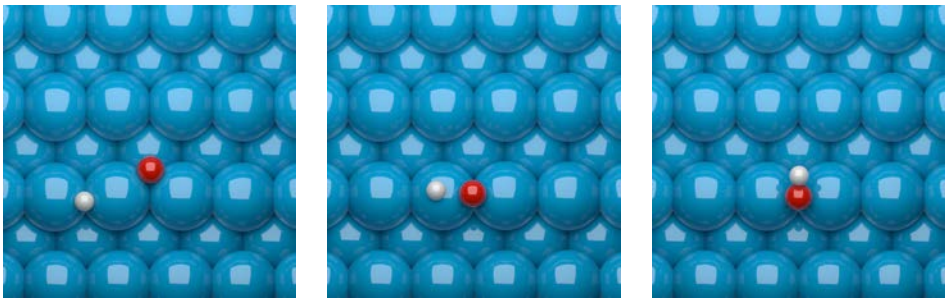

IS TS FS

Figure C.34: $O^* + H^* \rightarrow OH^* + *$

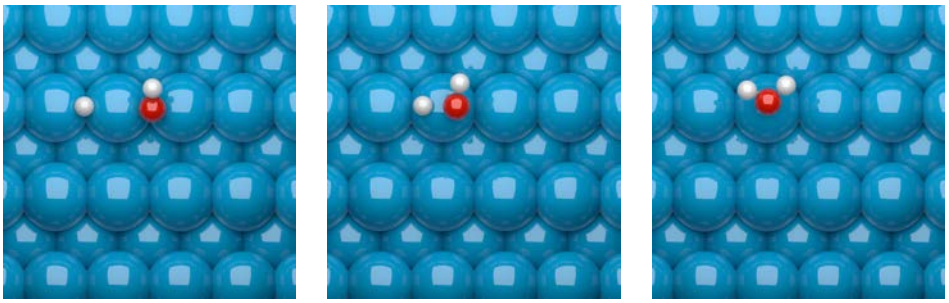

IS TS FS

Figure C.35: $OH^* + H^* \rightarrow H_2O^* + *$

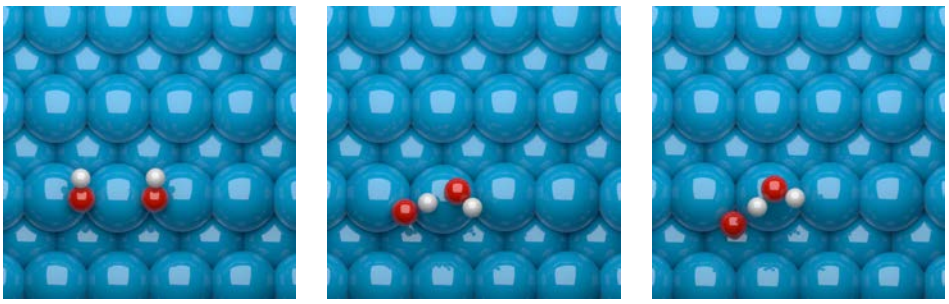

IS TS FS

Figure C.36: $2OH^* \rightarrow H_2O^* + O^*$

D Reaction barriers on Co FCC(110)

D.1 CO-dissociation

Table D.1: The reactions and their respective forward and backward acivation barriers for the dissociation of CO. Shown are the Direct and Hydrogen-assisted route to the formation of the CH- and OH-adsorbate

Reaction	$\Delta E_{act}^{forward}(kJ \cdot mol^{-1})$	$\Delta E_{act}^{backward}(kJ \cdot mol^{-1})$
CO + * $\rightarrow$ CO*	-154.73	-
H_2 + 2* $\rightarrow$ 2H*	-74.83	-
CO* + * $\rightarrow$ C* + O*	134.25	95.61
CO* + H* $\rightarrow$ HCO* + *	112.31	49.02
HCO* + * $\rightarrow$ CH* + O*	66.81	98.78
CO* + H* $\rightarrow$ COH* + *	173.03	72.81
COH* + * $\rightarrow$ C* + OH*	11.51	95.45

D.2 Methane formation

Table D.2: The activation energies in $(kJ \cdot mol^{-1})$ for the methanation reactions. The species denoted with an asterisk are surface species, the asterisk itself denotes an empty surface site.

Reaction	$\Delta E_{act}^{forward}(kJ \cdot mol^{-1})$	$\Delta E_{act}^{backward}(kJ \cdot mol^{-1})$
C* + H* $\rightarrow$ CH* + *	50.18	57.79
CH* + H* $\rightarrow$ CH_2^* + *	63.21	42.18
CH_2^* + H* $\rightarrow$ CH_3^* + *	52.74	58.11
CH_3^* + H* $\rightarrow$ CH4(g) + *	77.01	67.98

D.3 Carbon-carbon coupling and hydrogenation

Table D.3: The carbon-carbon coupling reactions and hydrogenation. Species denoted with an asterisk are surface adsorbates. The asterisk denotes and empty surface site. The coupling of two CH_3-adsorbates is assumed to be a stepped reaction. The protonshift is given in green. The pathway displayed in black is the pathway via the CH^* intermediate. The pathway displayed in blue is that pathway via CH_2^* and the red pathway is the pathway via the CH_3^*.

Reaction	$\Delta E_{forward}(kJ \cdot mol^{-1})$	$\Delta E_{backward}(kJ \cdot mol^{-1})$
$2C^* \rightarrow C_2^* + *$	79.89	47.64
$CH^* + C^* \rightarrow CCH^* + *$	83.51	128.68
$CH_2^* + C^* \rightarrow CCH_2^* + *$	141.63	174.35
$CH_3^* + C^* \rightarrow CCH_3^* + *$	75.52	87.50
$C_2^* + H^* \rightarrow CCH^* + *$	42.76	127.66
$CCH^* + H^* \rightarrow CCH_2^* + *$	84.01	50.44
$CCH_2^* + H^* \rightarrow CCH_3^* + *$	59.30	43.95
$CCH^* + H^* \rightarrow CHCH^* + *$	53.01	39.95
$CCH_2^* + H^* \rightarrow CHCH_2^* + *$	58.02	34.58
$CCH_3^* + H^* \rightarrow CHCH_3^* + *$	80.38	40.70
$CHCH^* + H^* \rightarrow CHCH_2^* + *$	85.00	21.95
$CHCH_2^* + H^* \rightarrow CHCH_3^* + *$	36.99	24.51
$CHCH_2^* + H^* \rightarrow CH_2CH_2^* + *$	24.38	55.07
$CHCH_3^* + H^* \rightarrow CH_2CH_3^* + *$	29.90	49.21
$CH_2CH_2^* + H^* \rightarrow CH_2CH_3^* + *$	137.79	113.93
$CH_2CH_3^* + H^* \rightarrow C_2H_6(g) + 2*$	82.45	62.25
$2CH^* \rightarrow CHCH^* + *$	53.71	78.49
$CH^* + CH_2 \rightarrow CHCH_2^* + *$	133.73	116.49
$CH^* + CH_3 \rightarrow CHCH_3^* + *$	122.26	87.17
$2CH_2^* \rightarrow CH_2CH_2^* + *$	135.79	170.27
$CH_2^* + CH_3^* \rightarrow CH_2CH_3^* + *$	102.78	108.02
$2CH_3^* \rightarrow C_2H_6(g) + 2*$	20.34	-
$CH_2CH2_2^* \rightarrow C_2H_4 + *$	97.09	-

D.4 Oxygen removal

Table D.4: Reactions that lead to oxygen being removed from the surface. Two pathways for the formation of water have been explored: hydrogenation of the oxygen species, the combination of two OH species and the combination of carbon-monoxide and oxygen to form carbon-dioxide. Species with an asterisk denote a surface species, the asterisk by itself denotes an empty surface site.

Reaction	$\Delta E_{forward}(kJ \cdot mol^{-1})$	$\Delta E_{backward}(kJ \cdot mol^{-1})$
$O^* + H^* \rightarrow OH^* + *$	109.42	131.95
$OH^* + H^* \rightarrow H_2O^* + *$	149.50	72.43
$2OH^* \rightarrow H_2O^* + O^*$	148.72	49.13
$H_2O^* \rightarrow H_2O(g) + *$	35.54	-
$CO^* + O^* \rightarrow CO2^* + *$	126.12	111.67
$CO_2^* \rightarrow CO_2(g) + *$	71.98	-
$2O^* \rightarrow O_2 + 2*$	471.45	-

E Reaction enthalpy

E.1 The PBE-functional

Table E.1: The calculated energies in electron volt using the PBE-potential by DFT calculation. The energetic correctio factor in eV, and the sum of the calculated DFT energy and the energy penalty. The formation enthalpies for several compounds in the reaction system, values taken from the website of the *National Institute of Standards and Technology*, or NIST for short. E_DFT is the calculate electronic energy and the zero-point-energy correction combined.

Compound	E_{DFT} (eV)	$E_{penalty}$ (eV)	$E_{DFT+penalty}(eV)$	$\Delta_f H_{NIST}$ (kJ/mol)
CO	-14,65	-0,23	-14,89	-110,52
H2	-6,48	0	-6,48	0
CO2	-22,66	0,19	-22,47	-393,52
H2O	-13,64	0	-13,64	-241,83
CH4	-22,83	0	-22,83	-74,87
C2H6	-38,49	0	-38,49	-84
C2H4	-30,59	0	-30,59	54,47
C3H8	-54,26	0	-54,26	-104,7
C3H6	-46,53	0	-46,53	20,41

Table E.2: The reaction enthalpies for the formation of methane, the watergasshift reaction, the formation of ethane, ethylene, propane and propylene. The column for $\Delta H_{r,DFT}$ displays the enthalpies as calculated using the DFT values. The column with $\Delta Hr, NIST$ displays the reaction enthalpies calculated using the $\Delta_f H_{NIST}$. $\Delta H_{r,corrected}$ displays the value for the reaction enthalpy per reaction using the $E_{DFT+penalty}$ from Table E.1. All values are given in kJ/mol, exept for the σ^2. The sum of squares is $\sum \sigma^2 = 7,38153 \cdot 10^{-14}$

Reaction	$\Delta H_{r,DFT}$	$\Delta H_{r,NIST}$	$\Delta H_{r,corrected}$	σ^2
$CO+3H_2 \rightarrow CH_4+H_2O$	-228,89	-206,17	-206,17	$8{,}25 \cdot 10^{-15}$
$CO+H_2O \rightarrow CO_2+H_2$	-81,77	-41,17	-41,17	$1{,}07 \cdot 10^{-14}$
$2CO+5H_2 \rightarrow C_2H_6+2H_2O$	-392,25	-346,60	-346,81	$1{,}26 \cdot 10^{-14}$
$2CO+4H_2 \rightarrow C_2H_4+2H_2O$	-255,58	-208,13	-210,13	$1{,}65 \cdot 10^{-14}$
$3CO+7H_2 \rightarrow C_3H_8+3H_2O$	-564,89	-498,60	-496,72	$7{,}93 \cdot 10^{-15}$
$3CO+6H_2 \rightarrow C_3H_6+3H_2O$	-445,04	-373,49	-376,88	$1{,}79 \cdot 10^{-14}$

E.2 The rPBE-functional

Table E.3: The calculated energies using DFT with the rPBE functional and for each component the penalty in kJ/mol. The energies is the column in E_{DFT} are the energies calculated by DFT and are the sum of the electronic and zero-point energies.

Substance	E_{DFT} (kJ/mol)	$E_{penalty}$ (kJ/mol)	$E_{DFT+penalty}$ (kJ/mol)
CO	-1465,20	-11,98	-1477,19
H2	-650,60	7,14	-643,45
H2O	-1362,57	-5,17	-1367,74
CO2	-2253,04	10,40	-2242,64
CH4	-2252,66	6,95	-2245,71
C2H4	-3010,57	9,73	-3000,84
C2H6	-3784,92	2,16	-3782,76
C3H6	-4567,81	5,25	-4562,56
C3H8	-5315,00	-16,12	-5331,12

Table E.4: The reaction enthalpies for different reactions with the energetic penalty using the rPBE functional in DFT. The error squared is calculated between the $\Delta H_{r,DFT+penalty}$ and the $\Delta H_{r,NIST}$ the latter can be found in Table E.2. The total sum of squares $\sum \sigma^2 = 3,84 \cdot 10^{-8}$

Reaction	$\Delta H_{r,DFT}$ (kJ/mol)	$\Delta H_{r,DFT+Penalty}$ (kJ/mol)	σ^2
$CO+3H_2 \rightarrow CH_4+H_2O$	-198,24	-205,90	$6,99 \cdot 10^{-9}$
$CO+H_2O \rightarrow CO_2+H_2$	-75,87	-41,17	$3,34 \cdot 10^{-9}$
$2CO+5H_2 \rightarrow C_2H_6+2H_2O$	-326,67	-346,60	$2,73 \cdot 10^{-8}$
$2CO+4H_2 \rightarrow C_2H_4+2H_2O$	-202,91	-208,13	$3,16 \cdot 10^{-10}$
$3CO+7H_2 \rightarrow C_3H_8+3H_2O$	-452,92	-498,60	$7,20 \cdot 10^{-15}$
$3CO+6H_2 \rightarrow C_3H_6+3H_2O$	-356,32	-373,49	$4,29 \cdot 10^{-10}$

E.3 Comparing PBE and rPBE

Table E.5: The reaction enthalpies for the different reaction as calculated using Equation 3.3 in kJ/mol along with the error in kJ/mol to the value obtained from NIST.

Reaction	$\Delta H_{r,PBE}$	$\Delta(\Delta H_r)_{PBE-NIST}$	$\Delta H_{r,rPBE}$	$\Delta(\Delta H_r)_{rPBE-NIST}$
$CO+3H_2 \rightarrow CH_4+H_2O$	-232,61	-26,44	-201,95	-3,95
$CO+H_2O \rightarrow CO_2+H_2$	-83,63	-42,46	-77,73	36,56
$2CO+5H_2 \rightarrow C_2H_6+2H_2O$	-401,54	-54,95	-335,96	-10,64
$2CO+4H_2 \rightarrow C_2H_4+2H_2O$	-261,15	-53,02	-208,49	0,36
$3CO+7H_2 \rightarrow C_3H_8+3H_2O$	-579,75	-81,16	-467,78	-30,81
$3CO+6H_2 \rightarrow C_3H_6+3H_2O$	-456,19	-82,71	-367,47	-6,02

F Shomate parameters

Table F.1: The parameters for the Shomate equations used in the microkinetic model, data is taken from ref [35].

compound	A	B	C	D
H_2O	30.09200	6.832514	6.793435	-2.534480
CO	25.56759	6.096130	4.054656	-2.671301
CO_2	24.99735	55.18696	-33.69137	7.948387
H_2	33.066178	-11.363417	11.432816	-2.772874
CH_4	-0.703029	108.4773	-42.52157	5.862788
C_2H_4	-6.387880	184.4019	-112.9718	28.49593
O_2	31.32234	-20.23531	57.86644	-36.50624
compound	E	F	G	H
H_2O	0.082139	-250.8810	223.3967	-241.8264
CO	0.131021	-118.0089	227.3665	-110.5271
CO_2	-0.136638	-403.6075	228.2431	-393.5224
H_2	-0.158558	-9.980797	172.707974	0.0
CH_4	0.678565	76.84376	158.7163	-74.87310
C_2H_4	0.315540	48.17332	163.1568	52.46694
O_2	-0.007374	-8.903471	246.7945	0.0

G blender settings

Table G.1: The Settings used for blender to render the images for this report in a script made by Dr.ir. B. Zijlstra. The script can be found at the TU/e gitlab: https://gitlab.tue.nl/

Command	Setting	Value
-r	resulotion	750×750
-g	render using the GPU	–
-e	copy unit cell	2
-E	atom types to copy	1
–no-bonds	do not render bonds	–
-m	surface-modifier	1
-s	samples per tile	1500
-l	the strength of the lighting	100
–mb	number of light bounces	5
–tile	the size of the tiles	200×200
-c	PNG compression	100

H MKM input files

H.1 Microkinetic model with only DFT

```
#!SEGFLOW
# This is the mkm file for the FT-synthesis on Co (110), C2H6_Formation_NoLats.mkm
# Made by Joost van der Meijs
# Under supervision of dr.ir. I.A.W. Filot and ir. M.P.C. van Etten
# (I.A.W.Filot@tue.nl) & (m.p.c.v.etten@tue.nl)
# With immense help from dr.ir. B. Zijlstra
################################################################################
################################################################################
### regex:                                                                   ###
################################################################################
################################################################################
&regex_rules_start
REGEX_COUNT      =   20
REGEX_BEGIN      =   ^[ \t]*@BEGIN[ \t]*;[ \t]*([0-9-]+)[ \t]*;[ \t]*([0-9-]+)[ \t]*
    $
REGEX_SWAP       =   ^.*@.*$
REGEX_SWAP_P     =   (^.*)@p([0-9]+)(.*$)
REGEX_SWAP_M     =   (^.*)@m([0-9]+)(.*$)
REGEX_SWAP_O     =   (^.*)@(.*$)
REGEX_END        =   ^[ \t]*@END[ \t]*$
&regex_rules_end
################################################################################
################################################################################
### variables:                                                               ###
################################################################################
################################################################################
###                          Simulation Variables
variable temp_test           =   true
variable sim_time            =   1e5
variable abs_tol             =   1e-15
variable rel_tol             =   1e-10
variable start_temp          =   473
variable step_size           =   5
variable nr_cores            =   4
### DeltaH corrections on CO and CO2:
variable COrrection          =   -22.72e3
variable CO2rrection         =   17.88e3
###                          Surface variables
variable site_size           =   1e-19
variable stick               =   1.0
###                          Shomate parameters
# A to H from https://webbook.nist.gov/
# Parameter name:                A          B          C          D          E
            F          G          H
variable CO_sho              =   25.56759;   6.096130;   4.054656;   -2.671301;
    0.131021;   -118.0089;  227.3665;   -110.5271
variable water_sho           =   -203.6060;  1523.290;   -3196.413;  2474.455;
    3.855326;   -256.5478;  -488.7163;  -285.8304
variable H_sho               =   33.066178;  -11.363417; 11.432816;  -2.772874;
    -0.158558;  -9.980797;  172.707974; 0.000000
variable methane_sho         =   -0.703029;  108.4773;   -42.52157;  5.862788;
    0.678565;   -76.84376;  158.7163;   74.87310
variable carb_sho            =   24.99735;   55.18696;   33.69137;   7.948387;
    -0.136638;  -403.6075;  228.2431;   -393.5224
variable ethe_sho            =   -6.387880;  184.4019;   -112.9718;  28.49593;
    0.315540;   48.17332;   163.1568;   52.46694
variable oxy_sho             =   31.32234;   -20.23531;  57.86644;   -36.50624;
    -0.007374;  -8.903471;  246.7945;   0.0
```

```
###                         Pressure
variable tot_syn_pres       =   1.0
variable H2_CO_RAT          =   2.0
variable Partial_P_CO       =   ($tot_syn_pres/(1+$H2_CO_RAT))
variable Partial_P_H2       =   ($tot_syn_pres-$tot_syn_pres/(1+$H2_CO_RAT))
###############################################################################
###############################################################################
### compounds:                                                              ###
###############################################################################
###############################################################################
&compounds
# Reagents:
        CO;             0;  [$Partial_P_CO]
        H2;             0;  [$Partial_P_H2]
# Products:
        H2O;            0;  0.00
        O2;             0;  0.00
        CO2;            0;  0.00
        CH4;            0;  0.00
        C2H4;           0;  0.00
        C2H6;           0;  0.00
# Empty surface sites:
        *;              1;  1.00
# Surface intermediates:
    # For CO dissociation:
        CO*;            1;  0.00
        HCO*;           1;  0.00
        COH*;           1;  0.00
    # Hydrogen, Oxygen, OH, H2O and CO2
        H*;             1;  0.00
        O*;             1;  0.00
        CO2*;           1;  0.00
        OH*;            1;  0.00
        H2O*;           1;  0.00
    # Single Carbon intermediates
        C*;             1;  0.00
        CH*;            1;  0.00
        CH2*;           1;  0.00
        CH3*;           1;  0.00
    # Double Carbon intermediates
        C2*;            1;  0.00
        CCH*;           1;  0.00
        CCH2*;          1;  0.00
        CCH3*;          1;  0.00
        CHCH*;          1;  0.00
        CHCH2*;         1;  0.00
        CHCH3*;         1;  0.00
        CH2CH2*;        1;  0.00
        CH2CH3*;        1;  0.00
###############################################################################
###############################################################################
### reactions:                                                              ###
###############################################################################
###############################################################################
&reactions
###################################
#   ADSORPTION / DESORPTION       #
###################################
HKN;    {CO}    +   {*}     =>  {CO*}    ;  $site_size;         28; $stick; $CO_sho
    ;       1.25e2; 154.73e3;   1   # (CO_Ads)
HKN;    {H2O}   +   {*}     =>  {H2O*}   ;  $site_size;         18; $stick;
    $water_sho;     1.16e2; 35.54e3;    1   # (H2O_Ads)
HKN;    {H2}    +   2{*}    =>  2{H*}    ;  $site_size;         2;  $stick; $H_sho;
```

```
                1.66e0; 74.83e3;     1    # (H2_Ads)
111 HKN;     {CO2}    +    {*}      =>  {CO2*}     ;   $site_size;          44; $stick;
    $carb_sho;        8.87e1; 71.98e3;     1    # (CO2_Ads)
112 HKN;     {O2}     +    2{*}     =>  2{O*}      ;   $site_size;          32; $stick;
    $oxy_sho;         1.96e1; 471.45e3;    1    # (A)
113 HKN;     {C2H4}   +    {*}      =>  {CH2CH2*};   $site_size;          28; $stick;
    $ethe_sho;        3.77e2; 97.09e3;     1    # (C2H4_Ads)
114 ###################################
115 #    SURFACE REACTIONS              #
116 ###################################
117 #
118     #    CO-Hydrogenation
119     #
120     ARQ;    {CO*}    +    {H*}     =>  {COH*}   +    {*};              0.234258;
    0.543187;    173.03e3;    72.81e3;     1    # (COH)
121     ARQ;    {CO*}    +    {H*}     =>  {HCO*}   +    {*};              0.000863;
    0.458237;    112.31e3;    49.02e3;     1    # (HCO)
122     #
123     #    CO - Dissociation:
124     #
125     ARQ;    {CO*}    +    {*}      =>  {C*}     +    {O*};             0.455723;
    5.020295;    134.25e3;    95.61e3;     1    # (Diss)
126     ARQ;    {COH*}   +    {*}      =>  {C*}     +    {OH*};            0.853567;
    1.932005;    11.51e3;     95.45e3;     1    # (COHDiss)
127     ARQ;    {HCO*}   +    {*}      =>  {CH*}    +    {O*};             0.130755;
    0.096524;    66.81e3;     98.78e3;     1    # (HCODiss)
128     #
129     #    Single C-Hydrogenation
130     #
131     ARQ;    {C*}     +    {H*}     =>  {CH*}    +    {*};              0.953095;
    0.387184;    50.18e3;     57.59e3;     1    # (AA)
132     ARQ;    {CH*}    +    {H*}     =>  {CH2*}   +    {*};              0.828829;
    0.661131;    63.21e3;     42.18e3;     1    # (AB)
133     ARQ;    {CH2*}   +    {H*}     =>  {CH3*}   +    {*};              0.920479;
    0.269246;    52.74e3;     58.11e3;     1    # (AC)
134     ARQ;    {CH3*}   +    {H*}     =>  {CH4}    +    2{*};             22.309831;
    0.285183;    77.01e3;     67.98e3;     1    # (HAE)
135 #
136 #    Oxygen Removal
137 #
138
139     #
140     #    CO2-Formation
141     #
142         ARQ;    {CO*}    +    {O*}         =>  {CO2*}   +    {*};      0.350083;
    2.179145;    126.12e3;    111.67e3;    1    # (CO2_Form)
143     #
144     #    Water-Formation
145     #
146         ARQ;    {O*}     +    {H*}         =>  {OH*}    +    {*};      0.173910;
    1.035713;    109.42e3;    131.95e3;    1    # (C)
147         ARQ;    {OH*}    +    {H*}         =>  {H2O*}   +    {*};      0.880259;
    0.116631;    149.50e3;    72.43e3;     1    # (D)
148         ARQ;    2{OH*}                    =>  {H2O*}   +    {O*};     0.350039;
    0.097347;    148.72e3;    49.13e3;     1    # (F)
149 #
150     #    Carbon Additions:
151     #
152     #    C Addition:
153     ARQ;    {C*}         +    {C*}     =>  {C2*}        +    {*};      1.064334;
    0.286005;    79.89e3;     47.64e3;     1    # (HAF)
154     ARQ;    {CH*}        +    {C*}     =>  {CCH*}       +    {*};      0.545304;
    0.555722;    83.51e3;     128.68e3;    1    # (HBA)
```

```
155     ARQ;    {CH2*}      +   {C*}    => {CCH2*}      + {*};      0.416975;
        0.399029;   141.63e3;   174.35e3;   1   # (HBB)
156     ARQ;    {CH3*}      +   {C*}    => {CCH3*}      + {*};      0.705084;
        1.446597;   75.52e3;    87.50e3;    1   # (AI)
157     #   CH Addition:
158     ARQ;    {CH*}       +   {CH*}   => {CHCH*}      + {*};      0.318600;
        1.298830;   53.71e3;    78.49e3;    1   # (CA)
159     ARQ;    {CH2*}      +   {CH*}   => {CHCH2*}     + {*};      0.374159;
        0.363990;   133.73e3;   116.49e3;   1   # (HCB)
160     ARQ;    {CH3*}      +   {CH*}   => {CHCH3*}     + {*};      0.341786;
        0.423427;   122.26e3;   87.17e3;    1   # (HCC)
161     #   CH2 Addition:
162     ARQ;    {CH2*}      +   {CH2*}  => {CH2CH2*}    + {*};      0.913969;
        0.415145;   135.79e3;   170.27e3;   1   # (DB)
163     ARQ;    {CH3*}      +   {CH2*}  => {CH2CH3*}    + {*};      0.147481;
        0.080704;   102.78e3;   108.02e3;   1   # (HDC)
164     #   CH3 Addition:
165     HK;     {C2H6}      +   2{*}    => {CH3*}       + {CH3*};       $site_size; 30;
        20; 6; $stick;  20.34e3;    1   # (HEC)
166     #   Double C-Hydrogenation:
167     ARQ;    {C2*}       +   {H*}    => {CCH*}       + {*};      0.496293;
        0.764613;   42.76e3;    127.66e3;   1   # (AM)
168     ARQ;    {CCH*}      +   {H*}    => {CHCH*}      + {*};      0.916129;
        1.488761;   53.01e3;    39.95e3;    1   # (HAJ)
169     ARQ;    {CCH*}      +   {H*}    => {CCH2*}      + {*};      0.828315;
        0.620432;   84.01e3;    50.44e3;    1   # (HAN)
170     ARQ;    {CCH2*}     +   {H*}    => {CHCH2*}     + {*};      0.972412;
        0.798395;   58.02e3;    34.58e3;    1   # (HAK)
171     ARQ;    {CCH2*}     +   {H*}    => {CCH3*}      + {*};      1.706890;
        1.070416;   59.30e3;    43.95e3;    1   # (HAO)
172     ARQ;    {CCH3*}     +   {H*}    => {CHCH3*}     + {*};      1.205931;
        0.323544;   80.38e3;    40.70e3;    1   # (HAL)
173     ARQ;    {CHCH*}     +   {H*}    => {CHCH2*}     + {*};      1.187132;
        0.225969;   85.00e3;    21.95e3;    1   # (HAP)
174     ARQ;    {CHCH2*}    +   {H*}    => {CHCH3*}     + {*};      0.479785;
        0.197346;   36.99e3;    24.51e3;    1   # (HAQ)
175     ARQ;    {CHCH2*}    +   {H*}    => {CH2CH2*}    + {*};      0.628289;
        0.234001;   24.38e3;    55.07e3;    1   # (HAR)
176     ARQ;    {CHCH3*}    +   {H*}    => {CH2CH3*}    + {*};      1.347048;
        0.433939;   29.90e3;    49.21e3;    1   # (HAS)
177     ARQ;    {CH2CH2*}   +   {H*}    => {CH2CH3*}    + {*};      5.552600;
        1.956700;   137.79e3;   113.93e3;   1   # (HAT)
178     ARQ;    {CH2CH3*}   +   {H*}    => {C2H6}       + 2{*};     0.290259;
        259.5823;   82.45e3;    62.25e3;    1   # (HAW)
179
180 ###############################################################################
181 ###############################################################################
182 ### Settings:                                                               ###
183 ###############################################################################
184 ###############################################################################
185 &settings
186 # General Settings
187     TYPE                =   SEQUENCERUN
188     DEBUG               =   0
189     NPAR                =   $nr_cores
190     PRESSURE            =   $tot_syn_pres
191     REAGENTS            =   {CO},{H2}
192     KEYCOMPONENTS       =   {CO}
193     NUMDIFF             =   1
194     SOLVERTYPE          =   1
195     SOLSTOPTIME         =   2
196     SOLMAXSTEP          =   50000
197     #Apparent Activation Energy:
```

```
    EACT            =   1
    EACTDIFF        =   0.00001
    # Degree of rate control:
    DRC             =   2
    DRCDIFF         =   0.001
    # Degree of selectivity control
    DSC             =   1
    # Thermodynamic degree of rate control
    # Reaction orders
    ORDERS          =   1
    ORDERSDIFF      =   0.001
    # Gibbs Energy Barriers
    GIBBS           =   1
    # Graphs:
    GRAPHDATA       =   1
    COLORBLIND      =   1
    MAKEPLOTS       =   1
##############################################################################
##############################################################################
### runs:                                                                  ###
##############################################################################
##############################################################################
&runs
# A full run, can be tuned from the top of the file.
if (!$temp_test){
    @BEGIN; 1;  11
        [$start_temp+@ml*$step_size];   $sim_time;  $abs_tol;   $rel_tol
    @END
}
if ($temp_test){
    493.15;     1e6;    1e-15;  1e-10
    513.15;     1e6;    1e-15;  1e-10
    533.15;     1e6;    1e-15;  1e-10
}
```

chapters/appendices/mkmfiles/C2H6_Formation_NoLats.mkm

H.2 Microkinetic model with DFT and lateral interaction

```
#!SEGFLOW
# This is the mkm file for the FT-synthesis on Co (110), C2H6_Formation.mkm
# Made by Joost van der Meijs
# Under supervision of dr.ir. I.A.W. Filot and ir. M.P.C. van Etten
# (I.A.W.Filot@tue.nl) & (m.p.c.v.etten@tue.nl)
# With immense help from dr.ir. B. Zijlstra
###############################################################################
###############################################################################
### regex:                                                                  ###
###############################################################################
###############################################################################
&regex_rules_start
REGEX_COUNT      =    20
REGEX_BEGIN      =    ^[ \t]*@BEGIN[ \t]*;[ \t]*([0-9-]+)[ \t]*;[ \t]*([0-9-]+)[ \t]*
    $
REGEX_SWAP       =    ^.*@.*$
REGEX_SWAP_P     =    (^.*)@p([0-9]+)(.*$)
REGEX_SWAP_M     =    (^.*)@m([0-9]+)(.*$)
REGEX_SWAP_O     =    (^.*)@(.*$)
REGEX_END        =    ^[ \t]*@END[ \t]*$
&regex_rules_end
###############################################################################
###############################################################################
### variables:                                                              ###
###############################################################################
###############################################################################
###                          Simulation Variables
variable Full_LTFT_Range          =    true
variable sim_time            =    1e4
variable abs_tol             =    1e-15
variable rel_tol             =    1e-10
variable start_temp          =    473
variable step_size           =    5
variable nr_cores            =    4
### DeltaH corrections on CO and CO2:
variable COrrection          =    -22.72e3
variable CO2rrection         =    17.88e3
###                          Surface variables
variable site_size           =    1e-19
variable stick               =    1.0
###                          Lateral Interactions; values taken from the model of ir
    . B. Zijlstra
variable CO_lat              =    450e3
variable C_lat               =    100e3
variable O__lat              =    100e3
variable H_lat               =    100e3
variable H2_lat              =    [2*($H_lat)]
variable H2O_lat             =    [($O__lat)+2*($H_lat)]
variable CH2_lat             =    [($C_lat)+2*($H_lat)]
variable CH3_lat             =    [($C_lat)+3*($H_lat)]
variable CH4_lat             =    [($C_lat)+4*($H_lat)]
variable CO2_lat             =    [($C_lat)+2*($O__lat)]
variable diss_lat            =    [$C_lat+$O__lat-$CO_lat]
variable CH2_r_lat           =    [-1*($C_lat)-2*($H_lat)]
variable CH3_r_lat           =    [-1*($C_lat)-3*($H_lat)]
variable CH4_r_lat           =    [-1*($C_lat)-4*($H_lat)]
variable eth_lat             =    [2*$C_lat+4*$H_lat]
variable olf_lat             =    [(2*$C_lat+3*$H_lat)]
variable lat_dir             =    0.50
variable lat_lb              =    0.00
variable lat_ub              =    1.00
```

```
variable lat_start          =   1.0
#variable latin            =   {*},0.5{H*}
variable latin              =   {*}
variable stand_lat          =   $lat_dir;   $lat_lb;    $lat_ub;    $lat_start;
    $latin
variable car_lat            =   0.00;       0.00;       1.00;       $lat_start;
    $latin
###                         Shomate parameters
# A to H from https://webbook.nist.gov/
# Parameter name:               A           B           C           D           E
            F           G           H
variable CO_sho             =   25.56759;   6.096130;   4.054656;   -2.671301;
    0.131021;   -118.0089;  227.3665;   -110.5271
variable water_sho          =   -203.6060;  1523.290;   -3196.413;  2474.455;
    3.855326;   -256.5478;  -488.7163;  -285.8304
variable H_sho              =   33.066178;  -11.363417; 11.432816;  -2.772874;
    -0.158558;  -9.980797;  172.707974; 0.000000
variable methane_sho        =   -0.703029;  108.4773;   -42.52157;  5.862788;
    0.678565;   -76.84376;  158.7163;   74.87310
variable carb_sho           =   24.99735;   55.18696;   33.69137;   7.948387;
    -0.136638;  -403.6075;  228.2431;   -393.5224
variable ethe_sho           =   -6.387880;  184.4019;   -112.9718;  28.49593;
    0.315540;   48.17332;   163.1568;   52.46694
variable oxy_sho            =   31.32234;   -20.23531;  57.86644;   -36.50624;
    -0.007374;  -8.903471;  246.7945;   0.0
###                         Pressure
variable tot_syn_pres       =   1.0
variable H2_CO_RAT          =   2.0
variable Partial_P_CO       =   ($tot_syn_pres/(1+$H2_CO_RAT))
variable Partial_P_H2       =   ($tot_syn_pres-$tot_syn_pres/(1+$H2_CO_RAT))
##############################################################################
##############################################################################
### compounds:                                                             ###
##############################################################################
##############################################################################
&compounds
# Reagents:
        CO;             0;  [$Partial_P_CO]
        H2;             0;  [$Partial_P_H2]
# Products:
        H2O;            0;  0.00
        O2;             0;  0.00
        CO2;            0;  0.00
        CH4;            0;  0.00
        C2H4;           0;  0.00
        C2H6;           0;  0.00
# Empty surface sites:
        *;              1;  1.00
# Surface intermediates:
    # For CO dissociation:
        CO*;            1;  0.00
        HCO*;           1;  0.00
        COH*;           1;  0.00
    # Hydrogen, Oxygen, OH, H2O and CO2
        H*;             1;  0.00
        O*;             1;  0.00
        CO2*;           1;  0.00
        OH*;            1;  0.00
        H2O*;           1;  0.00
    # Single Carbon intermediates
        C*;             1;  0.00
        CH*;            1;  0.00
        CH2*;           1;  0.00
```

```
113         CH3*;               1;  0.00
114     # Double Carbon intermediates
115         C2*;                1;  0.00
116         CCH*;               1;  0.00
117         CCH2*;              1;  0.00
118         CCH3*;              1;  0.00
119         CHCH*;              1;  0.00
120         CHCH2*;             1;  0.00
121         CHCH3*;             1;  0.00
122         CH2CH2*;            1;  0.00
123         CH2CH3*;            1;  0.00
124 ##############################################################################
125 ##############################################################################
126 ### reactions:                                                             ###
127 ##############################################################################
128 ##############################################################################
129 &reactions
130 ###################################
131 #   ADSORPTION / DESORPTION       #
132 ###################################
133 ADS;    {CO}    +   {*}     =>  {CO*}           ;   $CO_lat;        $stand_lat;
        $site_size;         28; $stick; $CO_sho;        1.25e2; 154.73e3;   1   # (
        CO_Ads)
134 ADS;    {H2O}   +   {*}     =>  {H2O*}          ;   $H2O_lat;       $stand_lat;
        $site_size;         18; $stick; $water_sho;     1.16e2; 35.54e3;    1   # (
        H2O_Ads)
135 ADS;    {H2}    +   2{*}    =>  2{H*}           ;   $H2_lat;        $stand_lat;
        $site_size;         2;  $stick; $H_sho;         1.66e0; 74.83e3;    1   # (
        H2_Ads)
136 ADS;    {CO2}   +   {*}     =>  {CO2*}          ;   $CO2_lat;       $stand_lat;
        $site_size;         44; $stick; $carb_sho;      8.87e1; 71.98e3;    1   # (
        CO2_Ads)
137 ADS;    {O2}    +   2{*}    =>  2{O*}           ;   $O__lat;        $stand_lat;
        $site_size;         32; $stick; $oxy_sho;       1.96e1; 471.45e3;   1   # (A)
138 ADS;    {C2H4}  +   {*}     =>  {CH2CH2*}       ;   $eth_lat;       $stand_lat;
        $site_size;         28; $stick; $ethe_sho;      3.77e2; 97.09e3;    1   # (
        C2H4_Ads)
139 ###################################
140 #   SURFACE REACTIONS             #
141 ###################################
142 #
143     #   CO-Hydrogenation
144     #
145     ARQL;   {CO*}   +   {H*}    =>  {COH*}  +   {*};            $diss_lat;
        $stand_lat;     0.234258;   0.543187;   173.03e3;   72.81e3;    1   # (COH)
146     ARQL;   {CO*}   +   {H*}    =>  {HCO*}  +   {*};            $diss_lat;
        $stand_lat;     0.000863;   0.458237;   112.31e3;   49.02e3;    1   # (HCO)
147     #
148     #   CO - Dissociation:
149     #
150     ARQL;   {CO*}   +   {*}     =>  {C*}    +   {O*};            $diss_lat;
        $stand_lat;     0.455723;   5.020295;   134.25e3;   95.61e3;    1   # (Diss)
151     ARQL;   {COH*}  +   {*}     =>  {C*}    +   {OH*};           $diss_lat;
        $stand_lat;     0.853567;   1.932005;   11.51e3;    95.45e3;    1   # (COHDiss)
152     ARQL;   {HCO*}  +   {*}     =>  {CH*}   +   {O*};            $diss_lat;
        $stand_lat;     0.130755;   0.096524;   66.81e3;    98.78e3;    1   # (HCODiss)
153     #
154     #   Single C-Hydrogenation
155     #
156     ARQ;    {C*}    +   {H*}    =>  {CH*}   +   {*};
                0.953095;   0.387184;   50.18e3;    57.59e3;    1   # (AA)
157     ARQ;    {CH*}   +   {H*}    =>  {CH2*}  +   {*};
                0.828829;   0.661131;   63.21e3;    42.18e3;    1   # (AB)
```

```
158     ARQ;    {CH2*}  +   {H*}    =>  {CH3*}  +   {*};
                0.920479;   0.269246;   52.74e3;    58.11e3;    1   # (AC)
159     ARQL;   {CH3*}  +   {H*}    =>  {CH4}   +   2{*};           $CH4_lat;
        $car_lat;       22.309831;  0.285183;   77.01e3;    67.98e3;    1   # (HAE)
160 #
161 #   Oxygen Removal
162 #
163
164     #
165     #   CO2-Formation
166     #
167         ARQ;    {CO*}   +   {O*}        =>  {CO2*}  +   {*};
                0.350083;   2.179145;   126.12e3;   111.67e3;   1   # (CO2_Form)
168     #
169     #   Water-Formation
170     #
171         ARQ;    {O*}    +   {H*}        =>  {OH*}   +   {*};
                2.173910;   1.035713;   109.42e3;   131.95e3;   1   # (C)
172         ARQ;    {OH*}   +   {H*}        =>  {H2O*}  +   {*};
                0.880259;   0.116631;   149.50e3;   72.43e3;    1   # (D)
173         ARQ;    2{OH*}                  =>  {H2O*}  +   {O*};
                0.350039;   0.097347;   148.72e3;   49.13e3;    1   # (F)
174 #
175     #   Carbon Additions:
176     #
177     #   C Addition:
178     ARQ;    {C*}        +   {C*}    =>  {C2*}       +   {*};
                1.064334;   0.286005;   79.89e3;    47.64e3;    1   # (HAF)
179     ARQ;    {CH*}       +   {C*}    =>  {CCH*}      +   {*};
                0.545304;   0.555722;   83.51e3;    128.68e3;   1   # (HBA)
180     ARQ;    {CH2*}      +   {C*}    =>  {CCH2*}     +   {*};
                0.416975;   0.399029;   141.63e3;   174.35e3;   1   # (HBB)
181     ARQL;   {CH3*}      +   {C*}    =>  {CCH3*}     +   {*};    $CH3_r_lat;
        $car_lat;       0.705084;   1.446597;   75.52e3;    87.50e3;    1   # (AI)
182     #   CH Addition:
183     ARQ;    {CH*}       +   {CH*}   =>  {CHCH*}     +   {*};
                0.318600;   1.298830;   53.71e3;    78.49e3;    1   # (CA)
184     ARQ;    {CH2*}      +   {CH*}   =>  {CHCH2*}    +   {*};
                0.374159;   0.363990;   133.73e3;   116.49e3;   1   # (HCB)
185     ARQL;   {CH3*}      +   {CH*}   =>  {CHCH3*}    +   {*};    $CH3_r_lat;
        $car_lat;       0.341786;   0.423427;   122.26e3;   87.17e3;    1   # (HCC)
186     #   CH2 Addition:
187     ARQ;    {CH2*}      +   {CH2*}  =>  {CH2CH2*}   +   {*};
                0.913969;   0.415145;   135.79e3;   170.27e3;   1   # (DB)
188     ARQL;   {CH3*}      +   {CH2*}  =>  {CH2CH3*}   +   {*};    $CH3_r_lat;
        $car_lat;       0.147481;   0.080704;   102.78e3;   108.02e3;   1   # (HDC)
189     #   CH3 Addition:
190     HK;     {C2H6}      +   2{*}    =>  {CH3*}      +   {CH3*};
                    $site_size; 30; 20; 6; $stick;  20.34e3;    1   # (HEC)
191     #   Double C-Hydrogenation:
192     ARQ;    {C2*}       +   {H*}    =>  {CCH*}      +   {*};
                0.496293;   0.764613;   42.76e3;    127.66e3;   1   # (AM)
193     ARQ;    {CCH*}      +   {H*}    =>  {CHCH*}     +   {*};
                0.916129;   1.488761;   53.01e3;    39.95e3;    1   # (HAJ)
194     ARQ;    {CCH*}      +   {H*}    =>  {CCH2*}     +   {*};
                0.828315;   0.620432;   84.01e3;    50.44e3;    1   # (HAN)
195     ARQ;    {CCH2*}     +   {H*}    =>  {CHCH2*}    +   {*};
                0.972412;   0.798395;   58.02e3;    34.58e3;    1   # (HAK)
196     ARQL;   {CCH2*}     +   {H*}    =>  {CCH3*}     +   {*};    $CH3_r_lat;
        $car_lat;       1.706890;   1.070416;   59.30e3;    43.95e3;    1   # (HAO)
197     ARQ;    {CCH3*}     +   {H*}    =>  {CHCH3*}    +   {*};
                1.205931;   0.323544;   80.38e3;    40.70e3;    1   # (HAL)
198     ARQ;    {CHCH*}     +   {H*}    =>  {CHCH2*}    +   {*};
```

```
                1.187132;    0.225969;    85.00e3;    21.95e3;    1    # (HAP)
    ARQL;    {CHCH2*}    +    {H*}    => {CHCH3*}    + {*};    $CH3_r_lat;
    $car_lat;        0.479785;    0.197346;    36.99e3;    24.51e3;    1    # (HAQ)
    ARQ;    {CHCH2*}    +    {H*}    => {CH2CH2*}    + {*};
                0.628289;    0.234001;    24.38e3;    55.07e3;    1    # (HAR)
    ARQ;    {CHCH3*}    +    {H*}    => {CH2CH3*}    + {*};
                1.347048;    0.433939;    29.90e3;    49.21e3;    1    # (HAS)
    ARQL;    {CH2CH2*}    +    {H*}    => {CH2CH3*}    + {*};    $CH3_r_lat;
    $car_lat;        5.552600;    1.956700;    137.79e3;    113.93e3;    1    # (HAT)
    ARQL;    {CH2CH3*}    +    {H*}    => {C2H6}    + 2{*};    $CH3_r_lat;
    $car_lat;        0.290259;    259.5823;    82.45e3;    62.25e3;    1    # (HAW)

################################################################################
################################################################################
### Settings:                                                                ###
################################################################################
################################################################################
&settings
# General Settings
    TYPE                =    SEQUENCERUN
    DEBUG               =    0
    NPAR                =    $nr_cores
    PRESSURE            =    $tot_syn_pres
    REAGENTS            =    {CO},{H2}
    KEYCOMPONENTS       =    {CO}
    NUMDIFF             =    1
    SOLVERTYPE          =    1
    SOLSTOPTIME         =    2
    SOLMAXSTEP          =    50000
    # SOLTESTFAIL         =    150
    #Apparent Activation Energy:
    EACT            =    1
    EACTDIFF        =    0.00001
    # Degree of rate control:
    DRC             =    2
    DRCDIFF         =    0.001
    # Degree of selectivity control
    DSC             =    1
    # Reaction orders
    ORDERS          =    1
    ORDERSDIFF      =    0.001
    # Gibbs Energy Barriers
    GIBBS           =    1
    # Graphs:
    GRAPHDATA       =    1
    COLORBLIND      =    1
    MAKEPLOTS       =    1
################################################################################
################################################################################
### runs:                                                                    ###
################################################################################
################################################################################
&runs
# A full run, can be tuned from the top of the file.
if (!$Full_LTFT_Range){
    @BEGIN; 1;  11
        [$start_temp+@m1*$step_size];    $sim_time;  $abs_tol;    $rel_tol
    @END
}
if ($Full_LTFT_Range){
    493.15;     1e6;    1e-15;  1e-10
    513.15;     1e6;    1e-15;  1e-10
    533.15;     1e6;    1e-15;  1e-10
```

```
256 }
```

chapters/appendices/mkmfiles/C2H6_Formation.mkm

H.3 Microkinetic model for the Fischer Tropsch Synthesis

```
#!SEGFLOW
# This is the mkm file for the FT-synthesis on Co (110), Carbon_growth.mkm
# Made by Joost van der Meijs
# Under supervision of dr.ir. I.A.W. Filot and ir. M.P.C. van Etten
# (I.A.W.Filot@tue.nl) & (m.p.c.v.etten@tue.nl)
# With immense help from dr.ir. B. Zijlstra
###############################################################################
###############################################################################
### regex:                    ###
###############################################################################
###############################################################################
&regex_rules_start
REGEX_COUNT  = 23
REGEX_BEGIN  =  ^[ \t]*@BEGIN[ \t]*;[ \t]*([0-9-]+)[ \t]*;[ \t]*([0-9-]+)[ \t]*$
REGEX_SWAP   =  ^.*@.*$
REGEX_SWAP_P =  (^.*)@p([0-9]+)(.*$)
REGEX_SWAP_M =  (^.*)@m([0-9]+)(.*$)
REGEX_SWAP_O =  (^.*)@(.*$)
REGEX_END    =  ^[ \t]*@END[ \t]*$
&regex_rules_end
###############################################################################
###############################################################################
### variables:                ###
###############################################################################
###############################################################################
###       Simulation Variables
variable temp_test    = true
variable sim_time     =  1e4
variable abs_tol      =  1e-15
variable rel_tol      =  1e-10
variable start_temp   = 473.15
variable step_size    = 5
variable nr_cores     = 3
### DeltaH corrections:
variable COrrection          =   -22.72e3
variable CO2rrection         =   17.88e3
###       Lateral Interactions; values taken from the model of ir. B. Zijlstra
variable CO_lat     =  450e3
variable C_lat      =  300e3
variable O__lat     =  300e3
variable H_lat      =  100e3
variable H2_lat     =  [2*($H_lat)]
variable H2O_lat    = [($O__lat)+2*($H_lat)]
variable CH2_lat    = [($C_lat)+2*($H_lat)]
variable CH3_lat    = [($C_lat)+3*($H_lat)]
variable CH4_lat    = [($C_lat)+4*($H_lat)]
variable CO2_lat    = [($C_lat)+2*($O__lat)]
variable diss_lat    = [$C_lat+$O__lat-$CO_lat]
variable C_r_lat     = [-1*($C_lat)-0*($H_lat)]
variable CH_r_lat     = [-1*($C_lat)-1*($H_lat)]
variable CH2_r_lat    = [-1*($C_lat)-2*($H_lat)]
variable CH3_r_lat    = [-1*($C_lat)-3*($H_lat)]
variable CH4_r_lat    = [-1*($C_lat)-4*($H_lat)]
variable eth_lat    = [2*$C_lat+4*$H_lat]
variable olf_lat    = [(2*$C_lat+3*$H_lat)]
variable lat_dir    = 0.50
variable lat_lb     = 0.00
variable lat_ub     = 1.0
variable lat_start    = 1.0
#variable latin     = {*},0.5{H*}
variable latin     = {*}
```

```
variable stand_lat   = $lat_dir;  $lat_lb;  $lat_ub;  $lat_start; $latin
variable car_lat   = 0.00;  0.00;  1.00;  $lat_start; $latin
###       Surface variables
# Size of a Co(0001) (1x1)
variable site_size   = 5.38e-20
variable stick     = 1.0
###       Shomate parameters
# A to H from https://webbook.nist.gov/
# Parameter name:    A     B     C     D     E     F     G     H
variable CO_sho    = 25.56759; 6.096130; 4.054656; -2.671301; 0.131021; -118.0089;
    227.3665; -110.5271
variable water_sho   = -203.6060; 1523.290; -3196.413; 2474.455;  3.855326;
    -256.5478; -488.7163; -285.8304
variable H_sho     = 33.066178; -11.363417; 11.432816; -2.772874; -0.158558;
    -9.980797; 172.707974; 0.000000
variable methane_sho  = -0.703029; 108.4773; -42.52157; 5.862788; 0.678565;
    -76.84376; 158.7163; 74.87310
variable carb_sho   = 24.99735; 55.18696; 33.69137; 7.948387; -0.136638; -403.6075;
     228.2431; -393.5224
variable ethe_sho   = -6.387880; 184.4019; -112.9718; 28.49593; 0.315540; 48.17332;
     163.1568; 52.46694
variable oxy_sho   = 31.32234; -20.23531; 57.86644; -36.50624; -0.007374;
    -8.903471; 246.7945; 0.0
###                          Pressure
variable tot_syn_pres       =   1.0
variable H2_CO_RAT          =   2.0
variable Partial_P_CO       =   ($tot_syn_pres/(1+$H2_CO_RAT))
variable Partial_P_H2       =   ($tot_syn_pres-$tot_syn_pres/(1+$H2_CO_RAT))
##########################################################################################
##########################################################################################
### compounds:                    ###
##########################################################################################
##########################################################################################
&compounds
# Reagents:
 CO;          0; [$Partial_P_CO]
 H2;          0; [$Partial_P_H2]
# Products:
 H2O;         0; 0.00
 O2;          0; 0.00
 CO2;         0; 0.00
 CH4;         0; 0.00
 C2H4;         0; 0.00
 C2H6;         0; 0.00
 CH2_CH_CH3;        0; 0.00
 @BEGIN;1;0
  CH3_@CH2_CH3;      0; 0.00
 @END
 @BEGIN;2;0
  CH2_CH_@m1CH2_CH3;     0; 0.00
 @END
# Empty surface sites:
 *;          1; 1.00
# Surface intermediates:
 # For CO dissociation:
 CO*;         1; 0.00
 HCO*;         1; 0.00
 COH*;         1; 0.00
 # Hydrogen, Oxygen, OH, H2O and CO2
 H*;          1; 0.00
 O*;          1; 0.00
 CO2*;         1; 0.00
 OH*;         1; 0.00
```

```
H2O*;          1; 0.00
# Single Carbon intermediates
C*;            1; 0.00
CH*;           1; 0.00
CH2*;          1; 0.00
CH3*;          1; 0.00
# Double Carbon intermediates
C2*;           1; 0.00
CCH*;          1; 0.00
CCH2*;         1; 0.00
CCH3*;         1; 0.00
CHCH*;         1; 0.00
CHCH2*;        1; 0.00
CHCH3*;        1; 0.00
CH2CH2*;       1; 0.00
CH2CH3*;       1; 0.00
# Multi Carbon intermediates
CH2_C_CH3*;       1; 0.00
CH2_CH_CH3*;      1; 0.00
C_CH_CH3*;       1; 0.00
CH_CH_CH3*;       1; 0.00
C_C_CH3*;        1; 0.00
CH_C_CH3*;       1; 0.00
@BEGIN;1;0
 CH2_@CH2_CH3*;     1; 0.00
 CH_@CH2_CH3*;      1; 0.00
 C_@CH2_CH3*;     1; 0.00
@END
@BEGIN;2;0
 CH2_CH_@m1CH2_CH3*;    1; 0.00
 CH_CH_@m1CH2_CH3*;     1; 0.00
 C_CH_@m1CH2_CH3*;    1; 0.00
 CH2_C_@m1CH2_CH3*;    1; 0.00
 CH_C_@m1CH2_CH3*;    1; 0.00
 C_C_@m1CH2_CH3*;    1; 0.00
@END
#############################################################################
#############################################################################
### reactions:                    ###
#############################################################################
#############################################################################
&reactions
 ###################################
 # ADSORPTION / DESORPTION   #
 ###################################
 ADS; {CO}  +  {*}  => {CO*}    ; $CO_lat;   $stand_lat; $site_size;   28; $stick;
    $CO_sho;  1.25e2; 154.73e3; 1 # (CO_Ads)
 ADS; {H2O} +  {*}  => {H2O*}    ; $H2O_lat;  $stand_lat; $site_size;   18; $stick;
    $water_sho;  1.16e2; 35.54e3; 1 # (H2O_Ads)
 ADS; {H2}  +  2{*} => 2{H*}    ; $H2_lat;   $stand_lat; $site_size;   2; $stick;
    $H_sho;   1.66e0; 74.83e3; 1 # (H2_Ads)
 ADS; {CO2} + {*}  => {CO2*}    ; $CO2_lat;  $stand_lat; $site_size;   44; $stick;
    $carb_sho;  8.87e1; 71.98e3; 1 # (CO2_Ads)
 ADS; {O2}  + 2{*} => 2{O*}    ; $O__lat;   $stand_lat; $site_size;   32; $stick;
    $oxy_sho;  1.96e1; 471.45e3; 1 # (A)
 ADS; {C2H4} + {*}  => {CH2CH2*}  ; $eth_lat;  $stand_lat; $site_size;   28; $stick
    ; $ethe_sho;  3.77e2; 97.09e3; 1 # (C2H4_Ads)
 ###################################
 # SURFACE REACTIONS     #
 ###################################
 #
 # CO-Hydrogenation
 #
```

```
175 ARQL; {CO*} + {H*} => {COH*} + {*};   $diss_lat; $stand_lat;                0.234258;
      0.543187; 173.03e3; 72.81e3; 1 # (COH)
176 ARQL; {CO*} + {H*} => {HCO*} + {*};   $diss_lat; $stand_lat;                0.000863;
      0.458237; 112.31e3; 49.02e3; 1 # (HCO)
177 #
178 # CO - Dissociation:
179 #
180 ARQL; {CO*} + {*}  => {C*} + {O*};   $diss_lat; $stand_lat;                0.455723;
      5.020295; 134.25e3; 95.61e3; 1 # (Diss)
181 ARQL; {COH*} + {*}  => {C*} + {OH*};   $diss_lat; $stand_lat;
     0.853567; 1.932005; 11.51e3; 95.45e3; 1 # (COHDiss)
182 ARQL; {HCO*} + {*}  => {CH*} + {O*};   $diss_lat; $stand_lat;
     0.130755; 0.096524; 66.81e3; 98.78e3; 1 # (HCODiss)
183 #
184 # Single C-Hydrogenation
185 #
186 ARQ; {C*} + {H*} => {CH*} + {*};                          0.953095; 0.387184; 50.18
     e3; 57.59e3; 1 # (AA)
187 ARQ; {CH*} + {H*} => {CH2*} + {*};                        0.828829; 0.661131; 63.21
     e3; 42.18e3; 1 # (AB)
188 ARQ; {CH2*} + {H*} => {CH3*} + {*};                      0.920479; 0.269246; 52.74
     e3; 58.11e3; 1 # (AC)
189 ARQL; {CH3*} + {H*} => {CH4}  + 2{*};   $CH4_lat; $car_lat;
     22.309831; 0.285183; 77.01e3; 67.98e3; 1 # (HAE)
190 #
191 # Carbon Additions:
192 #
193 # C Addition:
194 ARQ; {C*}  + {C*} => {C2*}  + {*};                       1.064334; 0.286005; 79.89e3
     ; 47.64e3; 1 # (HAF)
195 ARQ; {CH*}  + {C*} => {CCH*}  + {*};                     0.545304; 0.555722; 83.51
     e3; 128.68e3; 1 # (HBA)
196 ARQ; {CH2*}  + {C*} => {CCH2*}  + {*};                   0.416975; 0.399029;
     141.63e3; 174.35e3; 1 # (HBB)
197 ARQL; {CH3*}  + {C*} => {CCH3*}  + {*};  $CH3_r_lat; $car_lat;
     0.705084; 1.446597; 75.52e3; 87.50e3; 1 # (AI)
198 # CH Addition:
199 ARQ; {CH*}  + {CH*} => {CHCH*}  + {*};                   0.318600; 1.298830;
     53.71e3; 78.49e3; 1 # (CA)
200 ARQ; {CH2*}  + {CH*} => {CHCH2*}  + {*};                 0.374159; 0.363990;
     133.73e3; 116.49e3; 1 # (HCB)
201 ARQL; {CH3*}  + {CH*} => {CHCH3*}  + {*};  $CH3_r_lat; $car_lat;
     0.341786; 0.423427; 122.26e3; 87.17e3; 1 # (HCC)
202 # CH2 Addition:
203 ARQ; {CH2*}  + {CH2*} => {CH2CH2*} + {*};                 0.913969; 0.415145;
     135.79e3; 170.27e3; 1 # (DB)
204 ARQL; {CH3*}  + {CH2*}  => {CH2CH3*} + {*};  $CH3_r_lat; $car_lat;
     0.147481; 0.080704; 102.78e3; 108.02e3; 1 # (HDC)
205 # CH3 Addition:
206 HK;  {C2H6}  + 2{*} => {CH3*}  + {CH3*};                  $site_size; 30; 20;
     6; $stick;  20.34e3; 1 # (HEC)
207 # Double C-Hydrogenation:
208 ARQ; {C2*}  + {H*} => {CCH*}  + {*};                     0.496293; 0.764613;
     42.76e3; 127.66e3; 1 # (AM)
209 ARQ; {CCH*}  + {H*} => {CHCH*}  + {*};                   0.916129; 1.488761;
     53.01e3; 39.95e3; 1 # (HAJ)
210 ARQ; {CCH*}  + {H*} => {CCH2*}  + {*};                  0.828315; 0.620432;
     84.01e3; 50.44e3; 1 # (HAN)
211 ARQ; {CCH2*}  + {H*} => {CHCH2*}  + {*};                0.972412; 0.798395;
     58.02e3; 34.58e3; 1 # (HAK)
212 ARQL; {CCH2*}  + {H*} => {CCH3*}  + {*};  $CH3_r_lat; $car_lat;
     1.706890; 1.070416; 59.30e3; 43.95e3; 1 # (HAO)
213 ARQ; {CCH3*}  + {H*} => {CHCH3*}  + {*};                1.205931; 0.323544;
```

```
    80.38e3; 40.70e3; 1 # (HAL)
214 ARQ; {CHCH*} + {H*} => {CHCH2*} + {*}; 1.187132; 0.225969;
    85.00e3; 21.95e3; 1 # (HAP)
215 ARQL; {CHCH2*} + {H*} => {CHCH3*} + {*}; $CH3_r_lat; $car_lat;
    0.479785; 0.197346; 36.99e3; 24.51e3; 1 # (HAQ)
216 ARQ; {CHCH2*} + {H*} => {CH2CH2*} + {*}; 0.628289; 0.234001;
    24.38e3; 55.07e3; 1 # (HAR)
217 ARQ; {CHCH3*} + {H*} => {CH2CH3*} + {*}; 1.347048; 0.433939;
    29.90e3; 49.21e3; 1 # (HAS)
218 ARQL; {CH2CH2*} + {H*} => {CH2CH3*} + {*}; $CH3_r_lat; $car_lat;
    5.552600; 1.956700; 137.79e3; 113.93e3; 1 # (HAT)
219 ARQL; {CH2CH3*} + {H*} => {C2H6} + 2{*}; $CH3_r_lat; $car_lat;
    0.290259; 259.5823; 82.45e3; 62.25e3; 1 # (HAW)
220 #
221 # CO2-Formation
222 #
223 ARQ; {CO*} + {O*} => {CO2*} + {*}; 0.350083; 2.179145; 126.12
    e3; 111.67e3; 1 # (CO2_Form)
224 #
225 # Water-Formation
226 #
227 ARQ; {O*} + {H*} => {OH*} + {*}; 2.173910; 1.035713; 109.42e3
    ; 131.95e3; 1 # (C)
228 ARQ; {OH*} + {H*} => {H2O*} + {*}; 0.880259; 0.116631; 149.50
    e3; 72.43e3; 1 # (D)
229 ARQ; 2{OH*} => {H2O*} + {O*}; 0.350039; 0.097347; 148.72e3;
     49.13e3; 1 # (F)
230
231 # The First C3 Carbon species, for use in the loops:
232 ARQL; {C*} + {CH2CH3*} => {C_1CH2_CH3*} + {*}; $CH2_r_lat; $car_lat;
    0.705084; 1.446597; 75.52e3; 87.50e3; 1 # (AI)
233 ARQL; {CH*} + {CH2CH3*} => {CH_1CH2_CH3*} + {*}; $CH2_r_lat; $car_lat;
    0.341789; 0.463118; 122.26e3; 87.17e3; 1 # (HCC)
234 ARQL; {CH2*} + {CH2CH3*} => {CH2_1CH2_CH3*} + {*}; $CH2_r_lat; $car_lat;
     0.147481; 0.080704; 102.78e3; 108.02e3; 1 # (HDC)
235 ARQ; {C*} + {CHCH3*} => {C_CH_CH3*} + {*}; 0.416975; 0.399029;
    141.63e3; 174.35e3; 1 # (HBB)
236 ARQ; {CH*} + {CHCH3*} => {CH_CH_CH3*} + {*}; 0.374159; 0.363990;
    133.73e3; 116.49e3; 1 # (HCB)
237 ARQ; {CH2*} + {CHCH3*} => {CH2_CH_CH3*} + {*}; 0.913969;
    0.415145; 135.79e3; 170.27e3; 1 # (DB)
238 ARQ; {C*} + {CCH3*} => {C_C_CH3*} + {*}; 0.545304; 0.555722;
    83.51e3; 128.68e3; 1 # (HBA)
239 ARQ; {CH*} + {CCH3*} => {CH_C_CH3*} + {*}; 0.318600; 1.298830;
    53.71e3; 78.49e3; 1 # (CA)
240 ARQ; {CH2*} + {CCH3*} => {CH2_C_CH3*} + {*}; 0.374159; 0.363990;
     133.73e3; 116.49e3; 1 # (HCB)
241 # The C3 Hydrogenation:
242 ARQL; {CH2_CH_CH3*} + {H*} => {CH2_1CH2_CH3*} + {*}; $CH2_r_lat; $car_lat;
      5.552600; 1.956700; 137.79e3; 113.93e3; 1 # (HAT)
243 ARQ; {CH2_C_CH3*} + {H*} => {CH2_CH_CH3*} + {*}; 0.628289;
    0.234001; 24.38e3; 55.07e3; 1 # (HAR)
244 ARQL; {CH_CH_CH3*} + {H*} => {CH_1CH2_CH3*} + {*}; $CH2_r_lat; $car_lat;
     0.479785; 0.197346; 36.99e3; 24.51e3; 1 # (HAQ)
245 ARQ; {C_CH_CH3*} + {H*} => {CH_CH_CH3*} + {*}; 0.972412;
    0.798395; 58.02e3; 34.58e3; 1 # (HAK)
246 ARQL; {C_CH_CH3*} + {H*} => {C_1CH2_CH3*} + {*}; $CH2_r_lat; $car_lat;
    1.706890; 1.070416; 59.30e3; 43.95e3; 1 # (HAO)
247 ARQ; {CH_CH_CH3*} + {H*} => {CH2_CH_CH3*} + {*}; 0.628289;
    0.234001; 24.38e3; 55.07e3; 1 # (HAR)
248 ARQ; {C_C_CH3*} + {H*} => {CH_C_CH3*} + {*}; 0.916129; 1.488761;
     53.01e3; 39.95e3; 1 # (HAJ)
249 ARQ; {C_C_CH3*} + {H*} => {C_CH_CH3*} + {*}; 0.828315; 0.620432;
```

```
    84.01e3; 50.44e3; 1 # (HAN)
ARQ; {CH_C_CH3*}    + {H*}    => {CH_CH_CH3*}    + {*};            1.187132;
   0.225969; 85.00e3; 21.95e3; 1 # (HAP)
# C3-Desorption:
ADS; {CH2_CH_CH3}    + {*}    => {CH2_CH_CH3*};       $olf_lat; $stand_lat;
   $site_size; 42;  $stick; $ethe_sho; 3.77e2;  97.09e3; 1 # (C2H4_Ads)
@BEGIN; 1; 0
 # Alkane Desorption/Adsorption:
 ARQL; {CH2_@CH2_CH3*}    + {H*}    => {CH3_@CH2_CH3}    + 2{*}; $CH2_r_lat; $car_lat
   ;     0.290259; 259.5823; 82.45e3; 62.25e3; 1 # (HAW)
 # Hydrogenation:
 ARQ; {CH_@CH2_CH3*}    + {H*}    => {CH2_@CH2_CH3*}    + {*};          1.347048;
   0.433939; 29.90e3; 49.21e3; 1 # (HAS)
 ARQ; {C_@CH2_CH3*}    + {H*}    => {CH_@CH2_CH3*}    + {*};          1.205931;
   0.323544; 80.38e3; 40.70e3; 1 # (HAL)
@END
@BEGIN; 2; 0
 # Alkene Desorption:
 ADS; {CH2_CH_@m1CH2_CH3}  + {*}    => {CH2_CH_@m1CH2_CH3*};    $olf_lat;
   $stand_lat; $site_size; [42+@m1*14]; $stick; $ethe_sho; 3.77e2; 97.09e3; 1 # (
   C2H4_Ads)
 # Alkane formation through CH3 addition:
 HK;  {CH3_@CH2_CH3}    + 2{*}    => {CH2_@m1CH2_CH3*}  + {CH3*};       $site_size;
   [30+@*14]; 20; 6; $stick;    20.34e3; 1 # (HEC)
 # Hydrogenation:
 ARQL; {CH2_CH_@m1CH2_CH3*} + {H*}    => {CH2_@CH2_CH3*}    + {*}; $CH2_r_lat;
   $car_lat;     5.552600; 1.956700; 137.79e3; 113.93e3; 1 # (HAT)
 ARQ; {CH_CH_@m1CH2_CH3*}  + {H*}    => {CH2_CH_@m1CH2_CH3*} + {*};
   0.628289; 0.234001; 24.38e3; 55.07e3; 1 # (HAR)
 ARQL; {CH_CH_@m1CH2_CH3*}  + {H*}    => {CH_@CH2_CH3*}    + {*}; $CH2_r_lat;
   $car_lat;     0.479785; 0.197346; 36.99e3; 24.51e3; 1 # (HAQ)
 ARQ; {C_CH_@m1CH2_CH3*}  + {H*}    => {CH_CH_@m1CH2_CH3*}  + {*};
   0.972412; 0.798395; 58.02e3; 34.58e3; 1 # (HAK)
 ARQL; {C_CH_@m1CH2_CH3*}  + {H*}    => {C_@CH2_CH3*}    + {*}; $CH2_r_lat; $car_lat
   ;     1.706890; 1.070416; 59.30e3; 43.95e3; 1 # (HAO)
 ARQ; {CH2_C_@m1CH2_CH3*}  + {H*}    => {CH2_CH_@m1CH2_CH3*} + {*};
   0.628289; 0.234001; 24.38e3; 55.07e3; 1 # (HAR)
 ARQ; {CH_C_@m1CH2_CH3*}  + {H*}    => {CH2_C_@m1CH2_CH3*}  + {*};
   1.187132; 0.225969; 85.00e3; 21.95e3; 1 # (HAP)
 ARQ; {CH_C_@m1CH2_CH3*}  + {H*}    => {CH_CH_@m1CH2_CH3*}  + {*};
   1.187132; 0.225969; 85.00e3; 21.95e3; 1 # (HAP)
 ARQ; {C_C_@m1CH2_CH3*}  + {H*}    => {CH_C_@m1CH2_CH3*}  + {*};          0.916129;
    1.488761; 53.01e3; 39.95e3; 1 # (HAJ)
 ARQ; {C_C_@m1CH2_CH3*}  + {H*}    => {C_CH_@m1CH2_CH3*}  + {*};          0.828315;
    0.620432; 84.01e3; 50.44e3; 1 # (HAN)
@END
@BEGIN; 2; 0
 # Carbon-Carbon Coupling:
 ARQL; {CH2_@m1CH2_CH3*}  + {C*}    => {C_@CH2_CH3*}    + {*}; $CH2_r_lat; $car_lat;
       0.705084; 1.446597; 75.52e3; 87.50e3; 1 # (AI)
 ARQL; {CH2_@m1CH2_CH3*}  + {CH*}    => {CH_@CH2_CH3*}    + {*}; $CH2_r_lat;
   $car_lat;     0.341789; 0.463118; 122.26e3; 87.17e3; 1 # (HCC)
 ARQL; {CH2_@m1CH2_CH3*}  + {CH2*}    => {CH2_@CH2_CH3*}    + {*}; $CH2_r_lat;
   $car_lat;     0.147481; 0.080704; 102.78e3; 108.02e3; 1 # (HDC)
@END
@BEGIN; 3; 0
 # Carbon-Carbon Coupling:
 ARQ; {CH_@m2CH2_CH3*}  + {C*}    => {C_CH_@m2CH2_CH3*}  + {*};          0.416975;
   0.399029; 141.63e3; 174.35e3; 1 # (HBB)
 ARQ; {CH_@m2CH2_CH3*}  + {CH*}    => {CH_CH_@m2CH2_CH3*}  + {*};
   0.374159; 0.363990; 133.73e3; 116.49e3; 1 # (HCB)
 ARQ; {CH_@m2CH2_CH3*}  + {CH2*}    => {CH2_CH_@m2CH2_CH3*} + {*};
   0.913969; 0.415145; 135.79e3; 170.27e3; 1 # (DB)
```

```
  ARQ; {C_@m2CH2_CH3*}    + {C*}    => {C_C_@m2CH2_CH3*}   + {*};            0.545304;
    0.555722; 83.51e3; 128.68e3; 1 # (HBA)
  ARQ; {C_@m2CH2_CH3*}    + {CH*}    => {CH_C_@m2CH2_CH3*}   + {*};            0.318600;
     1.298830; 53.71e3; 78.49e3; 1 # (CA)
  ARQ; {C_@m2CH2_CH3*}    + {CH2*}    => {CH2_C_@m2CH2_CH3*}   + {*};
    0.374159; 0.363990; 133.73e3; 116.49e3; 1 # (HCB)
 @END
##############################################################################
##############################################################################
### Settings:                  ###
##############################################################################
##############################################################################
&settings
# General Settings
 TYPE      =  SEQUENCERUN
 DEBUG      =  0
 NPAR      =  $nr_cores
 NUMDIFF     =  1
 SOLVERTYPE     = 1
 SOLSTOPTIME    =  1
 SOLMAXSTEP    = 50000
 SOLTESTFAIL    = 150
# Reaction Settings:
 PRESSURE     =  $tot_syn_pres
 REAGENTS     =  {CO},{H2}
 KEYCOMPONENTS    =  {CO}
 SIMPLE_LAT_FAC    =  1
# Apparent Activation Energy:
 EACT      =  1
 EACTDIFF     =  0.00001
# Degree of rate control:
 DRC      = 2
 DRCDIFF     =  0.001
# Degree of Chain Growth Control (w/ DRC=2)
 DCGC      =  1
# Degree of selectivity control
 DSC      =  1
# Thermodynamic degree of rate control
 TDRC      =   0
 TDRCDIFF     =  0.1
# Reaction orders
 ORDERS      =  1
 ORDERSDIFF     =  0.001
# Gibbs Energy Barriers
 GIBBS      = 1
# Graphs:
 GRAPHDATA     =  1
 COLORBLIND    =  1
 MAKEPLOTS     = 1
# Networks
 NETWORK     =  1
 NETWORK_RATES   = 1
 NETWORK_STRICT   = 1
 NETWORK_NODAL_PROD = 1
##############################################################################
##############################################################################
### runs:                    ###
##############################################################################
##############################################################################
&runs
# A full run, can be tuned from the top of the file.
if (!$temp_test){
 @BEGIN; 1; 11
```

```
  [$start_temp+@ml*$step_size]; $sim_time; $abs_tol; $rel_tol
 @END
}
if ($temp_test){
 493.15;  1e6; 1e-15; 1e-10
 513.15;  1e6; 1e-15; 1e-10
 533.15;  1e6; 1e-15; 1e-10
}
##############################################################################
##############################################################################
### selectivity:                ###
##############################################################################
##############################################################################
&selectivity
 carbon_balance; {CO}; {CH4}
  carbon_balance; {CO}; 2{C2H4}
  carbon_balance; {CO}; 2{C2H6}
  carbon_balance; {CO}; {CO2}
  @BEGIN;1;0
   carbon_balance; {CO}; @p2{CH3_@CH2_CH3}
  @END
  @BEGIN;2;0
   carbon_balance; {CO}; @p2{CH2_CH_@m1CH2_CH3}
  @END
  oxygen_banance; {CO}; {H2O},2{CO2}
##############################################################################
##############################################################################
### Anderson-Schulz-Flory:              ###
##############################################################################
##############################################################################
&asf
 asf;  5; {CH4}
 asf;  5; 2{C2H6}
 asf;  5; 2{C2H4}
 parafin; 5; {CH4}
 parafin; 5; {C2H6}
 olefin; 5; 2{C2H4}
 @BEGIN;1;0
  asf; 5; @p2{CH3_@CH2_CH3}
  parafin; 5; @p2{CH3_@CH2_CH3}
 @END
 @BEGIN;2;0
  asf; 5; @p2{CH2_CH_@m1CH2_CH3}
  olefin; 5; @p2{CH2_CH_@m1CH2_CH3}
 @END

##############################################################################
##############################################################################
### Networks:                   ###
##############################################################################
##############################################################################
&networkplot
  NODAL_ROOT   = {CO}
  ROOT_NODE    = {CO}
  NODAL_START  = {CO},{H2},{*}
  NODAL_EXCLUDE = {*}
  NODAL_END    = {CH4},{C2H6},{C2H4},{H2O},{CO2}
  EXCLUDE_LIMIT = 1E-5
  @BEGIN;1;0
   NODAL_END = {CH3_@CH2_CH3}
  @END
  @BEGIN;2;0
   NODAL_END = {CH2_CH_@m1CH2_CH3}
```

```
411 @END
```

chapters/appendices/mkmfiles/Carbon_growth.mkm